THE CRESCERIN PROTEIN FAMILY USES ARRAYED TOG DOMAINS TO REGULATE MICROTUBULES IN CILIA

Alakananda Das

A dissertation submitted to the faculty at the University of North Carolina at Chapel Hill in partial fulfillment of the requirements for the degree of Doctor of Philosophy in the Department of Biochemistry and Biophysics in the School of Medicine.

Chapel Hill
2016

Approved by:

Kevin Slep

Saskia Neher

Brian Kuhlman

Eva Anton

Matthew Redinbo

ABSTRACT

Alakananda Das: The Crescerin protein family uses arrayed TOG domains to regulate microtubules in cilia
(Under the direction of Kevin C. Slep)

The eukaryotic primary cilium is a solitary, antenna-like projection from the surface of a cell, critical for sensing the extracellular environment. Many mammalian cell types have a primary cilium, which acts as a hub for different signaling pathways depending upon the cell type. Primary cilia play an important role in cell differentiation and cell fate determination in response to rapidly switching cues during embryonic development. Due to the widespread occurrence of primary cilium in different tissues, mutation in proteins affecting cilia structure can present a wide variety of developmental defects and sensory disorders, collectively termed ciliopathies.

A microtubule-based scaffold, known as the axoneme, forms the core of the primary cilium. The structure of the axoneme is highly conserved across different eukaryotic species. However, mechanisms that regulate the structure and microtubule dynamics in the axoneme are poorly understood. TOG domain array-containing proteins ch-TOG and CLASP are key regulators of cytoplasmic microtubules. Whether TOG array proteins also regulate ciliary microtubules is unknown. In this dissertation, we have identified the conserved Crescerin protein family as a cilia-specific TOG array-containing microtubule regulator. We present the crystal structure of mammalian Crescerin1 TOG2, revealing a canonical TOG fold with

conserved tubulin-binding determinants. Crescerin1′s TOG domains possess inherent microtubule-binding activity and promote microtubule polymerization *in vitro*. Using Cas9-triggered homologous recombination in *Caenorhabditis elegans*, we demonstrate that the worm Crescerin family member CHE-12 requires TOG domain-dependent tubulin-binding activity for sensory cilia development. Thus, Crescerin expands the TOG domain array-based MT regulatory paradigm beyond ch-TOG and CLASP, representing a distinct regulator of cilia structure.

ACKNOWLEDGEMENTS

First and foremost, I would like to thank my advisor, Dr. Kevin Slep for providing invaluable guidance and support through the last five years, for allowing me the freedom to take my project in new directions, encouraging me to explore outside my comfort zone and brave uncharted territories. I would also like to thank my thesis committee, Dr. Eva Anton, Dr. Brian Kuhlman, Dr. Saskia Neher and Dr. Matthew Redinbo for providing feedback on my research. I have enjoyed sharing my work with them and their suggestions helped me overcome many challenges I have faced along the way. I thank Dr. Stephen Rogers, Dr. Mark Peifer, Drs. Paul and Amy Maddox, Dr. Ashutosh Tripathy, Dr. Mike Miley and Victoria Madden for their expert advice and help with reagents and instruments. Special thanks to our collaborators, Dr. Bob Goldstein and Dr. Daniel Dickinson, and the entire Goldstein lab for granting me access into their lab space and reagents and for always being ready to answer my questions.

I would like to thank all the wonderful people I have had the pleasure to work with in the Slep lab. I could not have asked for a more congenial workplace. I am grateful for all the knowledge that they shared with me and I have a learnt a lot from each and every one of them. Above all, I thank them for their friendship and support.

Lastly, I would like to thank my family for always being there for me.

PREFACE

Parts of the work in Chapters 2, 3 and 4 previously appeared as an article in the journal Molecular Biology of the Cell, in 2015, under the direction of Dr. Kevin Slep and in collaboration with Dr. Bob Goldstein and Dr. Daniel Dickinson. In Chapter 2, I performed the sequence analysis, crystallization, data collection, model building and refinement of Crescerin1 TOG2. The phylogenetic analysis presented here in Chapter 2 section 2.4.2 has been modified from the one published in the article, by the addition of the PP2A family of HEAT repeat containing proteins. Cameron Wood collected the light scattering data for the *in vitro* microtubule polymerization experiments under my supervision. The light scattering and circular dichroism experiments were done in the Macromolecular Interactions Facility at UNC, with help from Dr. Ashutosh Tripathy. In Chapter 3, I performed the assays to analyze the cilia localization and cytoplasmic microtubule lattice-binding of Crescerin in mammalian cells. In Chapter 4, Daniel Dickinson created the GFP-tagged and CHE-12 mutant *C. elegans* strains, while I performed the chemotaxis assay, dye-filling assay and fluorescence imaging. The transmission electron microscopy of *C. elegans* was performed in the Microscopy Services Laboratory at UNC, with great help from Victoria C. Madden. The citation for this manuscript is as follows: Das, A.; Dickinson, D. J.; Wood, C. C.; Goldstein, B.; Slep, K. C. Crescerin uses a TOG domain array to regulate microtubules in the primary cilium. *Mol. Biol. Cell* **2015**, *26*, 4248–4264 DOI: 10.1091/mbc.E15-08-0603.

The work presented in Chapter 3, section 3.4.2, is an ongoing project attempting to understand the mechanism of Crescerin's entry into the ciliary compartment. In Chapter 4, the time-lapse imaging of *C. elegans* amphid cilia and the development of conditional tagging scheme is also part of an ongoing project to analyze the dynamics of CHE-12 in the cilia and its interactions with tubulin and intra-flagellar transport proteins.

The work highlighted in this dissertation was supported through several funding sources from March of Dimes, National Institutes of Health, National Science Foundation, HHMI International Student Research Fellowship and Dissertation Completion Fellowship awarded by the UNC Graduate School.

TABLE OF CONTENTS

LIST OF FIGURES.....xii

LIST OF ABBREVIATIONS AND SYMBOLS.....xiv

CHAPTER 1: INTRODUCTION.....1

1.1. Cilia: Types and functions.....1

1.2. Ciliogenesis.....3

1.3. Ultrastructure of cilia.....3

1.4. ch-TOG and CLASP families of MAPs regulate MT dynamics in cells.....7

References.....11

CHAPTER 2: CRESCERIN DEFINES A CONSERVED PROTEIN FAMILY WITH A TOG DOMAIN ARRAY.....16

2.1. Summary.....16

2.2. Introduction.....16

2.3. Experimental procedures.....19

2.3.1. Sequence analysis.....19

2.3.2. Phylogenetic analysis.....20

2.3.3. Cloning and expression.....20

2.3.4. Protein purification.....21

2.3.5. Crystallization.....22

2.3.6. Data collection, structure determination, and refinement.....22

2.3.7. Circular dichroism.....23

2.3.8. In vitro MT polymerization assay.....23

2.4. Results.....24

2.4.1. Sequence analysis.....24

2.4.2. Phylogenetic analysis.....30

2.4.3. Structure of the Crescerin1 second conserved domain reveals a bona fide TOG domain.....31

2.4.4. Crescerin1 TOG2 has a unique C-terminal β-hairpin that promotes domain stability.....33

2.4.5. The Crescerin1 TOG2 tubulin-binding surface is similar to Stu2 TOG1.....37

2.4.6. Crescerin1 TOG domains can bind to microtubules and promote microtubule polymerization in vitro.....38

2.5. Discussion.....40

References.....43

CHAPTER 3: CRESCERIN1 LOCALIZES TO THE PRIMARY CILIUM IN MAMMALIAN CELLS.....47

3.1. Summary.....47

3.2. Introduction.....46

3.3. Experimental Procedures.....50

3.3.1. Mammalian expression plasmids.....50

3.3.2. Cell culture and transfection.....51

3.3.3. Immunofluorescence microscopy of mammalian cells.....51

3.4. Results.....52

3.4.1. Crescerin1 localizes to cilia in mammalian cells.....52

3.4.2. Cilia import signals in Crescerin1.....55

3.4.3. Crescerin1 C-terminal TOG domains promote microtubule lattice binding in cells....56

3.5. Discussion....59

References....62

CHAPTER 4: THE MICROTUBULE REGULATORY FUNCTION OF CHE-12 IS NECESSARY FOR PROPER CILIA DEVELOPMENT IN *C. ELEGANS*....67

4.1. Summary....67

4.2. Introduction....67

4.3. Experimental Procedures....72

4.3.1. C. elegans culture and strain construction....72

4.3.2. Conditional endogenous tagging of C. elegans genes....74

4.3.3. Chemotaxis assays....74

4.3.4. Dye-filling assay....76

4.3.5. Fluorescence microscopy of C. elegans....76

4.3.6. Transmission electron microscopy of C. elegans....77

4.4 Results....78

4.4.1. CHE-12 localizes to a subset of amphid and phasmid cilia in C. elegans....78

4.4.2. CHE-12 is required for proper chemotaxis and dye-filling in amphid neurons....81

4.4.3. CHE-12 is necessary for proper amphid cilia development and organization in C. elegans....84

4.5. Discussion....86

References....89

CHAPTER 5: DISCUSSION AND FUTURE WORK....91

5.1. Why is Crescerin specific to cilia and how does this compare and contrast with the regulation of MT dynamics in the cytoplasm?....91

5.2. Future directions....92

References....96

APPENDIX 2.1: CH-TOG FAMILY OF TOG DOMAIN CONTAINING PROTEINS....98

APPENDIX 2.2: CLASP FAMILY OF TOG DOMAIN CONTAINING PROTEINS....99

APPENDIX 2.3: NCBI SEQUENCE IDENTIFIERS FOR CRESCERIN HOMOLOGS IN DIFFERENT SPECIES....100

APPENDIX 2.4: CRYSTALLOGRAPHIC DATA, PHASING AND REFINEMENT STATISTICS FOR THE CRESCERIN1 TOG2 STRUCTURE....101

APPENDIX 2.5: CRESCERIN FAMILY TOG1 SEQUENCE ALIGNMENT....102

APPENDIX 2.6: CRESCERIN FAMILY TOG2 SEQUENCE ALIGNMENT....103

APPENDIX 2.7: CRESCERIN FAMILY TOG3 SEQUENCE ALIGNMENT....104

APPENDIX 2.8: CRESCERIN FAMILY TOG4 SEQUENCE ALIGNMENT....105

APPENDIX 2.9: CIRCULAR DICHROISM OF CRESCERIN1 TOG DOMAINS....106

APPENDIX 3.1: OVER-EXPRESSED CRESCERIN1 ASSOCIATES WITH CYTOPLASMIC MICROTUBULES....107

APPENDIX 3.2: CRESCERIN1 CONSTRUCTS SPANNING RESIDUES 1-1242 AND 577-1242 MISLOCALIZE TO LARGE CYTOPLASMIC PUNCTAE....108

APPENDIX 3.3: PY-NLS SEQUENCES FROM KNOWN IMPORTIN-β2 BINDING PROTEINS AND CRESCERIN1....109

APPENDIX 4.1: LIST OF *C. ELEGANS* STRAINS USED IN THIS STUDY AND THEIR GENOTYPES....110

APPENDIX 4.2: GENOME EDITING IN *C. ELEGANS*....111

APPENDIX 4.3: CONDITIONAL ENDOGENOUS TAGGING OF *C. ELEGANS* GENES....112

LIST OF FIGURES

Figure 1.1 - Schematic diagram outlining the major steps during ciliogenesis.....2

Figure 1.2 - Schematic representation of the ultrastructure of cilia.....4

Figure 1.3 - Arrayed TOG domain containing protein families, ch-TOG and CLASP regulate microtubule dynamics.....8

Figure 2.1 - Structures of TOG domains and structural basis of tubulin binding.....19

Figure 2.2 - The Crescerin protein family has conserved TOG domains across a wide range of ciliated eukaryotes.....27

Figure 2.3 - Matrix showing sequence identity between pairs of TOG domains in human Crescerin, ch-TOG and CLASP families.....28

Figure 2.4 - Cladogram showing phylogenetic relationship between Crescerin, ch-TOG and CLASP family TOG domains.....29

Figure 2.5 - The Crescerin1 second conserved domain is a *bona fide* TOG domain.....32

Figure 2.6 - Crescerin1 TOG2 has a unique C-terminal β-hairpin.....35

Figure 2.7 - The Crescerin1 TOG2 tubulin-binding surface is similar to Stu2 TOG1.....36

Figure 2.8 - Crescerin1 TOG domains affect MT polymerization *in vitro*.....39

Figure 3.1 - Crescerin1 localizes to the primary cilium in mammalian cells.....53

Figure 3.2 - Localization of Crescerin1 truncation constructs to cilia, nucleus, or cytoplasm.....54

Figure 3.3 - Crescerin1 C-terminal TOG domains have MT lattice-binding activity.....58

Figure 4.1 - Diagram of amphid and phasmid sensillae.....69

Figure 4.2 - Map of *che-12* locus in *che-12* EMS mutant strains and CRISPR strains.....70

Figure 4.3 - In *C. elegans*, the endogenously tagged CHE-12 localizes to cilia in amphid and phasmid neurons.....79

Figure 4.4 - Deleting *che-12* or mutating tubulin-binding residues in CHE-12 TOG domains affects amphid cilia function.....82

Figure 4.5 - Deleting *che-12* or mutating tubulin-binding residues in CHE-12 TOG domains results in shorter and disorganized cilia in *C. elegans* amphid neurons.....85

LIST OF ABBREVIATIONS AND SYMBOLS

Å	Ångstrom
ATP	adenosine triphosphate
BBS	Bardet-Biedl syndrome
β-ME	β-mercaptoethanol
CD	circular dichroism
CLS	cilia localization signal
CMV	cytomegalovirus
CPC	cilia pore complex
CRISPR	clustered regularly-interspaced short palindromic repeats
DAPI	4',6-diamidino-2-phenylindole
DiI	1,1’-dioctadecyl-3,3,3’3’-tetramethylindocarbocyanine perchlorate
DiO	3,3’-dioctadecyloxacarbocyanine perchlorate
DMEM	Dulbecco’s modified eagle medium
DTT	dithiothriotol
EGTA	ethylene glycol tetraacetic acid
FBS	fetal bovine serum
FITC	Fluorescein isothiocyanate
FL	full-length
FRAP	fluorescence recovery after photobleaching
GFP	green fluorescent protein
GDP	guanosine diphosphate
GTP	guanosine triphosphate

HEAT	Huntingtin, elongation factor 3 (EF3), protein phosphatase 2A (PP2A), and the yeast kinase TOR1
HEK-293	Human embryonic kidney cells
HEPES	4-(2-hydroxyethyl)-1-piperazineethanesulfonic acid
HR	HEAT repeat
IFT	intra-flagellar transport
IMCD3	mouse inner medullary collecting duct cells
IPTG	isopropyl β-D-1-thiogalactopyranoside
JBTS	Joubert's syndrome
kDa	kiloDalton
M	molar
MAP	microtubule associated protein
mg	milligram
µg	microgram
MES	2-(N-morpholino)ethanesulfonic acid
min	minute
MKS	Meckel-Gruber syndrome
mL	milliliter
µl	microliter
µm	micrometer
ML	maximum likelihood
MLHL	maximum likelihood target based on amplitudes plus prior phase information encoded by Hendrickson-Lattman coefficients
mM	millimolar

μM	micromolar
MT	microtubule
NES	nuclear export signal
NLS	nuclear localization signal
nm	nanometer
NPC	nuclear pore complex
NPHP	Nephronophthisis
NTA	Nitrilotriacetic acid
NUP	nucleoporin
PBS	phosphate-buffered saline
Pctn	Pericentrin
PDB	Protein Data Bank (pdb.org)
PDGF	platelet derived growth factor
PEG	polyethylene glycol
PIPES	piperazine-N,N′-bis(2-ethanesulfonic acid)
PKD	polycystic kidney disease
PMSF	Phenylmethylsulfonyl fluoride
PTM	post-translational modification
RFP	red fluorescent protein
RMSD	root-mean-square deviation
SDS	sodium dodecyl sulfate
SeMet	selenomethionine
TIRF	total internal reflection fluorescence

TOG	tumor overexpressed gene
UTR	un-translated region
WT	wild type

CHAPTER 1: INTRODUCTION

1.1. Cilia: Types and functions

Eukaryotic cilia and flagella are specialized organelles projecting from the surface of cells. The beating of flagella and motile cilia drive the motility of free-swimming unicellular eukaryotes such as *Chlamydomonas reinhardtii*, *Tetrahymena*, *Paramecium* and sperm cells from a wide variety of species including humans, and direct extracellular fluid flow in adherent cells lining the trachea and oviduct in mammals (Satir and Christensen, 2008; Shah, 2009; Takeda and Narita, 2012; Kobayashi and Takeda, 2012). Additionally, most mammalian cell types contain a single non-motile cilium, whose importance has only recently come to light after decades of being considered to be a vestigial structure. This solitary antenna-like extension, known as the primary cilium, is an important sensory organelle that receives extracellular chemical and mechanical stimuli, and transduces signals to the cell body to elicit a response (Marshall and Nonaka, 2006; Satir and Christensen, 2007; Christensen et al., 2008; Veland et al., 2009; Hoey et al., 2012). Signaling pathways like Hedgehog, PDGFα, etc. that are important in development, morphogenesis and maintaining homeostasis, operate through the primary cilium. Mutations affecting cilia structure can negatively impact proper localization and translocation of these signaling components into and out of the primary cilium. Due to the widespread occurrence of primary cilia across many cell types, genetic anomalies disrupting cilia mediated signaling can have far reaching consequences resulting in a multitude of symptoms including cystic kidneys, retinal

degeneration, central nervous system malformation, skeletal abnormalities, polydactyly and *Situs inversus*, collectively termed ciliopathies (Marshall, 2008).

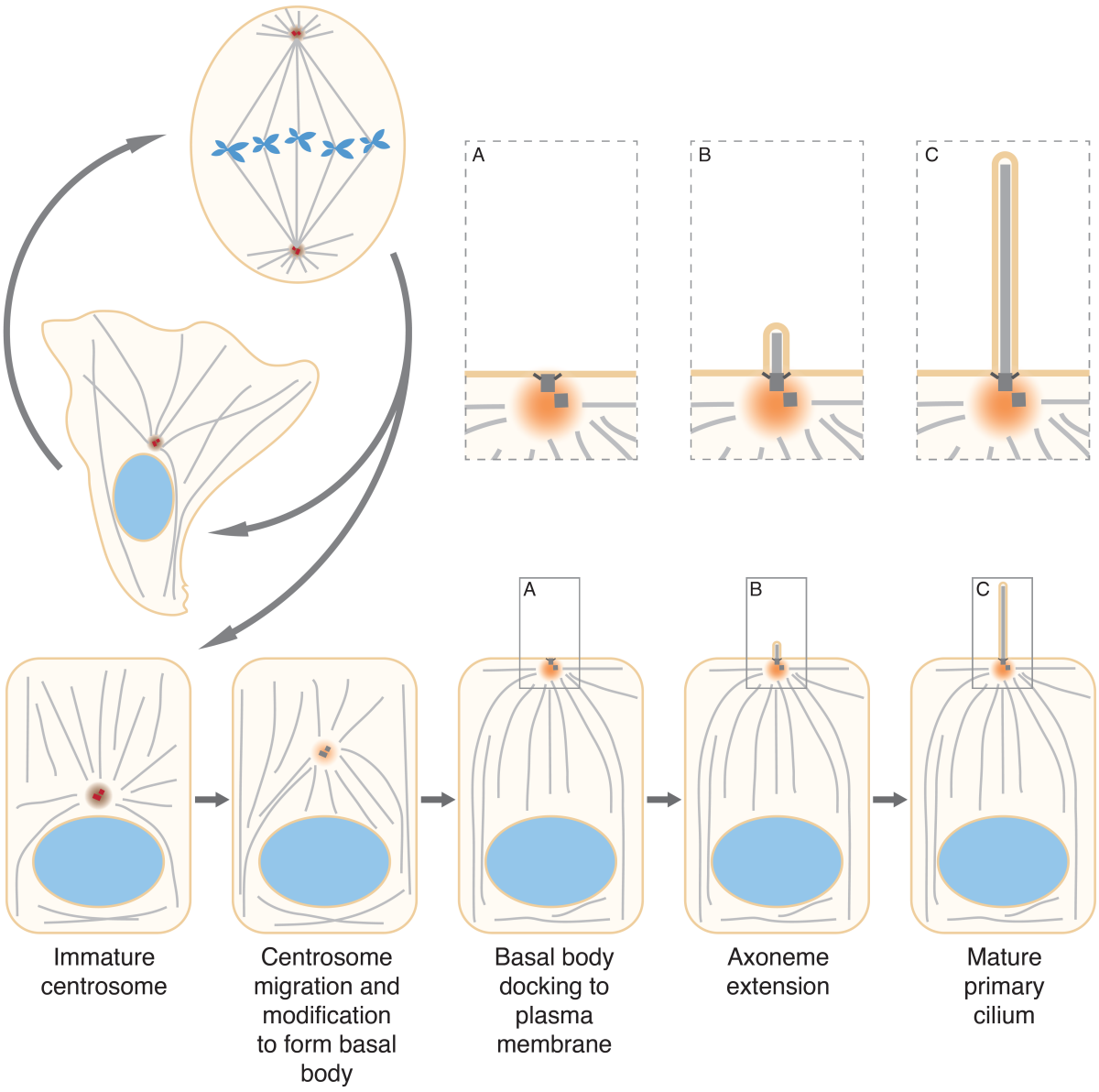

Figure 1.1. Schematic diagram outlining the major steps during ciliogenesis.
Ciliogenesis starts after the cell exits the mitotic cycle and enters the G_0 phase. The centrosome gets modified to form the basal body and migrates to the cell surface. At the cell surface the basal body docks on to the plasma membrane. The axoneme then nucleates from the basal body and elongates to form the mature primary cilium.

1.2. Ciliogenesis

Ciliogenesis occurs when the cell exits the mitotic cycle and enters the G_0 phase. In many mammalian tissues this occurs in terminally differentiated cells. The process of ciliogenesis begins with the modification of the centriole to form a basal body. The basal body migrates to the cell surface, docks to the plasma membrane and nucleates the growth of the axoneme. The growing axoneme pushes the cell membrane outward thereby elongating the cilia (Figure 1.1) (Sorokin, 1968; Avasthi and Marshall, 2012). Ciliated cells can often be made to re-enter cell cycle, under the influence of mitogenic signals. In such conditions, the primary cilium gets resorbed; the basal body undocks from the plasma membrane and undergoes maturation to form centrosomes that then nucleate the bipolar mitotic spindle.

1.3. Ultrastructure of cilia

The axoneme, composed of parallel microtubules (MT) arranged in 9-fold radial symmetry is the structural core of cilia and flagella (Figure 1.2A). The axoneme arises from the basal body, a modified centriole docked at the plasma membrane, which templates the nine-fold radial MT symmetry and anchors the MT minus ends. The MT doublets, composed of fused A and B tubules, span the length of the cilia middle zone. At the middle/distal zone transition, B tubules terminate and singlet A tubules extend into the distal zone. The axonemal MTs provide structural support, serve as tracks along which anterograde and retrograde intra-flagellar transport (IFT) complexes traffic ciliary components, and in motile cilia serve as the substrate for axonemal dynein motors that drive motility (Scholey, 2003, 2008; Ishikawa et al., 2012; Kobayashi and Takeda, 2012). Axonemal MTs are more complex in structure and composition compared to cytoplasmic MTs, which are dynamic

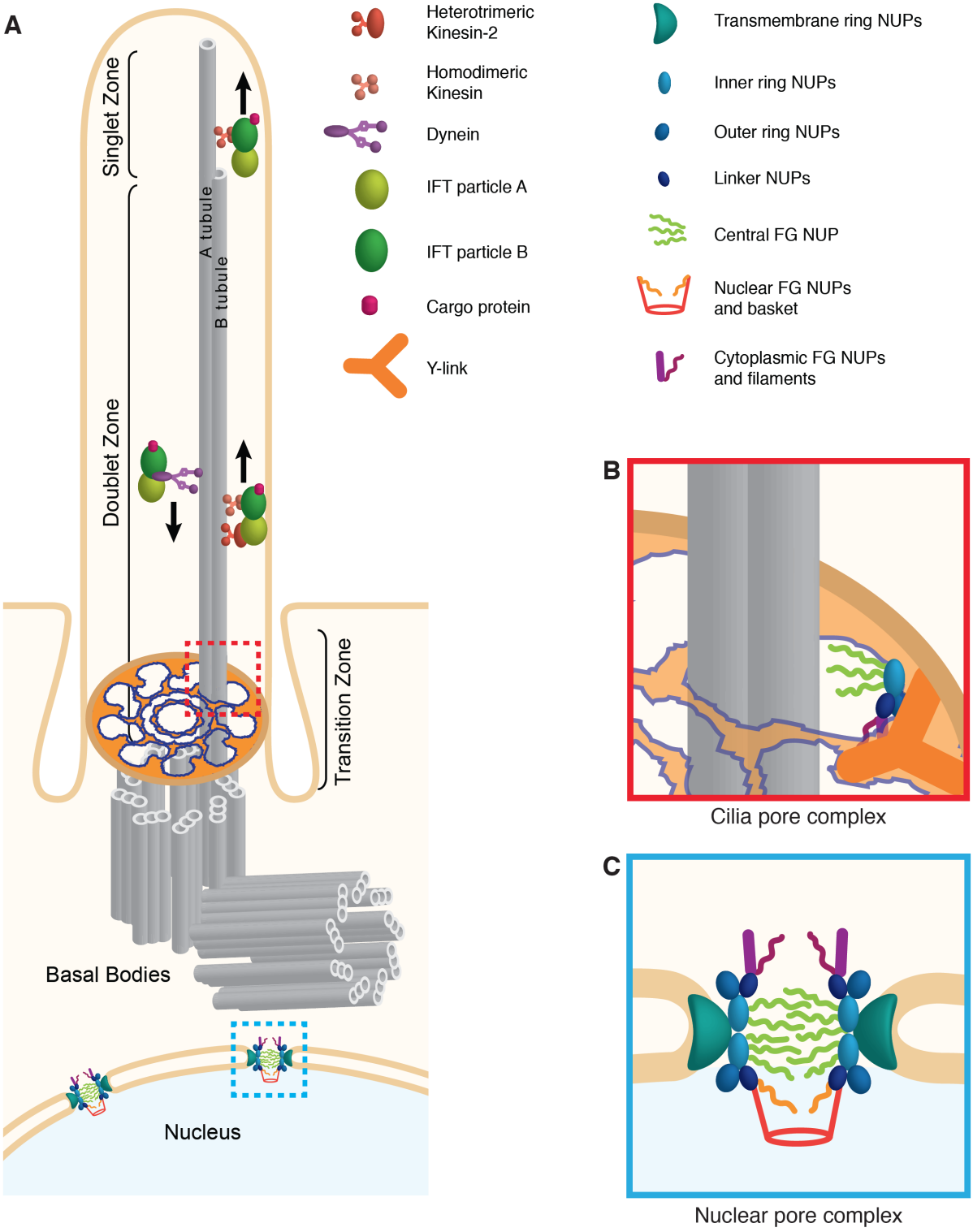

Figure 1.2. Schematic representation of the ultrastructure of cilia.
(A) Diagram of a cilium showing basal body and axonemal microtubules (grey), IFT particles and associated molecular motors, cilia pore complex and nuclear pore complex. (B) Expanded view of the cilia pore complex (area bound by the red square in A) showing the probable arrangement of nuclear pore complex proteins and Y-link proteins. (C) Expanded view of the nuclear pore complex (area bound by the blue square in A).

tubular polymers of αβ-tubulin heterodimers. For example, specific tubulin isotypes are enriched in axonemal MTs. In mammals, the β-tubulin isotype β_I is found in both ciliary and non-ciliary MTs, whereas the isotype β_{IV} is typically only found in the cilia (Renthal et al., 1993; Roach et al., 1998; Jensen-Smith et al., 2003). Multiple cilia-specific α and β-tubulin isotypes namely, TBA-6, TBA-9 and TBB-4 have been identified in the invertebrate species, *Caenorhabditis elegans*, which contains simple cilia at the dendritic termini of several sensory neurons (Hurd et al., 2010; Hao et al., 2011b). The axonemal MTs accumulate extensive post-translational modifications (PTM) such as acetylation of K40 in the MT lumen, detyrosination of the C-terminal tail, and addition of polyglutamyl and polyglycyl chains of variable length to the side chains of multiple glutamic acid residues in the C-terminal tails of α and β-tubulin. The extent and pattern of some of these PTMs on the axoneme are species and cell-type specific, and often regulate ciliary beating of motile cilia (Gaertig and Wloga, 2008). PTMs are also seen in cytoplasmic MTs but typically at much lower densities compared to axonemal MTs. Antibodies that recognize tubulin PTMs are therefore widely used to label cilia and flagella.

The IFT system is a kinesin and dynein driven bidirectional transport system along the axoneme (Figure 1.2A). IFT particles A and B are two large multimeric protein complexes that bind to a variety of cargo proteins. The two particles are connected to each other through another complex known as the BBSome (Taschner et al., 2012). The BBSome acts as a linker between IFT and membrane associated proteins such as signal receptors, and as such, mutations in the BBSome proteins causes the ciliopathy known as the Bardet-Biedl syndrome (Bisgrove and Yost, 2006; Nachury et al., 2007; Waters and Beales, 2011). A heterotrimeric kinesin (composed of KIF3A, KIF3B and KAP) binds to IFT-particle A and a

homodimeric kinesin (KIF17) binds to IFT-particle B. The concerted walk of these two kinesin motors along the axonemal B-tubules transports the IFT particles in the anterograde direction (cilia base to cilia tip) (Prevo et al., 2015). In *C. elegans* sensory cilia, these two motors function redundantly to build the doublet region of the axoneme (Snow et al., 2004; Evans et al., 2006), while the KIF17 homolog OSM-3 is responsible for building the distal singlet MTs (Perkins et al., 1986; Snow et al., 2004; Evans et al., 2006). Dynein motors transport the complexes back from the tip to the base in the retrograde direction (Hao et al., 2011a). The IFT system is highly conserved across all ciliated and flagellated eukaryotes and is crucial for cilia growth, maintenance and turnover of ciliary proteins (Marshall and Rosenbaum, 2001; Scholey, 2003; Snow et al., 2004; Ou et al., 2005; Pan et al., 2006; Pedersen and Rosenbaum, 2008; Hao et al., 2011b; Ishikawa and Marshall, 2011; Taschner et al., 2012).

The assembly of tubulin subunits to the axoneme leading to cilia growth occurs only at the distal end of the cilium. Hence, tubulin and other accessory factors required to regulate ciliogenesis need to be able to enter into the ciliary compartment from the cytosol and travel to the distal tip. The ciliary compartment is separated from the cytosol by a selectively permeable barrier at the base of the cilia (Nachury et al., 2010; Chih et al., 2011; Kee et al., 2012; Reiter et al., 2012; Kee and Verhey, 2013; Ounjai et al., 2013; Takao et al., 2014). Electron cryotomographic analysis of isolated basal bodies from *Tetrahymena* showed the presence of plate like structures, which could be a part of the cilia partitioning system (Ounjai et al., 2013) (Figure 1.2A). Although the exact molecular structure and composition of the cilia partitioning system is still unknown, Kristen Verhey's lab at the University of Michigan, showed the presence of nuclear pore complex proteins at the cilia base, thereby

raising the speculation that a structure analogous to that of the nuclear pore complex exists at the base of the cilia that regulates the trafficking of proteins into and out of the ciliary compartment (Kee et al., 2012) (Figure 1.2B-C). The Verhey lab further showed that proteins involved in the nuclear import pathway, including Importin-β2 and Ran-GTP, are necessary for trafficking some ciliary proteins across the "cilia pore complex" (Fan and Margolis, 2011; Kee et al., 2012; Obado and Rout, 2012). Inside the ciliary compartment, many ciliary proteins are further transported along the axoneme by the IFT system.

Different regions along the ciliary axoneme vary in the degrees of MT dynamics. Doublet MTs in the middle zone are highly stable and are even resistant to MT depolymerizing agents including colchicine (Tilney and Gibbins, 1968). In contrast, singlet MTs in the distal segment are dynamic and change their length in response to external stimuli (Marshall and Rosenbaum, 2001; Mukhopadhyay et al., 2008; Rich and Clark, 2012). The plus ends of both the A and B tubules exhibit rapid tubulin turnover (Hao et al., 2011b) and this localized dynamicity is necessary to maintain proper axoneme structure. However, the identities and mechanisms of MT associated proteins (MAPs) involved in regulating ciliary MT organization and dynamics are not well understood. This contrasts with our current knowledge and understanding of the regulators of cytoplasmic microtubules, of which two key regulators: ch-TOG and CLASP, have been extensively investigated in the Slep lab.

1.4. ch-TOG and CLASP families of MAPs regulate MT dynamics in cells

While MT polymerization-dependent GTP hydrolysis confers the αβ-tubulin polymer with inherent dynamics (Figure 1.3A), a host of cytoplasmic MAPs regulate MT dynamics in space and time to facilitate dynamic cellular changes as required during mitosis, polarized

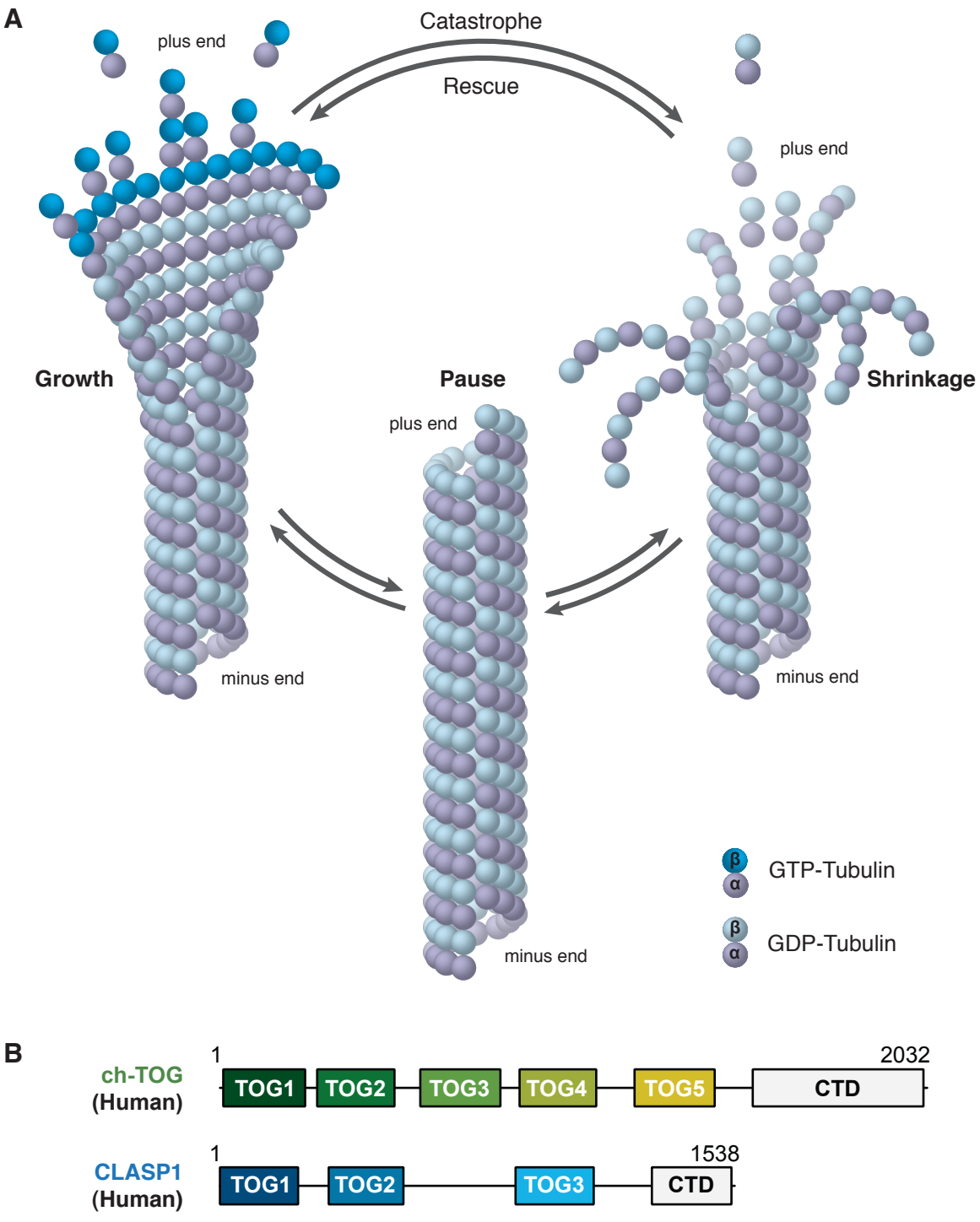

Figure 1.3. Arrayed TOG domain containing protein families, ch-TOG and CLASP regulate microtubule dynamics.

(A) Diagram showing dynamic instability of microtubules. Microtubules switch between growth, shrinkage and pause states. Arrayed TOG domain containing proteins, ch-TOG and CLASP regulate microtubule dynamics, with ch-TOG promoting the polymerization state and CLASP promoting the pause state. (B) Diagram showing domain architecture of ch-TOG and CLASP. ch-TOG has an array of five TOG domains followed by a C-terminal domain. CLASP has an array of three TOG domains followed by a C-terminal domain.

cell migration, and ciliogenesis. ch-TOG and CLASP represent two distinct MAP families that promote MT polymerization and pause respectively (Akhmanova et al., 2001; Brittle and Ohkura, 2005; Drabek et al., 2006; Sousa et al., 2007; Widlund et al., 2011). Both ch-TOG and CLASP use arrayed tubulin-binding TOG domains to regulate MT dynamics (Al-Bassam et al., 2007; Slep, 2009; Al-Bassam and Chang, 2011). The number of TOG domains in each array differs, as does the architecture and tubulin-binding activity of each TOG domain. Higher eukaryotic ch-TOG family members use a pentameric TOG domain array to promote MT polymerization (Widlund et al., 2011) while CLASP members use a trimeric TOG domain array to stabilize MTs and promote MT pause (Al-Bassam et al., 2010; Patel et al., 2012) (Figure 1.3B). A TOG domain consists of six pairs of antiparallel α-helices, termed HEAT repeats (HRs), which form an oblong solenoid-like structure. TOG domains bind tubulin using a series of intra-HEAT loops that are discontinuous in the primary sequence but line one face of the domain in the tertiary structure. The helices and inter-HEAT loops that buttress the tubulin-binding determinants have diverged in sequence, both within a given TOG array, and across the ch-TOG and CLASP families, making it challenging to identify TOG domain-containing proteins using BLAST searches. Using structure-based methodology, the Slep lab previously predicted and confirmed the existence of a cryptic TOG domain (TOG2) in CLASP (Slep and Vale, 2007; Leano et al., 2013), establishing a TOG array-based paradigm for ch-TOG and CLASP family MT regulatory activity.

We asked whether we could identify another TOG domain-containing protein family in eukaryotes based on our knowledge of TOG structural features and tubulin-binding determinants and if so, ascertain whether this protein family plays a role in regulating MTs in cilia. In 2005, Hepner *et al.* identified a hypothetical protein, KIAA0423 by 2D-gel

electrophoresis followed by mass spectroscopy, in tissue samples of human fetal perireticular nucleus, a key structure in human brain development (Hepner et al., 2005). Based on primary sequence analysis they predicted that KIAA0423 contained HEAT repeats. In 2008, the ortholog of KIAA0423 in *C. elegans*, CHE-12 was shown to play a role in the development of specific types of cilia in *C. elegans* sensory neurons (Bacaj et al., 2008). In this study, we describe how we structurally and functionally characterized this protein to establish its identity as TOG domain array-containing protein that regulates cilia structure. We have renamed this protein family Crescerin (Latin "*crescere*"=grow), for its role in cilia growth.

REFERENCES

Akhmanova, A., C.C. Hoogenraad, K. Drabek, T. Stepanova, B. Dortland, T. Verkerk, W. Vermeulen, B.M. Burgering, C.I. De Zeeuw, F. Grosveld, and N. Galjart. 2001. CLASPs are CLIP-115 and -170 associating proteins involved in the regional regulation of microtubule dynamics in motile fibroblasts. *Cell*. 104:923–935. doi:10.1016/S0092-8674(01)00288-4.

Al-Bassam, J., and F. Chang. 2011. Regulation of microtubule dynamics by TOG-domain proteins XMAP215/Dis1 and CLASP. *Trends Cell Biol.* 21:604–614. doi:10.1016/j.tcb.2011.06.007.

Al-Bassam, J., H. Kim, G. Brouhard, A. van Oijen, S.C. Harrison, and F. Chang. 2010. CLASP promotes microtubule rescue by recruiting tubulin dimers to the microtubule. *Dev. Cell*. 19:245–258. doi:10.1016/j.devcel.2010.07.016.

Al-Bassam, J., N.A. Larsen, A.A. Hyman, and S.C. Harrison. 2007. Crystal structure of a TOG domain: Conserved features of XMAP215/Dis1-family TOG domains and implications for tubulin binding. *Structure*. 15:355–362. doi:10.1016/j.str.2007.01.012.

Avasthi, P., and W.F. Marshall. 2012. Stages of ciliogenesis and regulation of ciliary length. *Differentiation*. 83:S30–42. doi:10.1016/j.diff.2011.11.015.

Bacaj, T., Y. Lu, and S. Shaham. 2008. The conserved proteins CHE-12 and DYF-11 are required for sensory cilium function in *Caenorhabditis elegans*. *Genetics*. 178:989–1002. doi:10.1534/genetics.107.082453.

Bisgrove, B.W., and H.J. Yost. 2006. The roles of cilia in developmental disorders and disease. *Development*. 133:4131–4143. doi:10.1242/dev.02595.

Brittle, A.L., and H. Ohkura. 2005. Mini spindles, the XMAP215 homologue, suppresses pausing of interphase microtubules in *Drosophila*. *EMBO J.* 24:1387–1396. doi:10.1038/sj.emboj.7600629.

Chih, B., P. Liu, Y. Chinn, C. Chalouni, L.G. Komuves, P.E. Hass, W. Sandoval, and A.S. Peterson. 2011. A ciliopathy complex at the transition zone protects the cilia as a privileged membrane domain. *Nat. Cell Biol.* 14:61–72. doi:10.1038/ncb2410.

Christensen, S.T., S.F. Pedersen, P. Satir, I.R. Veland, and L. Schneider. 2008. The primary cilium coordinates signaling pathways in cell cycle control and migration during development and tissue repair. *In* Current Topics in Developmental Biology. 261–301.

Drabek, K., M. van Ham, T. Stepanova, K. Draegestein, R. van Horssen, C.L. Sayas, A. Akhmanova, T. ten Hagen, R. Smits, R. Fodde, F. Grosveld, and N. Galjart. 2006. Role of CLASP2 in microtubule stabilization and the regulation of persistent motility. *Curr. Biol.* 16:2259–2264. doi:10.1016/j.cub.2006.09.065.

Evans, J.E., J.J. Snow, A.L. Gunnarson, G. Ou, H. Stahlberg, K.L. McDonald, and J.M. Scholey. 2006. Functional modulation of IFT kinesins extends the sensory repertoire of ciliated neurons in *Caenorhabditis elegans*. *J. Cell Biol.* 172:663–669. doi:10.1083/jcb.200509115.

Fan, S., and B. Margolis. 2011. The Ran importin system in cilia trafficking. *Organogenesis*. 7:147–153. doi:10.4161/org.7.3.17084.

Gaertig, J., and D. Wloga. 2008. Ciliary tubulin and its post-translational modifications. *In* Current Topics in Developmental Biology. Elesvier Inc. 83–113.

Hao, L., E. Efimenko, P. Swoboda, and J.M. Scholey. 2011a. The retrograde IFT machinery of *C. elegans* cilia: two IFT dynein complexes? *PLoS One*. 6:e20995. doi:10.1371/journal.pone.0020995.

Hao, L., M. Thein, I. Brust-Mascher, G. Civelekoglu-Scholey, Y. Lu, S. Acar, B. Prevo, S. Shaham, and J.M. Scholey. 2011b. Intraflagellar transport delivers tubulin isotypes to sensory cilium middle and distal segments. *Nat. Cell Biol.* 13:790–798. doi:10.1038/ncb2268.

Hepner, F., J.-K. Myung, N. Ulfig, A. Pollak, and G. Lubec. 2005. Detection of hypothetical proteins in human fetal perireticular nucleus. *J. Proteome Res.* 4:2379–2385. doi:10.1021/pr050133p.

Hoey, D.A., M.E. Downs, and C.R. Jacobs. 2012. The mechanics of the primary cilium: An intricate structure with complex function. *J. Biomech.* 45:17–26. doi:10.1016/j.jbiomech.2011.08.008.

Hurd, D.D., R.M. Miller, L. Nunez, and D.S. Portman. 2010. Specific α- and β-tubulin isotypes optimize the functions of sensory cilia in *Caenorhabditis elegans*. *Genetics*. 185:883–896. doi:10.1534/genetics.110.116996.

Ishikawa, H., and W.F. Marshall. 2011. Ciliogenesis: building the cell's antenna. *Nat. Rev. Mol. Cell Biol.* 12:222–234. doi:10.1038/nrm3085.

Ishikawa, H., J. Thompson, J.R. Yates, and W.F. Marshall. 2012. Proteomic analysis of mammalian primary cilia. *Curr. Biol.* 22:414–419. doi:10.1016/j.cub.2012.01.031.

Jensen-Smith, H.C., R.F. Luduena, and R. Hallworth. 2003. Requirement for the βI and βIV tubulin isotypes in mammalian cilia. *Cell Motil. Cytoskeleton*. 55:213–220. doi:10.1002/cm.10122.

Kee, H.L., J.F. Dishinger, T.L. Blasius, C.-J. Liu, B. Margolis, and K.J. Verhey. 2012. A size-exclusion permeability barrier and nucleoporins characterize a ciliary pore complex that regulates transport into cilia. *Nat. Cell Biol.* 14:431–437. doi:10.1038/ncb2450.

Kee, H.L., and K.J. Verhey. 2013. Molecular connections between nuclear and ciliary import processes. *Cilia*. 2:11. doi:10.1186/2046-2530-2-11.

Kobayashi, D., and H. Takeda. 2012. Ciliary motility: The components and cytoplasmic preassembly mechanisms of the axonemal dyneins. *Differentiation*. 83:S23–29. doi:10.1016/j.diff.2011.11.009.

Leano, J.B., S.L. Rogers, and K.C. Slep. 2013. A cryptic TOG domain with a distinct architecture underlies CLASP-dependent bipolar spindle formation. *Structure*. 21:939–950. doi:10.1016/j.str.2013.04.018.

Marshall, W.F., and S. Nonaka. 2006. Cilia: Tuning in to the Cell's Antenna. *Curr. Biol.* 16:R604–614. doi:10.1016/j.cub.2006.07.012.

Marshall, W.F., and J.L. Rosenbaum. 2001. Intraflagellar transport balances continuous turnover of outer doublet microtubules: implications for flagellar length control. *J. Cell Biol.* 155:405–414. doi:10.1083/jcb.200106141.

Mukhopadhyay, S., Y. Lu, S. Shaham, and P. Sengupta. 2008. Sensory signaling-dependent remodeling of olfactory cilia architecture in *C. elegans*. *Dev. Cell*. 14:762–774. doi:10.1016/j.devcel.2008.03.002.

Nachury, M. V., A. V. Loktev, Q. Zhang, C.J. Westlake, J. Peranen, A. Merdes, D.C. Slusarski, R.H. Scheller, J.F. Bazan, V.C. Sheffield, and P.K. Jackson. 2007. A core complex of BBS proteins cooperates with the GTPase Rab8 to promote ciliary membrane biogenesis. *Cell*. 129:1201–1213. doi:10.1016/j.cell.2007.03.053.

Nachury, M. V., E.S. Seeley, and H. Jin. 2010. Trafficking to the ciliary membrane: How to get across the periciliary diffusion barrier? *Annu. Rev. Cell Dev. Biol.* 26:59–87. doi:10.1146/annurev.cellbio.042308.113337.

Obado, S.O., and M.P. Rout. 2012. Ciliary and nuclear transport: Different places, similar routes? *Dev. Cell*. 22:693–694. doi:10.1016/j.devcel.2012.04.002.

Ou, G., O.E. Blacque, J.J. Snow, M.R. Leroux, and J.M. Scholey. 2005. Functional coordination of intraflagellar transport motors. *Nature*. 436:583–587. doi:10.1038/nature03818.

Ounjai, P., K.D. Kim, H. Liu, M. Dong, A.N. Tauscher, H.E. Witkowska, and K.H. Downing. 2013. Architectural insights into a ciliary partition. *Curr. Biol.* 23:339–344. doi:10.1016/j.cub.2013.01.029.

Pan, X., G. Ou, G. Civelekoglu-Scholey, O.E. Blacque, N.F. Endres, L. Tao, A. Mogilner, M.R. Leroux, R.D. Vale, and J.M. Scholey. 2006. Mechanism of transport of IFT particles in *C. elegans* cilia by the concerted action of kinesin-II and OSM-3 motors. *J. Cell Biol.* 174:1035–1045. doi:10.1083/jcb.200606003.

Patel, K., E. Nogales, and R. Heald. 2012. Multiple domains of human CLASP contribute to microtubule dynamics and organization in vitro and in *Xenopus* egg extracts. *Cytoskeleton*. 69:155–165. doi:10.1002/cm.21005.

Pedersen, L.B., and J.L. Rosenbaum. 2008. Intraflagellar transport (IFT): Role in ciliary assembly, resorption and signalling. *In* Current Topics in Developmental Biology. Elesvier Inc. 23–61.

Perkins, L.A., E.M. Hedgecock, J.N. Thomson, and J.G. Culotti. 1986. Mutant sensory cilia in the nematode *Caenorhabditis elegans*. *Dev. Biol.* 117:456–487. doi:10.1016/0012-1606(86)90314-3.

Prevo, B., P. Mangeol, F. Oswald, J.M. Scholey, and E.J.G. Peterman. 2015. Functional differentiation of cooperating kinesin-2 motors orchestrates cargo import and transport in *C. elegans* cilia. *Nat. Cell Biol.* 17:1536–1545. doi:10.1038/ncb3263.

Reiter, J.F., O.E. Blacque, and M.R. Leroux. 2012. The base of the cilium: roles for transition fibres and the transition zone in ciliary formation, maintenance and compartmentalization. *EMBO Rep.* 13:608–618. doi:10.1038/embor.2012.73.

Renthal, R., B.G. Schneider, M.M. Miller, and R.F. Ludueña. 1993. Beta IV is the major beta-tubulin isotype in bovine cilia. *Cell Motil. Cytoskeleton*. 25:19–29. doi:10.1002/cm.970250104.

Rich, D.R., and A.L. Clark. 2012. Chondrocyte primary cilia shorten in response to osmotic challenge and are sites for endocytosis. *Osteoarthr. Cartil.* 20:923–930. doi:10.1016/j.joca.2012.04.017.

Roach, M.C., V.L. Boucher, C. Walss, P.M. Ravdin, and R.F. Luduena. 1998. Preparation of a monoclonal antibody specific for the class I isotype of β-tubulin: The β isotypes of tubulin differ in their cellular distributions within human tissues. *Cell Motil. Cytoskeleton*. 39:273–285. doi:10.1002/(SICI)1097-0169(1998)39:4<273::AID-CM3>3.0.CO;2-4.

Satir, P., and S.T. Christensen. 2007. Overview of structure and function of mammalian cilia. *Annu. Rev. Physiol.* 69:377–400. doi:10.1146/annurev.physiol.69.040705.141236.

Satir, P., and S.T. Christensen. 2008. Structure and function of mammalian cilia. *Histochem. Cell Biol.* 129:687–693. doi:10.1007/s00418-008-0416-9.

Scholey, J.M. 2003. Intraflagellar transport. *Annu. Rev. Cell Dev. Biol.* 19:423–443. doi:10.1146/annurev.cellbio.19.111401.091318.

Scholey, J.M. 2008. Intraflagellar transport motors in cilia: Moving along the cell's antenna. *J. Cell Biol.* 180:23–29. doi:10.1083/jcb.200709133.

Shah, A.S. 2009. Motile cilia of human airway are chemosensory. *Science*. 325:1131–1134. doi:10.1126/science.1173869.

Slep, K.C. 2009. The role of TOG domains in microtubule plus end dynamics. *Biochem. Soc. Trans.* 37:1002–1006. doi:10.1042/BST0371002.

Slep, K.C., and R.D. Vale. 2007. Structural basis of microtubule plus end tracking by XMAP215, CLIP-170, and EB1. *Mol. Cell*. 27:976–991. doi:10.1016/j.molcel.2007.07.023.

Snow, J.J., G. Ou, A.L. Gunnarson, M.R.S. Walker, H.M. Zhou, I. Brust-Mascher, and J.M. Scholey. 2004. Two anterograde intraflagellar transport motors cooperate to build sensory cilia on *C. elegans* neurons. *Nat. Cell Biol.* 6:1109–1113. doi:10.1038/ncb1186.

Sorokin, S. 1968. Reconstructions of centriole formation and ciliogenesis in mammalian lungs. *J. Cell Sci.* 3:207–230.

Sousa, A., R. Reis, P. Sampaio, and C.E. Sunkel. 2007. The *Drosophila* CLASP homologue, Mast/Orbit regulates the dynamic behaviour of interphase microtubules by promoting the pause state. *Cell Motil. Cytoskeleton*. 64:605–620. doi:10.1002/cm.20208.

Takao, D., J.F. Dishinger, H.L. Kee, J.M. Pinskey, B.L. Allen, and K.J. Verhey. 2014. An assay for clogging the ciliary pore complex distinguishes mechanisms of cytosolic and membrane protein entry. *Curr. Biol.* 24:2288–2294. doi:10.1016/j.cub.2014.08.012.

Takeda, S., and K. Narita. 2012. Structure and function of vertebrate cilia, towards a new taxonomy. *Differentiation*. 83:S4–11. doi:10.1016/j.diff.2011.11.002.

Taschner, M., S. Bhogaraju, and E. Lorentzen. 2012. Architecture and function of IFT complex proteins in ciliogenesis. *Differentiation*. 83:S12–22. doi:10.1016/j.diff.2011.11.001.

Tilney, L.G., and J.R. Gibbins. 1968. Differential effects of antimitotic agents on the stability and behavior of cytoplasmic and ciliary microtubules. *Protoplasma*. 65:167–179. doi:10.1007/BF01666377.

Veland, I.R., A. Awan, L.B. Pedersen, B.K. Yoder, and S.T. Christensen. 2009. Primary cilia and signaling pathways in mammalian development, health and disease. *Nephron - Physiol.* 111:p39–53. doi:10.1159/000208212.

Waters, A.M., and P.L. Beales. 2011. Ciliopathies: An expanding disease spectrum. *Pediatr. Nephrol.* 26:1039–1056. doi:10.1007/s00467-010-1731-7.

Widlund, P.O., J.H. Stear, A. Pozniakovsky, M. Zanic, S. Reber, G.J. Brouhard, A.A. Hyman, and J. Howard. 2011. XMAP215 polymerase activity is built by combining multiple tubulin-binding TOG domains and a basic lattice-binding region. *Proc. Natl. Acad. Sci. U. S. A.* 108:2741–2746. doi:10.1073/pnas.1016498108.

CHAPTER 2: CRESCERIN DEFINES A CONSERVED PROTEIN FAMILY WITH A TOG DOMAIN ARRAY[1]

2.1. Summary

The role of arrayed TOG domain-containing cytoplasmic MT regulators, ch-TOG and CLASP, have been extensively investigated at interphase and during cell division. However, very limited information is available so far about the factors associated with the regulation of axonemal MT dynamics. Novel TOG domain containing proteins are difficult to identify due to low overall sequence identity between domains. Using our knowledge of previously solved TOG domain structures and the positions of conserved tubulin-binding residues that are discontinuous in primary sequence we predicted that the Crescerin protein family contains an array of TOG domains. In this chapter we present the steps that led to the identification of Crescerin as a novel TOG domain containing protein, through sequence analysis, structure determination by X-ray crystallography and MT-polymerization rate altering activity *in vitro*.

2.2. Introduction

The TOG domain containing protein family ch-TOG was first identified as a 215 kDa, MT assembly promoting factor in *Xenopus* egg extracts in 1987 (Gard and Kirschner,

[1]Parts of this chapter previously appeared as an article in the journal Molecular Biology of the Cell. The original citation is as follows: Das, A., D.J. Dickinson, C.C. Wood, B. Goldstein, and K.C. Slep. 2015. Crescerin uses a TOG domain array to regulate microtubules in the primary cilium. *Mol. Biol. Cell*. 26:4248–4264. doi:10.1091/mbc.E15-08-0603.

1987). In 1998, a homolog of this protein was found to be over-expressed in human colonic and hepatic tumors and consequently named the colonic, hepatic tumor over-expressed gene (ch-TOG) (Charrasse et al., 1998). In 2001, the domain architecture of XMAP215/ch-TOG was predicted to consist of an array of five domains, each containing multiple HEAT repeats (helix-loop-helix motifs found in Huntingtin, Elongation factor-3, PP2A and Tor-kinase) (Cassimeris et al., 2001; Popov et al., 2001). These domains were named TOG domains after ch-TOG, where they were first identified. Although the amino acid sequences of the five TOG domains within an array differ greatly, the sequence of each TOG domain in the array remains highly conserved across species. This leads to the speculation that each TOG domain has unique roles based on its position in the array. The XMAP215/ ch-TOG family proteins in human (ch-TOG), *Xenopus* (XMAP215) and *Drosophila* (Minispindles) each contain an array of five TOG domains, while its orthologs in *C. elegans* (ZYG-9) and *S. cerevisiae* (Stu2) contain three and two TOG domains, respectively (Appendix 2.1). Around the same time, another type of MT associated protein, CLASP/Mast/Orbit was predicted to contain TOG domain-like sequences at its N-terminus and additional conserved regions of unknown structural identity along its length (Lemos et al., 2000).

The first crystal structures of ch-TOG family TOG domains, published in 2007 show six HEAT repeats stacked against one another to form a paddle-shaped solenoid, with their intra-HEAT loops lining one face of the domain (Slep and Vale, 2007; Al-Bassam et al., 2007) (Figure 2.1A). Since then, the structures of several other TOG domains from ch-TOG and CLASP families have been solved to reveal similar domain fold but have different degrees of curvature (De la Mora-Rey et al., 2013; Leano et al., 2013; Fox et al., 2014; Maki et al., 2015; Howard et al., 2015) (Appendices 2.1 and 2.2). Presently, it is not completely

clear how these different curvatures contribute to their function in cells. Some recent studies suggest that the degree of curvature of TOG domains predisposes it to bind preferentially to microtubule protofilaments of different curvature, thus favoring the growth (straight protofilaments) vs. catastrophe (curled protofilaments) stages (Maki et al., 2015). The amino acid sequences of the HEAT repeats in TOG domains are poorly conserved with very low sequence identity to one another. However, many residues in the intra-HEAT loops are highly conserved across different TOG domains from ch-TOG and CLASP families. These residues were predicted to form the tubulin-binding face of TOG domains. This prediction was confirmed in 2012 with the publication of a crystal structure of TOG1 from Stu2 (Figure 2.1B), a ch-TOG family protein in *S. cerevisiae* bound to αβ-tubulin heterodimer (Ayaz et al., 2012).

Due to the low conservation of HEAT repeat amino acid sequences in TOG domains, it is difficult to identify TOG domains in uncharacterized proteins. Our lab devised a strategy to predict the existence of TOG domains from primary sequence. In this strategy, we first analyze secondary structure information obtained from modern prediction servers such as JPred and PSIPRED (Jones, 1999; Cole et al., 2008; Buchan et al., 2013; Drozdetskiy et al., 2015) to look for the presence of at least twelve tandem predicted alpha-helices of appropriate length. We then look for the presence of conserved intra-HEAT loop residues between the helices. Using this strategy, our lab previously predicted the existence of TOG domains in the central conserved region of CLASP, and confirmed the prediction by solving a crystal structure of this region (Leano et al., 2013). Given that the ch-TOG and CLASP families play central roles regulating MT dynamics, we asked whether any other conserved protein families might use a TOG domain array to regulate MT dynamics.

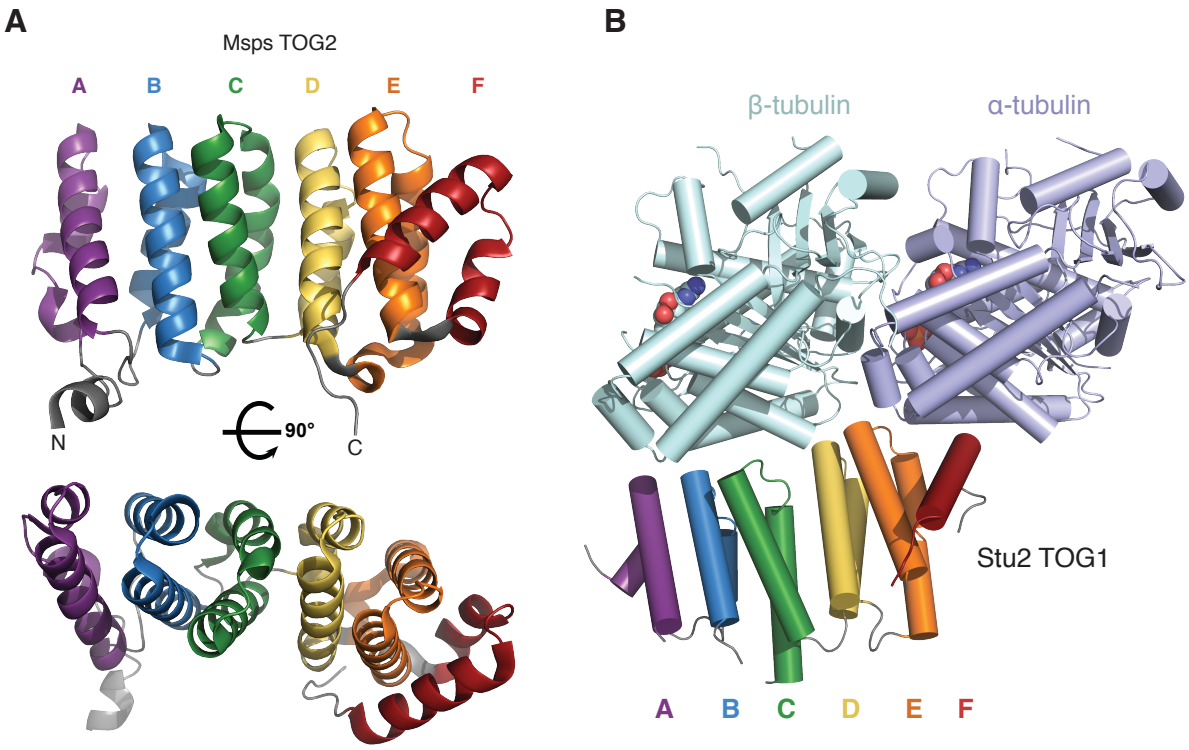

Figure 2.1. Structures of TOG domains and structural basis of tubulin binding.
(A) Structure of Minispindle TOG2 (PDB ID: 2QK2). Each HEAT repeat is shown in a different color and labeled A-F. (B) Structure of Stu2 TOG1 bound to αβ-tubulin heterodimer (PDB ID:4FFB) (Ayaz *et al*., 2012). HEAT repeats color coded as in A.

2.3. Experimental Procedures

2.3.1. Sequence analysis

Homologs of Crescerin from different organisms in the NCBI database were identified using the BLASTP algorithm (Gish et al., 1990). The NCBI accession numbers of Crescerin homologs used for sequence alignments are available in Appendix 2.3. Secondary structure predictions were performed using JPred 3 (Cole et al., 2008) and PSIPRED servers (Jones, 1999; Buchan et al., 2013). Amino acid sequence conservation across species was mapped using CLUSTAL Omega server (Goujon et al., 2010; Sievers et al., 2011; McWilliam et al., 2013).

2.3.2. Phylogenetic analysis

Phylogenetic and molecular evolutionary analyses were conducted using integrated algorithms in the server http://phylogeny.lirmm.fr/phylo_cgi/index.cgi (Anisimova and Gascuel, 2006; Dereeper et al., 2008; Guindon et al., 2010) and MEGA version 6 (Tamura et al., 2013). Sequence alignment was carried out using the MUSCLE algorithm with the Neighbor Joining method of clustering in MEGA. We used available structural data from previously solved TOG domain structures to further optimize the alignment in the intra-HEAT loops. We constructed the initial tree using the maximum likelihood method implemented in the PhyML program (v3.0). The LG substitution model was selected assuming an estimated proportion of invariant sites and 4 gamma-distributed rate categories to account for rate heterogeneity across sites. The gamma shape parameter was estimated directly from the data. Reliability for internal branch was assessed using the bootstrapping method (100 bootstrap replicates). We used this initial tree for tree inference using the Subtree-Pruning-Regrafting (extensive) algorithm with a very weak branch swap filter in MEGA version 6. Subsequent reliability for internal branch was assessed using the bootstrapping method (1000 bootstrap replicates). The final tree was prepared using FigTree v1.4.0.

2.3.3. Cloning and expression

Mouse Crescerin1 TOG2 (residues 332 – 620) was cloned into pET28b (Novagen), generating a thrombin-cleavable N-terminal His_6 tag. Crescerin1 TOG2 was transformed into BL21 DE3 *E. coli*, and grown in 6 L Luria Broth (50 μg/ml kanamycin) at 37 °C to an optical density of 0.6 at 600 nm. The temperature was lowered to 15 °C and protein expression

induced with 100 μM IPTG (final concentration) for 16 hours. Cells were centrifuged at 2100 x g for 10 min and pellets resuspended in 250 ml buffer A (25 mM Tris pH 8.0, 300 mM NaCl, 10 mM imidazole, 0.1% β-ME) and stored at -20 °C. To produce selenomethionine-substituted Crescerin1 TOG2, expression was conducted in the B834 methionine auxotrophic *E. coli* strain, and grown in L-selenomethionine-containing minimal media (MD12-501 and MD12-502, Molecular Dimensions) according to the manufacturer's instructions.

2.3.4. Protein purification

Native and selenomethionine-substituted Crescerin1 TOG2 cell pellets were thawed, 0.5 mM Phenylmethylsulfonyl fluoride (PMSF) added and the cells lysed by sonication. After lysis, additional PMSF was added to 1 mM final concentration and the lysate was centrifuged at 23,000 x g for 45 min. Supernatant was loaded onto a 10 ml Ni^{2+}-NTA column (Qiagen), washed with 300 ml buffer A and TOG2 eluted over a 250 ml linear gradient between buffer A and B (buffer B = buffer A supplemented with 290 mM imidazole). TOG2-containing fractions were pooled, $CaCl_2$ added to 2.5 mM, and 0.1 mg bovine α-thrombin added to remove the His_6-tag, leaving an N-terminal Gly-Ser-His-Met cloning artifact. Thrombin digest proceeded for at least 16 hours at 4 °C. Digested protein was filtered over 0.5 ml Benzamidine sepharose (GE Healthcare), and exchanged into buffer C (25 mM HEPES pH 7.0, 0.1 % β-ME) by dialysis. Protein was loaded onto a 10 ml SP-sepharose fast flow column (GE Healthcare), washed with 200 ml buffer C and eluted over a 250 ml linear gradient between buffer C and D (buffer D = buffer C supplemented with 1 M NaCl). Protein fractions were pooled, concentrated and exchanged into 10 mM HEPES pH 7.5, 100 mM NaCl, 0.1 % β-ME in a Millipore Ultrafree 10,000 MWCO concentrator to 15 mg/ml, frozen

in liquid nitrogen and stored at -80 °C. Purification of selenomethionine-substituted protein proceeded according to the above protocol.

2.3.5. Crystallization

Crescerin1 TOG2 was crystallized using the hanging drop vapor diffusion method. 2 μl of protein (native and selenomethionine-substituted protein) at 10 mg/ml was added to an equal volume of a well solution containing 25% PEG 3350, 0.25 M magnesium chloride, 0.1 M HEPES, pH 7.5 and incubated at 20 °C. Crystals appeared overnight and reached maximum dimensions over the course of 2-3 days. Crystals were transferred to Fomblin oil (Sigma Aldrich) and flash frozen in liquid nitrogen.

2.3.6. Data collection, structure determination, and refinement

Isomorphous Crescerin1 TOG2 native and selenium peak single wavelength anomalous dispersion data sets were collected on single crystals to a resolution of 2.1 and 2.3 Å respectively. Diffraction data was collected at the Advanced Photon Source 22-ID beamline at 100 K. Crescerin1 TOG2 crystals belong to the space group $P2_12_12$ with one molecule in the asymmetric unit. Data was indexed, integrated and scaled using HKL2000 (Otwinowski and Minor, 1997). Selenium sites were identified and used to generate initial experimental, density modified electron density maps (PHENIX) (Grosse-Kunstleve and Adams, 2003; Terwilliger, 2004; Zwart et al., 2005; McCoy et al., 2007; Terwilliger et al., 2007, 2008; Moriarty et al., 2009; Adams et al., 2010; Afonine et al., 2012). Initial models were built using AutoBuild (PHENIX) followed by reiterative manual building in Coot (Emsley et al., 2010) and refinement runs using phenix.refine (PHENIX). The

selenomethionine-substituted TOG2 structure was refined against a MLHL target function, the model converted to native methionine, and refined against native data using a ML target function to 2.2 Å resolution. Refinement was monitored using a Free R, based on 10% of the data randomly excluded from refinement. No clear electron density was evident for N-terminal residues 332-344, HR A loops residues 361-365, HR F residues 558-562, and the C-terminal residues 595-620. Lysine K380 was modeled as alanine. Information regarding data statistics, model building and refinement can be found in Appendix 2.4. Atomic coordinates have been deposited in the Protein Data Bank under accession code 5DN7.

2.3.7. Circular dichroism

Circular dichroism (CD) spectra of Crescerin1 TOG domains were collected at 20 °C and 94 °C using a Chirascan-plus CD spectrometer (Applied Photophysics, Leatherhead, UK). Each protein sample was diluted to a final concentration of 0.1 mg/ml in 10 mM sodium phosphate buffer (pH 7.5), 50 mM NaF. The spectra were recorded from 260 to 190 nm with a step size of 0.5 nm using a 1 mm path length cuvette. The time per point was kept at 1.25 sec. A base-line control CD spectrum was taken and subtracted from each spectrum. All spectra were smoothed in the Chirascan-plus software with a moving window of 5 points. In CD thermal melt experiments, data were collected at 1 °C intervals from 20 °C to 94 °C at 208 nm and 222 nm wavelengths.

2.3.8. In vitro MT polymerization assay

Crescerin1 constructs for MT polymerization assays (TOG1: 67-317, TOG2: 332-620, TOG2-Y364E, TOG3: 1243-1491, TOG4: 1533-1776, TOG4-F1559E, TOG(1+2): 67-

620, and TOG(3+4): 1243-1776) were cloned into *E. coli* expression vectors, expressed, and purified in a manner similar to that for TOG2 as detailed above. Tubulin was purified from bovine brain following protocols established by the Mitchison lab, Harvard Univ. (http://mitchison.med.harvard.edu/protocols/microtubules/Large Scale Tubulin Preparation.pdf). Tubulin polymerization was monitored using a SPEX Fluorolog-3 spectrophotometer (Horiba JobinYvon) in T-format, high voltage mode. The excitation and detection wavelengths were set at 350 nm and the excitation and emission slits set at 0.5 and 0.75 nm respectively. The cuvette holder was maintained at 37 °C. Clarified tubulin samples (18 μM final concentration) were prepared in the presence or absence of Crescerin1 TOG domain constructs each at 3 μM final concentration) in polymerization buffer (50 mM MES, pH 6.6, 3.4 M glycerol, 5 mM DTT, 1 mM EGTA, 5 mM $MgSO_4$, 1 mM GTP) and incubated on ice for 8 minutes. 300 μL samples were injected into a 4 mm path length quartz cuvette at room temperature, then immediately placed into the 37 °C cuvette holder. Scattering was recorded at 350 nm in 1 second intervals over 1500 seconds. Spikes in scattering within the first 100 seconds were the result of samples equilibrating to 37 °C.

2.4. Results

2.4.1. Sequence analysis

We performed structure-based BLAST searches using individual TOG domains from ch-TOG and CLASP family members and scanned weak hits for sequence identity in the discontinuous TOG domain intra-HEAT loop determinants that bind tubulin. Searching the human proteome we found an uncharacterized protein, FAM179B (previously known as KIAA0423), which showed discontinuous sequence similarity to CLASP TOG1 (BLAST E-

value of 1e-09). This novel protein is a member of a protein family conserved in ciliated/flagellated eukaryotes ranging from mammals to unicellular eukaryotes including *Chlamydomonas* (SSA6) and *Tetrahymena*, but absent in non-ciliated eukaryotes including yeast and *Dictyostelium* (Figure 2.2 and Appendix 2.3). We designate this protein family and its unnamed members Crescerin, derived from the Latin (*crescere*: to grow, as functional assays of protein family members revealed a mechanistic function in driving cilia formation and promoting microtubule polymerization). The only family member characterized to date is the *C. elegans* member CHE-12. The single study examining CHE-12 showed that it is expressed in a subset of amphid neurons possessing simple rod-like cilia and two phasmid sensory neurons under the transcriptional control of DAF-19, a transcription factor that controls numerous ciliary genes (Bacaj et al., 2008). Overexpressed CHE-12::GFP localizes to cilia, and mutations in *che-12* impair cilia formation (Bacaj et al., 2008). Concordant with a role in cilia structure, *che-12* mutant worms do not properly chemotax in response to sodium chloride (Bacaj et al., 2008).

Upon further investigation we found that mammals contain two closely related Crescerin family genes, *FAM179A* and *FAM179B* (Figure 2.2). Sequence analysis and secondary structure prediction of mouse FAM179B, revealed four conserved domains, an N-terminal pair and a C-terminal pair, connected by a long central linker (Figure 2.2). Each of the four domains contain twelve predicted α-helices that are predicted to form six tandem HRs (Appendices 2.5, 2.6, 2.7 and 2.8) with intra-HEAT loops displaying similarity to the intra-HEAT loop tubulin-binding determinants found in ch-TOG and CLASP family TOG domains. The mammalian FAM179A protein contains only two conserved TOG-like domains that share high sequence similarity with the FAM179B C-terminal pair of TOG

domains (Figure 2.2). A number of Crescerin family members from different species were found to contain fewer than four TOG domains. We classified all proteins that include TOG-like domains similar to the mammalian FAM179B TOG1 or TOG2 into the Crescerin1 sub-family and those that only contain FAM179B TOG3 and TOG4-like domains (i.e. more similar to FAM179A) into the Crescerin2 sub-family (Figure 2.2 and Appendix 2.3).

We then compared amino acid sequences from individual TOG and TOG-like domains among human Crescerin1, Crescerin2, ch-TOG, CLASP1 and CLASP2 and tabulated the pairwise percentage sequence identity between these domains (Figure 2.3). TOG domains occupying analogous positions in the array in CLASP1 and CLASP2 share high sequence identity to each other but not to other TOGs in the same array. Similarly, we found high sequence identity between Crescerin1 TOG3 and Crescerin2 TOG1 as well as between Crescerin1 TOG4 and Crescerin2 TOG2 (Figure 2.3). Such positional sequence conservation of TOG domains in an array strongly suggests that each TOG domain has a unique role in the overall function of the protein.

We found that the average percentage sequence identity between non-analogous TOG domains occupying different positions in an array of the same family as well as different families to be 16.8%. Interestingly, Crescerin1 TOG2 shares relatively high sequence identity to CLASP1 TOG1 (23.9%) and CLASP2 TOG1 (27.1%), and these are the highest sequence identities between any pair of TOG domains from different families (Figure 2.3).

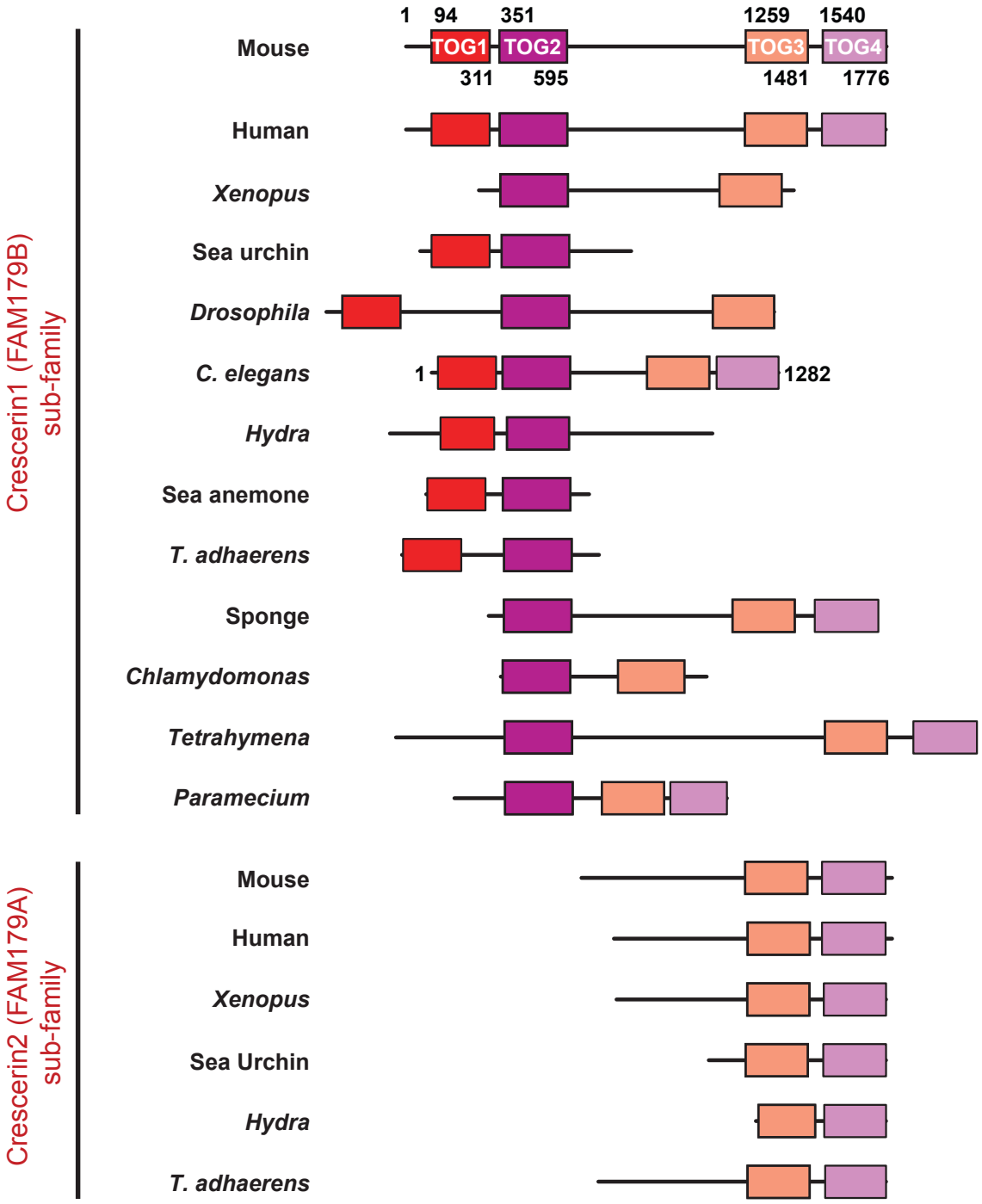

Figure 2.2. The Crescerin protein family has conserved TOG domains across a wide range of ciliated eukaryotes.
Sequence analysis of Crescerin family proteins across species reveals a variable number of TOG domains and variable lengths of inter-TOG domain linkers. In each organism, the domains are color coded according to the mouse Crescerin1 (FAM179B) TOG domain that they are most similar to in primary sequence. All variants that include TOG domains that are most similar to the N-terminal pair of TOG domains in mouse Crescerin1 are grouped under Crescerin1 sub-family. Some organisms including mammals contain a separate isotype (FAM179A)) containing two TOG domains that are most similar to the C-terminal pair of TOG domains in mouse Crescerin1. These variants are grouped under the Crescerin2 sub-family.

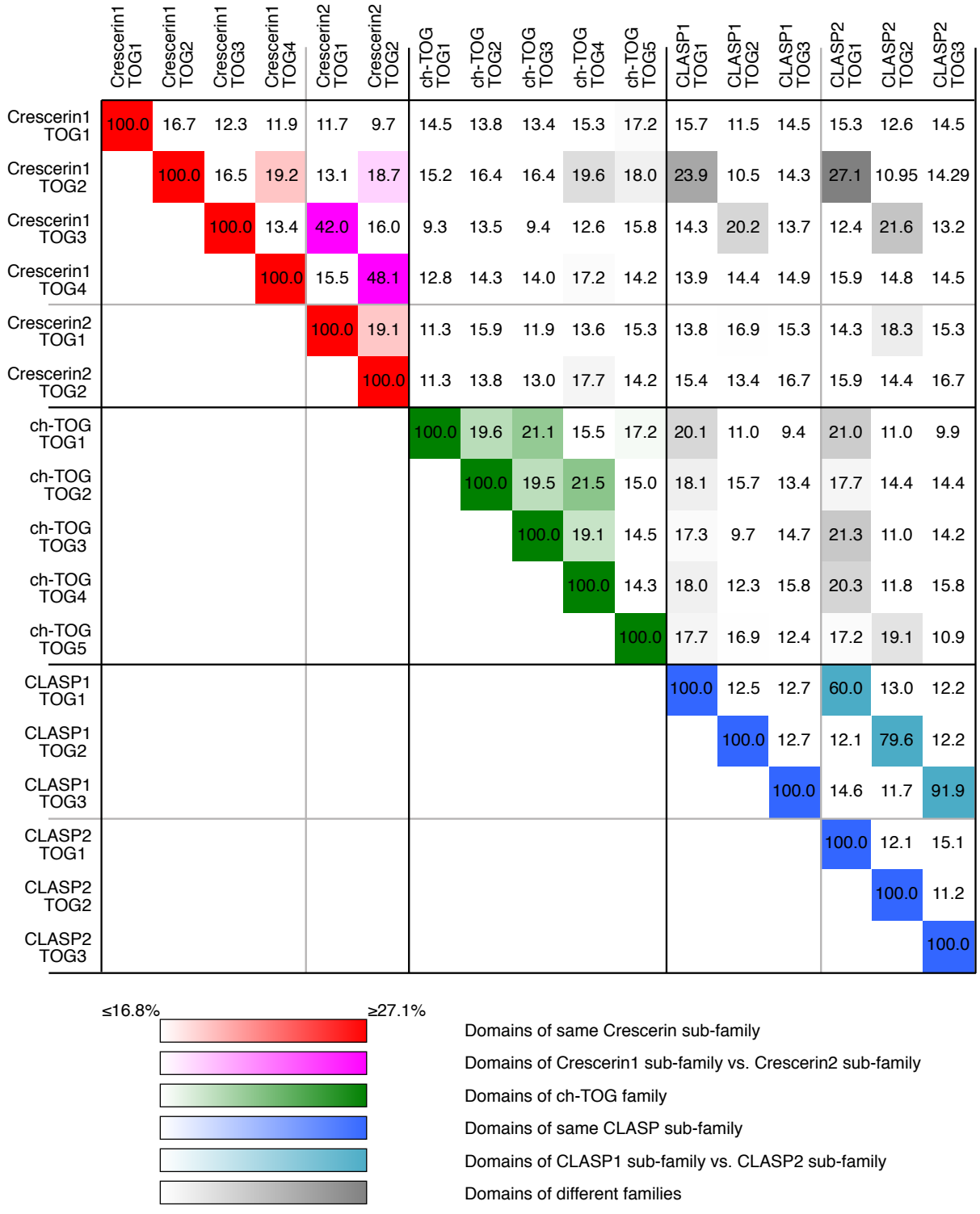

Figure 2.3. Matrix showing sequence identity between pairs of TOG domains in human Crescerin, ch-TOG and CLASP families.

The average and maximum sequence identity between pairs of different TOG domains is 16.8% and 27.1% respectively. The individual boxes are color coded according to the heat map shown below in the range between 16.8% to 27.1% to highlight the pairs with above average sequence identity.

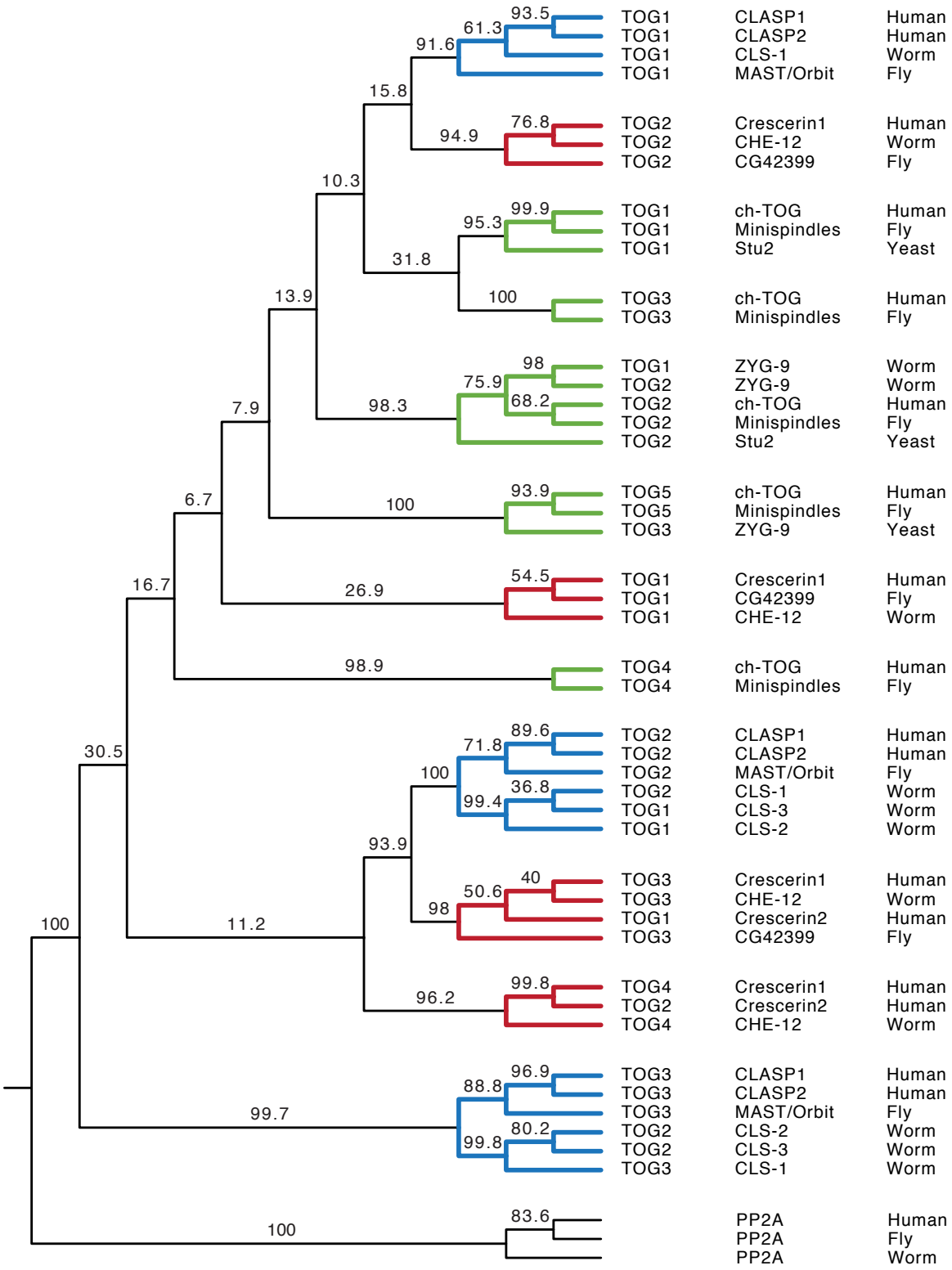

Figure 2.4. Cladogram showing phylogenetic relationship between Crescerin, ch-TOG and CLASP family TOG domains.

2.4.2. Phylogenetic analysis

In order to determine the evolutionary relationship between TOG domains from the ch-TOG, CLASP and Crescerin families, we performed phylogenetic analyses using available amino acid sequences of the TOG domains from human, fly, worm and yeast. The results of this analysis are presented as a cladogram (Figure 2.4) where the TOG domains in neighboring branches of the tree are more closely related in primary sequence than those that are further away. The numbers on the branches represent the bootstrap values of the analysis, which indicate the percentage of times the two interior branches were grouped together over many rebuilding cycles. Thus the bootstrap values are a measure of reliability of internal branch organization, where a higher bootstrap value on a branch indicates a greater likelihood that its interior branches are more closely related to each other than to other branches on the tree. We used amino acid sequences of Protein phosphatase 2A (PP2A), a HEAT repeat containing protein not related to TOG domains, from human, fly and worm, to serve as the root reference for comparison between TOG domains.

As expected, we found that the analogous TOG domains from different species are grouped together in closely related branches with the bootstrap values on the master branch connecting the group greater than 90. The major exceptions to this pattern are the Crescerin family TOG1 domains, which are grouped together only 269 times out of the 1000 bootstrap iterations. This indicates that TOG1 is the least conserved Crescerin family TOG domain across species. The other notable exception is ZYG-9 TOG1, which bears high sequence similarity with ZYG-9 TOG2 and is grouped together with TOG2 from other ch-TOG family members. The Crescerin family TOG domains were not grouped with any of the ch-TOG or

CLASP TOG domains indicating that Crescerin is an independent family, distinct from ch-TOG and CLASP. Interestingly, we observed that Crescerin1 TOG-like domains TOG2 and TOG3 are distantly related to CLASP family TOG domains TOG1 and TOG2 respectively. We set out to confirm the structures of the predicted TOG domains in Crescerin and determine whether it plays a role distinct from the ch-TOG and CLASP protein families, potentially specific to cilia structure and function.

2.4.3. Structure of the Crescerin1 second conserved domain reveals a bona fide TOG domain

To determine whether the Crescerin family represents a novel TOG domain array-containing protein family we cloned and purified all four conserved putative TOG domains from mouse Crescerin1. We obtained crystals of the second conserved domain (residues 332-620) in space group $P2_12_12$. We collected a native X-ray diffraction data set to 2.2 Å resolution and a single wavelength anomalous dispersion data set on selenomethionine-substituted protein to 2.37 Å resolution. We solved and built the structure, refining against the native data to 2.2 Å resolution, yielding R and R_{free} values of 0.18 and 0.24 respectively (Appendix 2.4). The model contains one molecule of Crescerin1 in the asymmetric unit and encompasses residues 345-594.

The Crescerin1 TOG2 structure reveals a *bona fide* TOG domain fold consisting of twelve helices that pair into six tandem HRs (A-F) and stack, forming a 60 Å oblong solenoid (Figure 2.5A). TOG domain HRs can be grouped into two triads: the first triad containing HRs A-C and the second triad containing HRs D-F. These HR triads have a canonical handedness and relative positioning similar to that observed in ch-TOG family

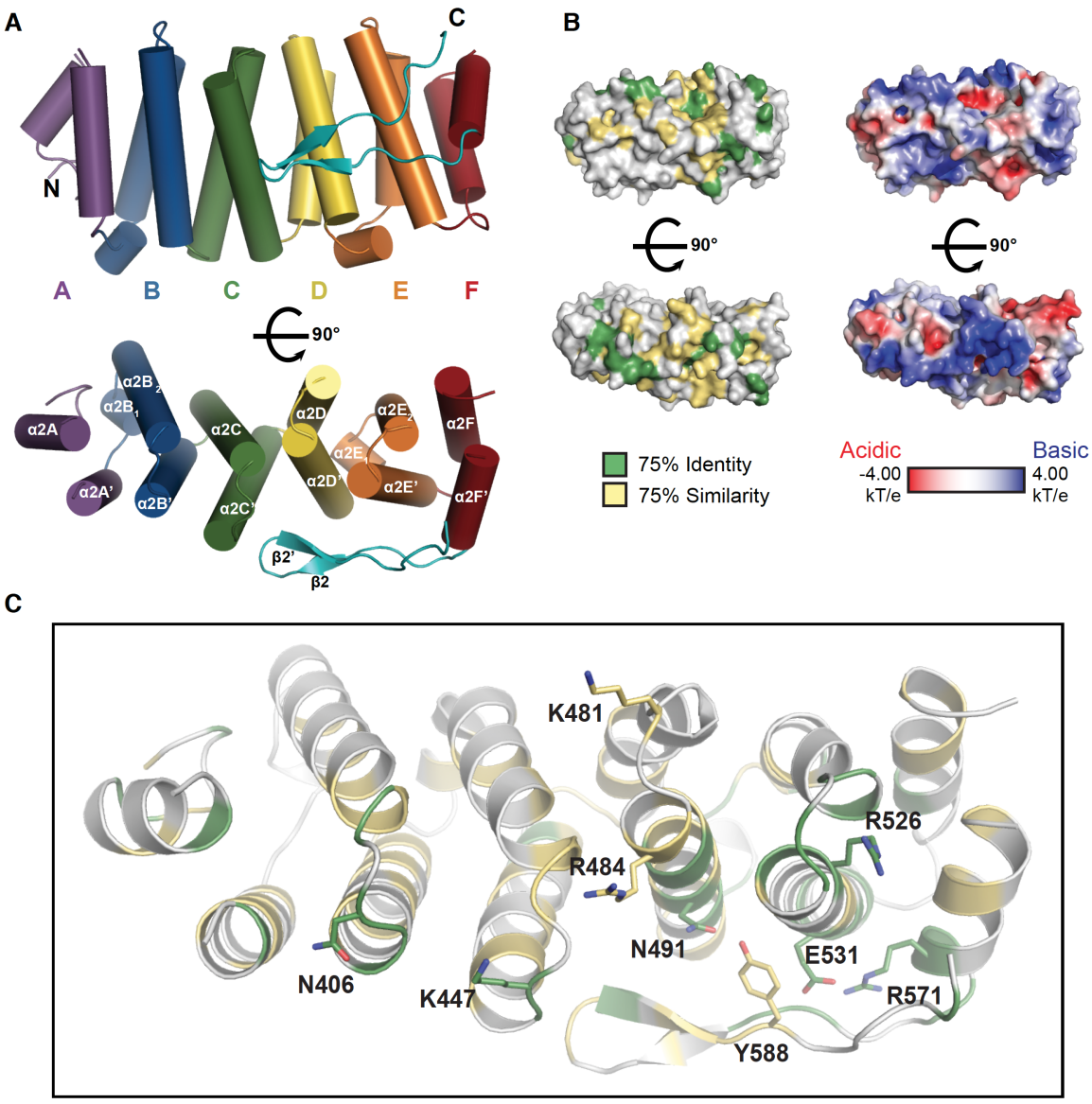

Figure 2.5. The Crescerin1 second conserved domain is a *bona fide* TOG domain.
(A) Crystal structure of Crescerin1 TOG2. Each HR (A-F) and the C-terminal β-hairpin are shown in a different color. See Appendix 2.4 for crystallographic data, phasing and refinement statistics. (B) Crescerin1 TOG2 shown in surface representation, oriented as in A, with cross species conservation (left) or electrostatic charge distribution (right) mapped on the surface. See Appendix 2.6 for multiple sequence alignment of Crescerin TOG2 showing conservation across species. (C) Crescerin1 TOG2 conserved residues (colored as in B) map to the tubulin-binding intra-HEAT loops and to the C-terminal β-hairpin-HR interface.

TOG domains (Al-Bassam et al., 2007; Slep and Vale, 2007; Fox et al., 2014). The HR A-C triad has a right-handed twist, while the HR D-F triad has a right-handed twist between repeats D and E, but transits to a left-handed twist between repeats E and F. Between the two

HR triads there is a lateral shift relative to the axis of the solenoid, a common feature found in all other TOG domain structures determined to date. The Crescerin1 TOG2 structure has inter-HR α-helices, $\alpha 2B_1$ situated between HR A and HR B, also found in hCLASP1 TOG2, and $\alpha 2E_1$, situated between HR D and HR E, also found in the hCLASP1 TOG2 structure as well as ch-TOG family structures of *Drosophila* Minispindles TOG2 and TOG4. To map conserved residues across the Crescerin family onto the structure, we aligned 13 diverse species and contoured conservation at 75% identity (green) and 75% similarity (yellow) (Figure 2.5B and Appendix 2.6). The majority of conserved residues map to the intra-HEAT loops that span one face of the domain. These conserved intra-HEAT loops are similar in composition and structure to the tubulin-binding intra-HEAT loops found in ch-TOG and CLASP protein family TOG domain structures (Figure 2.5C and Appendix 2.6). Additionally, the electrostatic charge distribution across the first five intra-HEAT loops (HR A-E) is basic (Figure 2.5B), and like other TOG domain structures determined to date, would complement the acidic nature of the αβ-tubulin TOG-binding site. Overall, the structure of the Crescerin1 second conserved domain conforms to a canonical TOG architecture with conserved intra-HEAT loop determinants, homologous in composition and charge to the tubulin-binding determinants in ch-TOG and CLASP TOG domains. We thus designate this domain a TOG domain and refer to it hereafter as TOG2. This confirms our prediction that Crescerin represents a third, unique TOG domain-containing protein family.

2.4.4. Crescerin1 TOG2 has a unique C-terminal β-hairpin that promotes domain stability

While Crescerin1 TOG2 has overall structural similarity with previously determined ch-TOG and CLASP family TOG domain structures, it also has architecturally unique

components that differentiate it from these other TOG domain structures. One striking feature is the presence of a 21-residue C-terminal β-hairpin that runs alongside the second HR triad and occupies the area created by the lateral shift between the HR A-C and D-F triads. The β-hairpin forms multiple hydrophobic interactions and hydrogen bonds with conserved residues in the α2C', α2D', and α2E' helices (We designate the helices of each HR as X and X', as notated in Slep and Vale, 2007, with "2" indicating TOG2). An invariant asparagine (N491) in α2D' forms a hydrogen bond with a conserved tyrosine residue (Y588) on the β2' strand of the β-hairpin (Figure 2.6A). The β-hairpin is further locked alongside the TOG domain by a network of hydrogen bonds formed between the A589 backbone amide and a conserved glutamate side-chain (E531) in α2E', as well as the T576 backbone carbonyl group and a conserved arginine side-chain (R571) in helix α2F' (Figure 2.6A). Commensurate with a stable, *bona fide* interaction between the β-hairpin and the central HRs, the β-hairpin has comparatively low B-factors that parallel those of the HRs it interacts with (Figure 2.6B). To further assess the contribution of the C-terminal β-hairpin to domain stability, we created a shorter TOG2 construct lacking the β-hairpin (TOG2-ΔβHP, residues 332-576) and performed secondary structure analysis by circular dichroism (CD). Although the overall α-helical signature was similar for both constructs (Figure 2.6C), the TOG2-ΔβHP construct had a lower melting temperature (T_m = 45.5 °C) compared to the TOG2 construct containing the β-hairpin (residues 332-620; T_m = 57.5 °C), indicating that the β-hairpin promotes TOG2 domain stability (Figure 2.6D). Secondary structure elements that flank TOG domains have previously been shown to stabilize other TOG domains (Leano et al., 2013). Crescerin family sequence alignments and secondary structure prediction analysis on the regions flanking TOG domains 1, 3, and 4 did not show conservation or similar

predicted secondary structure, suggesting that the TOG2 C-terminal β-hairpin is a unique stabilizing feature for Crescerin1 TOG2. Whether this β-hairpin plays additional functional roles remains to be determined.

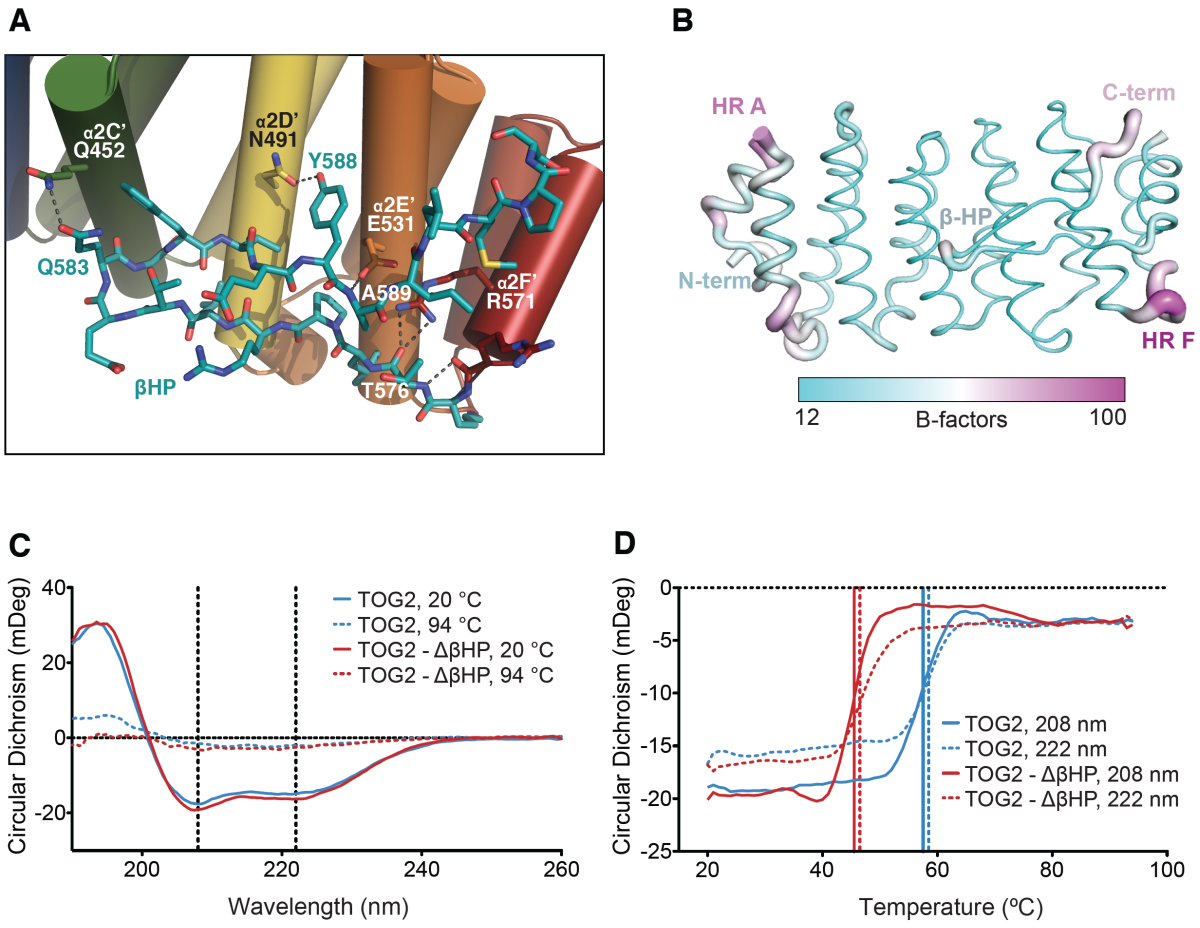

Figure 2.6. Crescerin1 TOG2 has a unique C-terminal β-hairpin.
(A) Expanded view of the Crescerin1 TOG2 C-terminal β-hairpin-HR interface. (B) Cα B-factor values mapped on the Crescerin1 TOG2 structure suggests that the domain has a non-plastic core. Regions with low and high B-factor are shown in cyan and magenta respectively. (C-D) Circular dichroism spectra (C) of Crescerin1 TOG2 (blue) and TOG2-ΔβHP (red) at 20 °C (solid lines) and 94 °C (dotted lines) and thermal melt curves (D) monitored using 208 nm (solid lines) and 222 nm (dotted lines) wavelength light.

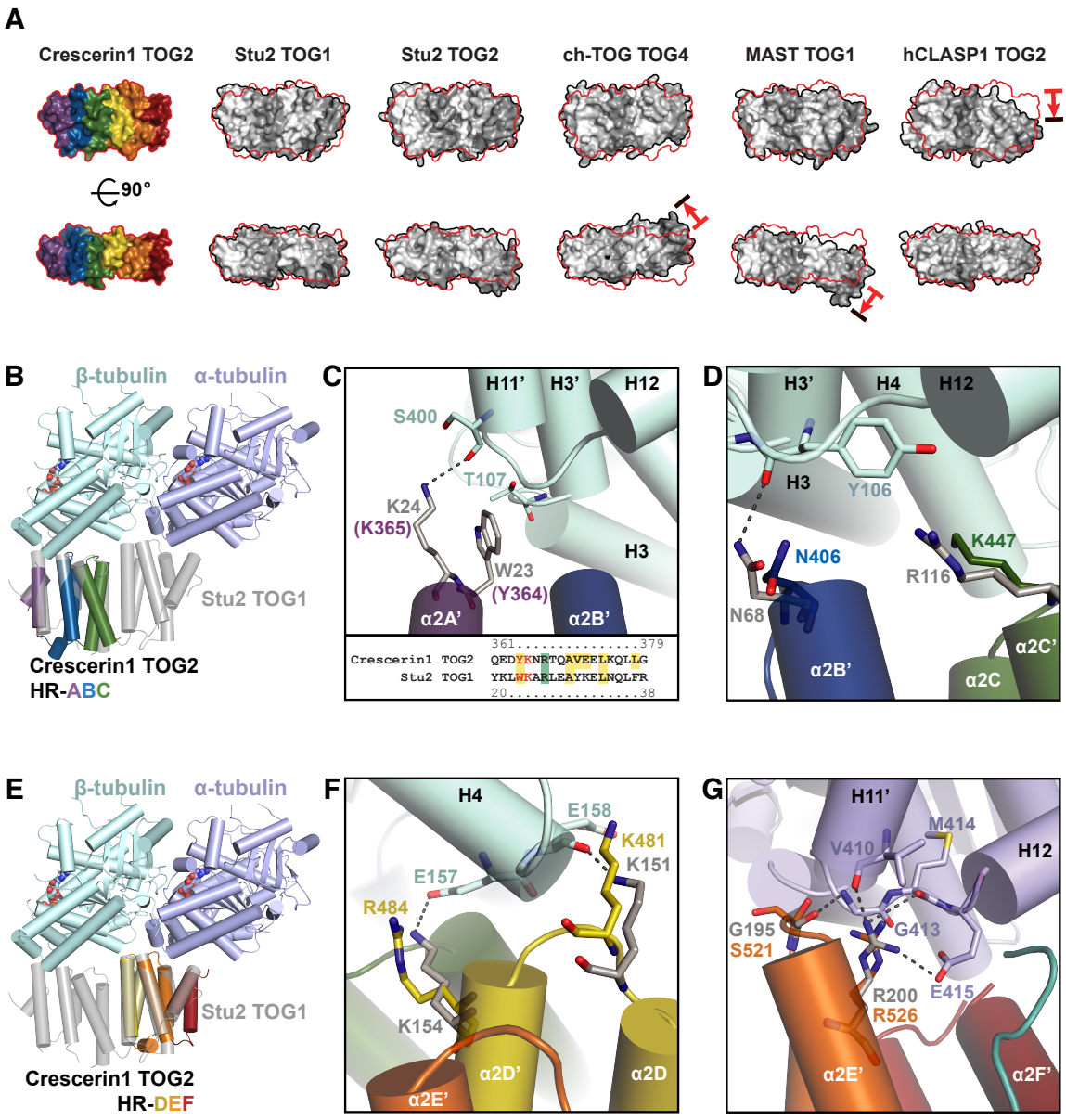

Figure 2.7. The Crescerin1 TOG2 tubulin-binding surface is similar to Stu2 TOG1.
(A) Comparison of Crescerin1 TOG2 structure (rainbow/red outline) with Stu2 TOG1 (4FFB), Stu2 TOG2 (2QK1), ch-TOG4 (4QMI), MAST TOG1 (4G3A) and hCLASP1 TOG2 (4K92) structures by aligning the first HR triad. Red arrows highlight major structural differences. (B-D) Alignment of the Crescerin1 TOG2 first HR triad to the Stu2 TOG1-αβ-tubulin complex (4FFB). (C) Stu2 TOG1 HR A loop residues W23 and K24 interact with T107 and S400 of β-tubulin. Although residues in the Crescerin1 TOG2 HR A loop could not be modeled due to weak electron-density, we anticipate that the homologous Crescerin1 residues Y364 and K365 (see alignment below) form similar interactions with β-tubulin. (D) Crescerin1 TOG2 residues N406 and K447 are positioned similar to Stu2 TOG1 residues N68 and R116 that interact with β-tubulin Y106. (E-G) Alignment of the Crescerin1 TOG2 second HR triad to the Stu2 TOG1-αβ-tubulin complex (4FFB). (F) Crescerin1 residues K481 and R484 occupy similar positions as Stu2 TOG1 K151 ad K154 that form salt-bridges with β-tubulin E158 and E157 respectively. (G) Crescerin1 TOG2 HR-E residues S521 and R526 occupy similar positions as Stu2 TOG1 G195 and R200 which interact with α-tubulin V410, G413, M414 and E415.

2.4.5. The Crescerin1 TOG2 tubulin-binding surface is similar to Stu2 TOG1

TOG domain structures determined to date from the ch-TOG and CLASP families reveal distinct structural variations that predict diversified interactions with αβ-tubulin. To determine which TOG structures Crescerin1 TOG2 is most similar to, we performed pairwise structural alignments using the DALI server (Holm and Rosenstrom, 2010), aligning the first HR triads as a point of reference since this region displays the highest conservation across TOG domains (Figure 2.7A). The Crescerin1 TOG2 intra-HEAT loop surface assumes a straight conformation that closely resembles Stu2 TOG1 and contrasts with the bent architectures observed in ch-TOG TOG4, MAST TOG1, and hCLASP1 TOG2 (Figure 2.7A, red arrows) (Slep and Vale, 2007; Ayaz et al., 2012; De la Mora-Rey et al., 2013; Leano et al., 2013; Fox et al., 2014).

To gain insight into whether Crescerin1 TOG2 could form contacts with tubulin as observed in the Stu2 TOG1-αβ-tubulin structure, we docked Crescerin1 TOG2 on the tubulin heterodimer by structurally aligning Crescerin1 TOG2 HRs A-C (first HR triad) and HRs D-F (second HR triad) to the coordinates of Stu2 TOG1 in the Stu2 TOG1-tubulin complex (Ayaz et al., 2012) (Figure 2.7B-D and Figure 2.7E-G respectively). Many of the Stu2 TOG1 tubulin-binding residues are conserved and similarly positioned in Crescerin1 TOG2 (Figure 2.7B-G). Prime β-tubulin binding determinants reside in Stu2 TOG1 HR A, including W23 and K24. While electron density for the Crescerin1 TOG2 HR-A loop was poor and precluded modeling of the homologous residues Y364 and K365, the HR-A helices are similarly positioned and we anticipate that Y364 and K365 form homologous contacts with β-tubulin T107 and S400 respectively (T109 and G410 in mammalian β-tubulin) (Figure

2.7C). In the Crescerin1 TOG2 HR-B and HR-C intra-HEAT loops, N406 and K447 occupy positions analogous to Stu2 N68 and R116 respectively, both of which interact with yeast β-tubulin Y106 (Y108 in mammalian β-tubulin) (Figure 2.7D). In Crescerin1 TOG2 HR-D, K481 and R484 are positioned similar to Stu2 K151 and K154, which interact with β-tubulin E158 and E157 respectively (E160 and E159 in mammalian β-tubulin) (Figure 2.7F). Similarly, the highly conserved R526 in Crescerin1 TOG2 HR-E is positioned analogous to Stu2 R200, which interacts with α-tubulin V410, and E415 (V409 and E414 in mammalian α-tubulin) (Figure 2.7G). The composition and conformational similarity between Stu2 TOG1 and Crescerin1 TOG2 intra-HEAT loops suggests that Crescerin1 TOG2 may be involved in binding free αβ-tubulin and/or MTs to regulate MT dynamics.

2.4.6. Crescerin1 TOG domains can bind to microtubules and promote microtubule polymerization in vitro

To determine whether Crescerin might regulate the MT cytoskeleton, we first tested whether Crescerin1 TOG domains could influence MT polymerization *in vitro*. We mixed different purified TOG domains (Figure 2.8A) with tubulin and monitored tubulin polymerization at 37 °C using a light scattering assay. The intrinsic polymerization activity of tubulin in the absence of other proteins is reflected as a characteristic sigmoidal increase in light scattering signal with an initial lag phase of about 500 seconds (Figure 2.8B, black curve). Addition of TOG1 or TOG3 to the reaction mixture did not affect the MT polymerization rate. In contrast, addition of either TOG2 or TOG4 dramatically increased the rate of MT polymerization. To determine whether TOG2 and TOG4 potentiated tubulin polymerization using canonical tubulin-binding determinants, we mutated a conserved

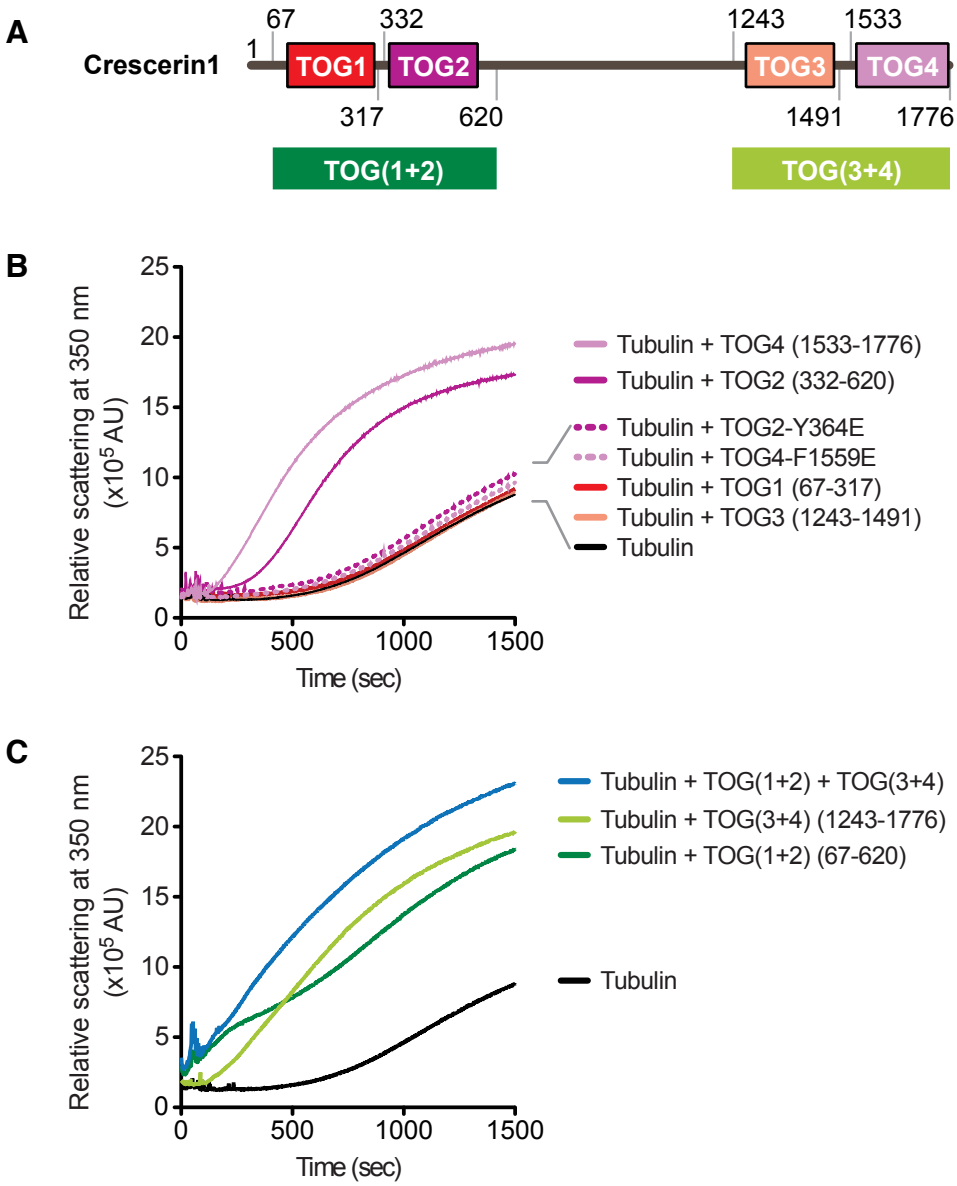

Figure 2.8. Crescerin1 TOG domains affect MT polymerization *in vitro*.
(A) Schematic of Crescerin1 TOG domain-containing fragments used for *in vitro* MT polymerization assays. (B) *In vitro* MT polymerization assays in the absence (black) or presence of purified Crescerin1 single TOG domains. TOG2 and TOG4-dependent MT polymerizing activity was lost when key tubulin-binding HR A loop residues Y364 (TOG2) and F1559 (TOG4) were mutated to glutamate (dotted lines). Addition of TOG1 (red) or TOG3 (orange) did not affect MT polymerization kinetics. See Appendix 2.9 for circular dichroism analysis of single TOG domain constructs used in B. (C) Larger constructs containing tandem TOG domains 1 and 2 (dark green) or 3 and 4 (light green) increased MT polymerization kinetics.

aromatic residue in the HR-A intra-HEAT loop in each TOG domain to glutamate (Y364E in TOG2 and F1559E in TOG4). Homologous mutations in other TOG domains have been shown to abrogate tubulin binding without affecting the TOG domain fold (Slep and Vale,

2007; Leano et al., 2013). We performed CD spectrum analysis on these constructs and confirmed that Y364E and F1559E mutations in TOG2 and TOG4, respectively, did not affect the alpha-helical fold and thermal stability of these domains (Appendix 2.9). The Y364E and F1559E mutations abrogated the ability of Crescerin1 TOG2 and TOG4, respectively, to accelerate tubulin polymerization, suggesting that both TOG2 and TOG4 use canonical tubulin-binding determinants to promote tubulin polymerization. Addition of larger fragments containing pairs of TOG domains (TOG(1+2): amino acids 67-620 and TOG(3+4): amino acids 1243-1776) resulted in distinct reproducible scattering curves with short lag times (Figure 2.8C). These data suggest that Crescerin family TOG domains have differential tubulin-binding activity and may function collectively to regulate MT dynamics.

2.5. Discussion

TOG-domain containing protein families, ch-TOG and CLASP regulate MT dynamics in the cytoplasm, both during interphase and cell division (Brittle and Ohkura, 2005; Sousa et al., 2007; Slep, 2009; Al-Bassam et al., 2010; Al-Bassam and Chang, 2011; Currie et al., 2011; Widlund et al., 2011; Patel et al., 2012; Leano et al., 2013; Fox et al., 2014). ch-TOG uses its array of five TOG domains to promote MT polymerization during interphase. CLASP has a trimeric TOG domain array that promotes MT pause in interphase. During mitosis, both the ch-TOG and CLASP families regulate spindle dynamics, facilitating proper segregation of sister chromatids between daughter cells. Both ch-TOG and CLASP require tubulin-binding activity across their TOG domain arrays in order to regulate MT dynamics. While the activities of ch-TOG, CLASP, and a host of other cytoplasmic regulators of MT dynamics have been extensively studied, little is known about factors that

regulate ciliary MTs. We have identified Crescerin as a novel TOG-domain array-containing protein family through structural characterization of its second TOG domain. The Crescerin family is conserved across a wide range of ciliated and flagellated eukaryotes and has been implicated to be involved in cilia structure and function regulation in *C. elegans*. We find that Crescerin1 uses its TOG domain array to promote MT polymerization *in vitro*. This highlights the emerging paradigm of MT regulators that mechanistically employ arrayed TOG domains with distinct structures and tubulin-binding activities to differentially regulate MT dynamics, whether during interphase, mitosis, or in specialized organelles like the primary cilium.

Concordant with the ability of Crescerin1 to promote MT polymerization *in vitro*, we find that Crescerin1 TOG2 is most similar to TOG1 from the ch-TOG family of MT polymerases. However, Crescerin1 TOG2 does have unique features including the presence of a β-hairpin at its C-terminal region that makes extensive contacts with HRs C, D and E and contributes to domain stability. The primary sequences of Crescerin's four TOG domains bear low sequence identity to one another and to TOG domains from ch-TOG and CLASP families. Comparing TOG domain structures solved to date, we find that the tubulin-binding surface of many of these domains adopts different conformations that imply different tubulin-binding modes as well as potential effects on the curvature of the tubulin heterodimer. Our data demonstrate that Crescerin1 TOG domain pairs promote tubulin polymerization *in vitro*. Studies analyzing the ability of ch-TOG family TOG domains to promote tubulin polymerization *in vitro* have found that a pair of TOG domains (TOG1 and TOG2 from yeast Stu2 or *Drosophila* Minispindles) are required for this activity while the individual TOG domains are not sufficient (Slep and Vale, 2007; Ayaz et al., 2012; Fox et al., 2014). In

contrast, a single TOG domain (TOG2) from human CLASP1 was sufficient to promote tubulin polymerization *in vitro*, suggesting that it either stabilized a conformation of tubulin more amenable for polymerization or aided in lattice contacts through a direct or allosteric mechanism (Leano et al., 2013). Interestingly, Crescerin TOG2 and TOG4 are also able to individually increase MT polymerization rates *in vitro*, similar to human CLASP1 TOG2 (Leano et al., 2013). The structural mechanism underlying the ability of these individual TOG domains to promote tubulin polymerization remains to be determined.

REFERENCES

Adams, P.D., P. V. Afonine, G. Bunkóczi, V.B. Chen, I.W. Davis, N. Echols, J.J. Headd, L.W. Hung, G.J. Kapral, R.W. Grosse-Kunstleve, A.J. McCoy, N.W. Moriarty, R. Oeffner, R.J. Read, D.C. Richardson, J.S. Richardson, T.C. Terwilliger, and P.H. Zwart. 2010. PHENIX: A comprehensive Python-based system for macromolecular structure solution. *Acta Crystallogr. Sect. D Biol. Crystallogr.* 66:213–221. doi:10.1107/S0907444909052925.

Afonine, P. V., R.W. Grosse-Kunstleve, N. Echols, J.J. Headd, N.W. Moriarty, M. Mustyakimov, T.C. Terwilliger, A. Urzhumtsev, P.H. Zwart, and P.D. Adams. 2012. Towards automated crystallographic structure refinement with phenix.refine. *Acta Crystallogr. Sect. D Biol. Crystallogr.* 68:352–367. doi:10.1107/S0907444912001308.

Al-Bassam, J., and F. Chang. 2011. Regulation of microtubule dynamics by TOG-domain proteins XMAP215/Dis1 and CLASP. *Trends Cell Biol.* 21:604–614. doi:10.1016/j.tcb.2011.06.007.

Al-Bassam, J., H. Kim, G. Brouhard, A. van Oijen, S.C. Harrison, and F. Chang. 2010. CLASP promotes microtubule rescue by recruiting tubulin dimers to the microtubule. *Dev. Cell*. 19:245–258. doi:10.1016/j.devcel.2010.07.016.

Al-Bassam, J., N.A. Larsen, A.A. Hyman, and S.C. Harrison. 2007. Crystal structure of a TOG domain: Conserved features of XMAP215/Dis1-family TOG domains and implications for tubulin binding. *Structure*. 15:355–362. doi:10.1016/j.str.2007.01.012.

Anisimova, M., and O. Gascuel. 2006. Approximate likelihood-ratio test for branches: A fast, accurate, and powerful alternative. *Syst. Biol.* 55:539–552. doi:10.1080/10635150600755453.

Ayaz, P., X. Ye, P. Huddleston, C.A. Brautigam, and L.M. Rice. 2012. A TOG:αβ-tubulin complex structure reveals conformation-based mechanisms for a microtubule polymerase. *Science.* 337:857–860. doi:10.1126/science.1221698.

Bacaj, T., Y. Lu, and S. Shaham. 2008. The conserved proteins CHE-12 and DYF-11 are required for sensory cilium function in *Caenorhabditis elegans*. *Genetics*. 178:989–1002. doi:10.1534/genetics.107.082453.

Brittle, A.L., and H. Ohkura. 2005. Mini spindles, the XMAP215 homologue, suppresses pausing of interphase microtubules in *Drosophila*. *EMBO J.* 24:1387–1396. doi:10.1038/sj.emboj.7600629.

Buchan, D.W.A., F. Minneci, T.C.O. Nugent, K. Bryson, and D.T. Jones. 2013. Scalable web services for the PSIPRED Protein Analysis Workbench. *Nucleic Acids Res.* 41:W349–357. doi:10.1093/nar/gkt381.

Cassimeris, L., D. Gard, P.T. Tran, and H.P. Erickson. 2001. XMAP215 is a long thin

molecule that does not increase microtubule stiffness. *J. Cell Sci.* 114:3025–3033.

Charrasse, S., M. Schroeder, C. Gauthier-Rouviere, F. Ango, L. Cassimeris, D.L. Gard, and C. Larroque. 1998. The TOGp protein is a new human microtubule-associated protein homologous to the Xenopus XMAP215. *J. Cell Sci.* 111:1371–1383.

Cole, C., J.D. Barber, and G.J. Barton. 2008. The Jpred 3 secondary structure prediction server. *Nucleic Acids Res.* 36:W197–201. doi:10.1093/nar/gkn238.

Currie, J.D., S. Stewman, G. Schimizzi, K.C. Slep, A. Ma, and S.L. Rogers. 2011. The microtubule lattice and plus-end association of *Drosophila* Mini spindles is spatially regulated to fine-tune microtubule dynamics. *Mol. Biol. Cell*. 22:4343–4361. doi:10.1091/mbc.E11-06-0520.

De la Mora-Rey, T., B.D. Guenther, and B.C. Finzel. 2013. The structure of the TOG-like domain of *Drosophila melanogaster* Mast/Orbit. *Acta Crystallogr. Sect. F Struct. Biol. Cryst. Commun.* 69:723–729. doi:10.1107/S1744309113015182.

Dereeper, A., V. Guignon, G. Blanc, S. Audic, S. Buffet, F. Chevenet, J.F. Dufayard, S. Guindon, V. Lefort, M. Lescot, J.M. Claverie, and O. Gascuel. 2008. Phylogeny.fr: robust phylogenetic analysis for the non-specialist. *Nucleic Acids Res.* 36:W465–469. doi:10.1093/nar/gkn180.

Drozdetskiy, A., C. Cole, J. Procter, and G.J. Barton. 2015. JPred4 : a protein secondary structure prediction server. *Nucleic Acids Res*. 43:389–394. doi:10.1093/nar/gkv332.

Emsley, P., B. Lohkamp, W.G. Scott, and K. Cowtan. 2010. Features and development of Coot. *Acta Crystallogr. Sect. D Biol. Crystallogr.* 66:486–501. doi:10.1107/S0907444910007493.

Fox, J.C., A.E. Howard, J.D. Currie, S.L. Rogers, and K.C. Slep. 2014. The XMAP215 family drives microtubule polymerization using a structurally diverse TOG array. *Mol. Biol. Cell*. 25:2375–2392. doi:10.1091/mbc.E13-08-0501.

Gard, D.L., and M.W. Kirschner. 1987. A microtubule-associated protein from *Xenopus* eggs that specifically promotes assembly at the plus-end. *J. Cell Biol.* 105:2203–2215. doi:10.1083/jcb.105.5.2203.

Gish, W., S.F. Altschul, D.J. Lipman, W. Miller, and E.W. Myers. 1990. Basic local alignment search tool. *J. Mol. Biol.* 215:403–10. doi:10.1016/S0022-2836(05)80360-2.

Goujon, M., H. McWilliam, W. Li, F. Valentin, S. Squizzato, J. Paern, and R. Lopez. 2010. A new bioinformatics analysis tools framework at EMBL-EBI. *Nucleic Acids Res.* 38:W695–W699. doi:10.1093/nar/gkq313.

Grosse-Kunstleve, R.W., and P.D. Adams. 2003. Substructure search procedures for macromolecular structures. *Acta Crystallogr. - Sect. D Biol. Crystallogr.* 59:1966–1973. doi:10.1107/S0907444903018043.

Guindon, S., J.F. Dufayard, V. Lefort, M. Anisimova, W. Hordijk, and O. Gascuel. 2010. New algorithms and methods to estimate maximum-likelihood phylogenies: Assessing the performance of PhyML 3.0. *Syst. Biol.* 59:307–321. doi:10.1093/sysbio/syq010.

Holm, L., and P. Rosenstrom. 2010. Dali server: Conservation mapping in 3D. *Nucleic Acids Res.* 38:W545–9. doi:10.1093/nar/gkq366.

Howard, A.E., J.C. Fox, and K.C. Slep. 2015. *Drosophila melanogaster* Msps TOG3 utilizes unique structural elements to promote domain stability and maintain a TOG1- and TOG2-like tubulin-binding surface. *J. Biol. Chem.* 290:10149–10162. doi:10.1074/jbc.M114.633826.

Jones, D.T. 1999. Protein secondary structure prediction based on position-specific scoring matrices. *Proc. Natl. Acad. Sci.* 292:195–202. doi:10.1006/jmbi.1999.3091.

Leano, J.B., S.L. Rogers, and K.C. Slep. 2013. A cryptic TOG domain with a distinct architecture underlies CLASP-dependent bipolar spindle formation. *Structure*. 21:939–950. doi:10.1016/j.str.2013.04.018.

Lemos, C.L., P. Sampaio, H. Maiato, M. Costa, L. V. Omel'yanchuk, V. Liberal, and C.E. Sunkel. 2000. Mast, a conserved microtubule-associated protein required for bipolar mitotic spindle organization. *EMBO J.* 19:3668–3682. doi:10.1093/emboj/19.14.3668.

Maki, T., A.D. Grimaldi, S. Fuchigami, I. Kaverina, and I. Hayashi. 2015. CLASP2 has two distinct TOG domains that contribute differently to microtubule dynamics. *J. Mol. Biol.* 427:2379–2395. doi:10.1016/j.jmb.2015.05.012.

McCoy, A.J., R.W. Grosse-Kunstleve, P.D. Adams, M.D. Winn, L.C. Storoni, and R.J. Read. 2007. Phaser crystallographic software. *J. Appl. Crystallogr.* 40:658–674. doi:10.1107/S0021889807021206.

McWilliam, H., W. Li, M. Uludag, S. Squizzato, Y.M. Park, N. Buso, A.P. Cowley, and R. Lopez. 2013. Analysis tool web services from the EMBL-EBI. *Nucleic Acids Res.* 41:W597–600. doi:10.1093/nar/gkt376.

Moriarty, N.W., R.W. Grosse-Kunstleve, and P.D. Adams. 2009. Electronic ligand builder and optimization workbench (eLBOW): A tool for ligand coordinate and restraint generation. *Acta Crystallogr. Sect. D Biol. Crystallogr.* 65:1074–1080. doi:10.1107/S0907444909029436.

Patel, K., E. Nogales, and R. Heald. 2012. Multiple domains of human CLASP contribute to microtubule dynamics and organization in vitro and in *Xenopus* egg extracts. *Cytoskeleton*. 69:155–165. doi:10.1002/cm.21005.

Popov, A. V., A. Pozniakovsky, I. Arnal, C. Antony, A.J. Ashford, K. Kinoshita, R. Tournebize, A.A. Hyman, and E. Karsenti. 2001. XMAP215 regulates microtubule dynamics through two distinct domains. *EMBO J.* 20:397–410. doi:10.1093/emboj/20.3.397.

Sievers, F., A. Wilm, D. Dineen, T.J. Gibson, K. Karplus, W. Li, R. Lopez, H. McWilliam, M. Remmert, J. Söding, J.D. Thompson, and D.G. Higgins. 2011. Fast, scalable generation of high-quality protein multiple sequence alignments using Clustal Omega. *Mol. Syst. Biol.* 7:539. doi:10.1038/msb.2011.75.

Slep, K.C. 2009. The role of TOG domains in microtubule plus end dynamics. *Biochem. Soc. Trans.* 37:1002–1006. doi:10.1042/BST0371002.

Slep, K.C., and R.D. Vale. 2007. Structural basis of microtubule plus end tracking by XMAP215, CLIP-170, and EB1. *Mol. Cell*. 27:976–991. doi:10.1016/j.molcel.2007.07.023.

Sousa, A., R. Reis, P. Sampaio, and C.E. Sunkel. 2007. The *Drosophila* CLASP homologue, Mast/Orbit regulates the dynamic behaviour of interphase microtubules by promoting the pause state. *Cell Motil. Cytoskeleton*. 64:605–620. doi:10.1002/cm.20208.

Tamura, K., G. Stecher, D. Peterson, A. Filipski, and S. Kumar. 2013. MEGA6: Molecular evolutionary genetics analysis version 6.0. *Mol. Biol. Evol.* 30:2725–2729. doi:10.1093/molbev/mst197.

Terwilliger, T. 2004. SOLVE and RESOLVE: Automated structure solution, density modification, and model building. *J. Synchrotron Radiat.* 11:49–52. doi:10.1107/S0909049503023938.

Terwilliger, T.C., R.W. Grosse-Kunstleve, P. V. Afonine, N.W. Moriarty, P.D. Adams, R.J. Read, P.H. Zwart, and L.W. Hung. 2008. Iterative-build OMIT maps: Map improvement by iterative model building and refinement without model bias. *Acta Crystallogr. Sect. D Biol. Crystallogr.* 64:515–524. doi:10.1107/S0907444908004319.

Terwilliger, T.C., R.W. Grosse-Kunstleve, P. V. Afonine, N.W. Moriarty, P.H. Zwart, L.W. Hung, R.J. Read, and P.D. Adams. 2007. Iterative model building, structure refinement and density modification with the PHENIX AutoBuild wizard. *Acta Crystallogr. Sect. D Biol. Crystallogr.* 64:61–69. doi:10.1107/S090744490705024X.

Widlund, P.O., J.H. Stear, A. Pozniakovsky, M. Zanic, S. Reber, G.J. Brouhard, A.A. Hyman, and J. Howard. 2011. XMAP215 polymerase activity is built by combining multiple tubulin-binding TOG domains and a basic lattice-binding region. *Proc. Natl. Acad. Sci. U. S. A.* 108:2741–2746. doi:10.1073/pnas.1016498108.

Zwart, P.H., G.-K.R. W., and P.D. Adams. 2005. Xtriage and Fest: automatic assessment of X-ray data and substructure structure factor estimation. *CCP4 Newsl.* 43:27–35.

CHAPTER 3: CRESCERIN1 LOCALIZES TO THE PRIMARY CILIUM IN MAMMALIAN CELLS[1]

3.1. Summary

Many mammalian cell types have a solitary primary cilium extending out from the cell surface. It is yet unknown whether TOG domain containing proteins play a role in regulating their structure and dynamics. In this chapter we investigate Crescerin1's association with the primary cilium and whether it can bind to MTs in cells.

3.2. Introduction

Primary cilia can be described as cellular antennae that relay signals from the external environment into the cell. They project from the surface of the cell into the extracellular matrix. They are usually 5-10 μm in length although they can range from 1 μm in chondrocytes to 30 μm in epithelial cells (Wheatley, 2005; Yoder, 2007; McGlashan et al., 2010; Rich and Clark, 2012). The primary cilium functions as a hub for signaling pathways like Hedgehog, which regulate cell differentiation, cell fate specification and body plan establishment during embryonic development. In post-embryonic stages, the Hedgehog pathway plays an important role in brain development and maintaining neurogenesis (Deshpande et al., 2001; Haycraft et al., 2005; Singla, 2006; Hochman et al., 2006; Wang et

[1]Parts of this chapter previously appeared as an article in the journal Molecular Biology of the Cell. The original citation is as follows: Das, A., D.J. Dickinson, C.C. Wood, B. Goldstein, and K.C. Slep. 2015. Crescerin uses a TOG domain array to regulate microtubules in the primary cilium. *Mol. Biol. Cell*. 26:4248–4264. doi:10.1091/mbc.E15-08-0603.

al., 2009; Wilson and Stainier, 2010; Goetz and Anderson, 2010; Zeng et al., 2010; Polizio et al., 2011; Uchida et al., 2011; Caparros-Martin et al., 2013). The PDGF-α pathway is another example of cilia-based signaling and is important for directed cell-migration in cultured fibroblasts (Schneider et al., 2005, 2010). Receptors for the Sonic Hedgehog (SHH) and PDGF-α ligands, namely Patched and PDGFR-α, localize to the cilia. In addition, many other downstream regulators of the Hedgehog pathway enter or leave the primary cilia in a signal dependent manner (Haycraft et al., 2005; Wang et al., 2009; Wilson and Stainier, 2010; Polizio et al., 2011). Thus, the primary cilium is capable of spatially and temporally segregating signaling components in response to external signals, even though it is not a membrane enclosed compartment.

The ciliary compartment is separated from the cytosolic compartment by a structure at the cilia base known as the cilia pore complex (CPC). Protein trafficking between the two compartments is thought to be regulated and gated at the CPC. Although the complete structure and composition of the CPC is not yet known, it is believed that the mechanism of soluble protein trafficking across the barrier is at least partially analogous to that of the nuclear pore complex (NPC) (Figure 1.2). This view is substantiated by the observed localization of nucleoporins (NUPs) including NUP214 (cytoplasmic FG NUP), NUP37 (outer ring NUP), NUP35 (inner ring NUP), NUP93 (linker NUP) and NUP62 (central FG NUP) at the base of the primary cilium in mammalian cells, as well as by the requirement of Importins and Ran-GTP gradient across the CPC for the proper localization of cilia proteins including Kif17 and retinitis pigmentosa 2 (RP2) (Dishinger et al., 2010; Hurd et al., 2011; Kee et al., 2012). Proteins that enter the cilium by this pathway have a special targeting peptide sequence analogous to the nuclear localization signal (NLS), known as the cilia

localization sequence (CLS), which is recognized by Importin-β2. The translocation of membrane proteins into the ciliary compartment follows a different gating mechanism involving a septin-based periciliary membrane diffusion barrier and the Y-link modules formed by the proteins linked to ciliopathies such as nephronophthisis/Meckel-Gruber Syndrome/Joubert's Syndrome (NPHP/MKS/JBTS) (Figure 1.2) (Craige et al., 2010; Chih et al., 2011; Dowdle et al., 2011; Garcia-Gonzalo et al., 2011; Williams et al., 2011; Hu et al., 2012; Cevik et al., 2013; Awata et al., 2014; Roberson et al., 2015). Once inside the ciliary compartment, the IFT particles A and B bind to many ciliary proteins and transport them to their appropriate location along the axoneme. The IFT cargo includes tubulin, which is delivered to the dynamic plus ends of microtubules at the distal tip of cilia to maintain axoneme length.

TOG domain-containing protein families, ch-TOG and CLASP play an important role in modulating MT dynamics spatially and temporally inside the cell. They belong to a larger MT plus end associated protein family known as the +TIPs. ch-TOG and CLASP localize to the plus ends of MTs by interacting with the MT end-binding protein, EB1, either directly via the EB1-binding SXIP motif in CLASP, or indirectly via secondary association with SLAIN2 in case of ch-TOG (Galjart, 2010; Li et al., 2011; van der Vaart et al., 2011). Although the exact mechanism is yet to be worked out, it is widely believed that these proteins associate with MTs and/or free tubulin via their TOG array and differentially modulate the rates of growth, shrinkage and pause states, to bring about complex MT driven cellular processes including cell migration and bipolar spindle formation during cell division (Cullen et al., 1999; Popov et al., 2001; Brittle and Ohkura, 2005; Drabek et al., 2006; Sousa et al., 2007; Barr and Gergely, 2008; Slep, 2009; Al-Bassam et al., 2010; Al-Bassam and Chang, 2011;

Currie et al., 2011; Widlund et al., 2011; Patel et al., 2012; Leano et al., 2013; Fox et al., 2014; Lacroix et al., 2014; Maki et al., 2015). The most prominent effect of depletion of these proteins in the cell is the failure to form a proper bipolar mitotic spindle resulting in mis-segregation of chromosomes during cell division. TOG family proteins have been studied extensively in the context of cell division and in fact, the *Drosophila* orthologs of ch-TOG and CLASP, Minispindles (Msps) and Multiple Asters (MAST) / Orbit, respectively, are named after their spindle phenotypes associated with mutations/deletions in the *msps* and *mast* genes (Cullen et al., 1999; Lemos et al., 2000). In contrast, very little is known about how the MT dynamics at the tip of the cilia are regulated.

In the previous chapter we have predicted and proved that the Crescerin protein family contains an array of TOG domains, which are capable of increasing MT polymerization rates *in vitro* using canonical TOG-tubulin interactions. Here, we investigate if the Crescerin family of TOG array containing MT associated protein has a role in primary cilia.

3.3. Experimental Procedures

3.3.1. Mammalian expression plasmids

For constitutive expression in mammalian cells driven by the cytomegalovirus (CMV) immediate early promoter, full length and truncated mouse Crescerin1 constructs (Figure 3 B-C and Figure 7) were cloned into pcDNA-DEST47 and pcDNA-DEST53 plasmids using the Gateway cloning system (Invitrogen) generating C-terminal and N-terminal GFP fusion proteins respectively.

3.3.2. Cell culture and transfection

IMCD3 cells were cultured in DMEM:F-12 (1:1) media (Gibco) supplemented with 10% FBS (Gibco) and 1X Anti-Anti (Gibco) at 37 °C and 5% CO_2. HEK-293 cells were cultured in DMEM media (Gibco) supplemented with 10% FBS (Gibco) and 1X antibiotic-antimycotic solution (Anti-Anti, Gibco) at 37 °C and 5% CO_2. For transfection, IMCD3 and HEK-293 cells were seeded in 6-well plates and transfected when they reached 70-80% confluence. One hour prior to transfection the media in the cell-culture plates were replaced with either Opti-MEM (IMCD3) or non-supplemented DMEM (HEK-293). Cells were transfected with 2.5-3 μg of the plasmid DNA per well of a 6-well plate using either Polyethelenimine or Lipofectamine® 3000 (Invitrogen) transfection reagents for HEK-293 cells and IMCD3 cells, respectively. After 6-8 hours of transfection, the cells were seeded on glass cover-slips in low-serum supplemented (0.25% FBS) DMEM. HEK-293 cells were serum-starved for 24-48 hours while IMCD3 cells were serum-starved for 4 days to promote growth arrest and induce ciliogenesis. For MT lattice-binding assays, HEK-293 cells (not serum starved) were fixed 24 hours after transfection.

3.3.3. Immunofluorescence microscopy of mammalian cells

For visualization of primary cilia in mammalian cells, the cells were first treated with PHEM buffer (60 mM PIPES, 21 mM HEPES, 10 mM EGTA, 2 mM $MgCl_2$, pH 7.5) containing 4% formaldehyde for 20 seconds, followed by permeabilization in PHEM buffer supplemented with 0.2% TritonX-100 for 2 minutes. The cells were then fixed in fresh PHEM buffer supplemented with 4% formaldehyde for 20 minutes and then blocked with 10 mg/ml BSA solution dissolved in PHEM buffer supplemented with 0.2% TritonX-100.

Polyclonal antibodies against mouse Crescerin1 were raised in guinea pig (Pocono Rabbit Farm and Laboratory) using purified fragments of TOG1 (residues 67-317) and TOG2 (residues 332-620) as antigen. Mouse monoclonal anti-acetylated tubulin antibody (clone 6-11B-1, T7451, Sigma-Aldrich) was used for labeling the primary cilium, anti-Pericentrin antibody raised in rabbit (ab4448, Abcam) was used for labeling centrioles and basal bodies. Mouse monoclonal anti-alpha tubulin antibody (Clone DM1A, T6199, Sigma-Aldrich) was used for labeling microtubules. Nuclei were stained with DAPI (Molecular Probes, Invitrogen). All samples were mounted with mounting medium (20 mM Tris, pH 8.5, 90% glycerol, 50 mg/ml n-propyl gallate). Images were collected on an inverted epifluorescence microscope (Nikon Eclipse Ti) using a 100X objective. Images were analyzed using NIS-Elements imaging software and ImageJ.

3.4. Results

3.4.1. Crescerin1 localizes to cilia in mammalian cells

We raised an antibody against mouse Crescerin1 N-terminal domains. We used this antibody to stain IMCD3 cells after fixation. This antibody co-localized with the cilia marker, acetylated tubulin and basal body marker, pericentrin, in IMCD3 cells (Figure 3.1A). This antibody is specific to mouse as we did not see similar staining in human cell lines (RPE1 and HEK-293). We also created GFP-tagged full-length mouse Crescerin1 constructs for expression in HEK-293 cells. Crescerin1-GFP localized along the length of the primary cilium and at the basal body at low expression levels (Figure 3.1B). At high expression Crescerin1-GFP accumulated at the basal body and distal tip of primary cilium as well as along cytoplasmic MTs (Figure 3.1C, Appendix 3.1). Cells were fixed and stained with anti-

acetylated tubulin antibody (red) to label cilia and anti-pericentrin antibody (blue) to label basal bodies and centrosomes. We never observed Crescerin1-GFP at the plus ends of cytoplasmic MTs, which is a major difference between Crescerin1 and the other two major TOG–family proteins, ch-TOG and CLASP. This also suggests that Crescerin1 does not preferentially localize to the distal cilia tip through recognition of a GTP-MT cap.

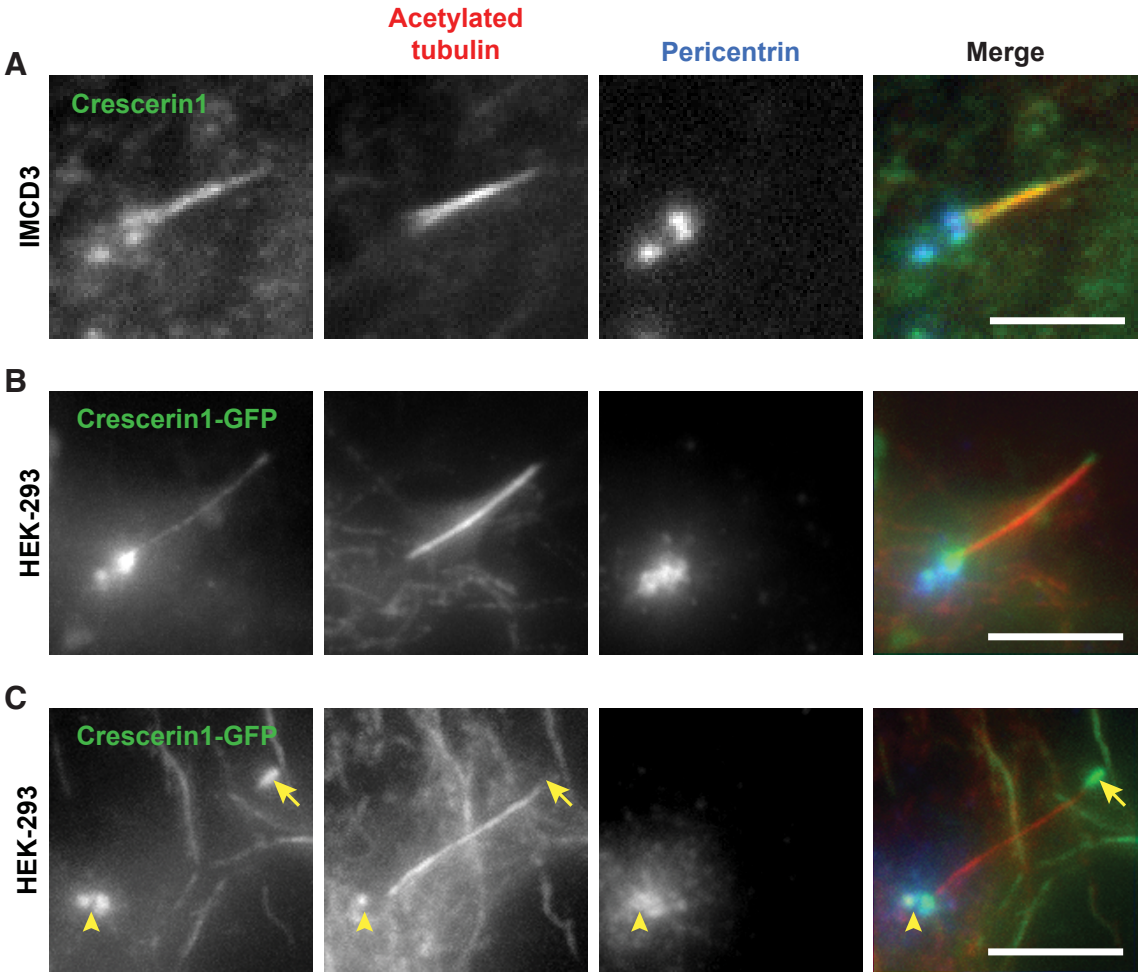

Figure 3.1. Crescerin1 localizes to the primary cilium in mammalian cells.
(A) Antibody staining against endogenous Crescerin1 in IMCD3 cells shows localization to the primary cilium and basal body. (B) GFP-tagged mouse Crescerin1 localizes along the primary cilium and to the basal body in HEK-293 cells. (C) At high expression levels, GFP-tagged Crescerin1 accumulates at the basal body (yellow arrowhead) and distal tip (yellow arrow) of the primary cilium, as well as along the lattice of cytoplasmic microtubules. Primary cilia are labeled using antibody against acetylated tubulin (red) and basal bodies are labeled using antibody against pericentrin (blue). All scale bars = 5 μm.

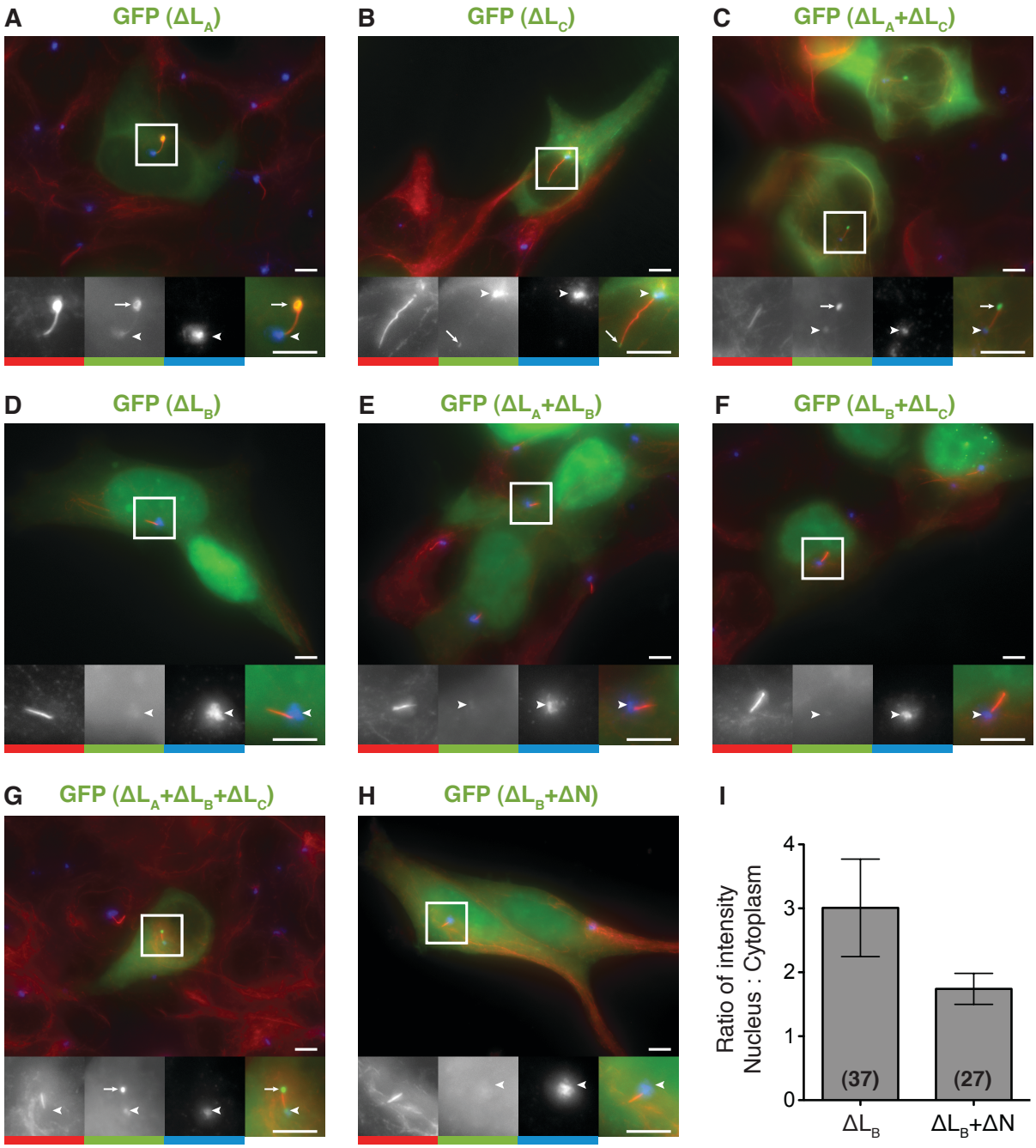

Figure 3.2. Localization of Crescerin1 truncation constructs to cilia, nucleus, or cytoplasm.
(A-C) Crescerin1 truncation constructs lacking fragments L_A or L_C or both can localize to the primary cilium. (D-F) Crescerin1 truncation constructs lacking fragments L_B , L_A+L_B or L_B+L_C localize primarily to the nucleus. (G) Crescerin1 truncation constructs lacking all three linker fragments (L_A+L_B+L_C) can localize to the primary cilium. (H) Crescerin1 truncation constructs lacking L_B as well as the residues 10-67 from the N-terminal unstructured region show reduced localization to the nucleus compared to D, E and F. (I) Quantification of ratio of nuclear vs. cytoplasmic GFP intensity in cells expressing ΔL_B and ΔL_B+ΔN constructs. Primary cilium is labeled with antibody against acetylated tubulin (red) and basal bodies are labeled with antibody against pericentrin (blue). White arrows indicate cilia distal tips and white arrowheads indicate basal bodies. All scale bars = 5 μm.

3.4.2. Cilia import signals in Crescerin1

We then proceeded to identify the sequences that allowed Crescerin1 entry into the ciliary compartment. We created several GFP-tagged constructs truncating Crescerin1 from the N- and C-termini, or deleting regions in the central linker. We found that while the full length protein always localizes to the cilium and basal body, deleting the unstructured N-terminal region preceding TOG1, resulted in a decreased frequency of cilia localization to ~52%. This indicates that the extreme N-terminus of Crescerin1 contains sequences important for cilia localization. However since cilia localization was not completely abolished, we hypothesized that there could be other motifs in Crescerin1 that were important for its cilia localization. Therefore, we tested more constructs with deletions in the large central linker region.

Since the central linker of mouse Crescerin1 is quite large, we denoted three sub-regions within this linker, namely L_A, L_B, and L_C, spanning residues 621-838, 839-1048 and 1049-1242 respectively. Deleting region L_A or L_C did not have any effect on the cilia localization of Crescerin1 (Figure 3.2A-C). Interestingly, we found that when we deleted L_B the protein strongly localized to the nucleus (Figure 3.3D). We saw similar nuclear localization when we extended the deletion on either the N or C-terminal side ($\Delta L_A+\Delta L_B$ and $\Delta L_B+\Delta L_C$) (Figure 3.2E-F) but surprisingly not when we deleted the entire central linker ($\Delta L_A+\Delta L_B+\Delta L_C$) (Figure 3.2G). From this data we concluded that there are at least two regions in the central linker that confer nuclear localization (in region L_A and L_C) as well as at least one nuclear export signal in the region L_B. Given the similarity between nuclear and

cilia localization pathways, we hypothesized that selectively deleting a few of the signals tipped the balance in favor of nuclear or cilia localization.

To test this hypothesis, we then proceeded to see if the N-terminal cilia localization sequence also affected nuclear localization. To test this we created a construct where we deleted residues 6-67 as well as L_B. Deleting the N-terminal cilia localization sequence reduced the nuclear localization of Crescerin1 by almost 40% relative to the ΔL_B construct. This indicates that cilia localization of Crescerin1 is mediated by multiple signals located in different regions of the protein that co-ordinate with each other and possibly with other transport proteins in the cell.

3.4.3. Crescerin1 C-terminal TOG domains promote microtubule lattice binding in cells

We previously noticed that overexpression of full-length Crescerin1 in both HEK-293 and IMCD3 cells caused cytoplasmic MT bundling with Crescerin1 localizing along the MT lattice (Figure 3.1C and Appendix 3.1). Crescerin1 MT-colocalization did not correlate with increased MT acetylation, a post-translational modification common to ciliary MTs. This suggests that Crescerin1 has an inherent ability to associate with MTs. Although Crescerin1's cytoplasmic MT-colocalization is unlikely to be biologically relevant, since it is only observed upon over-expression, we took advantage of this phenotype as an assay to probe the contribution of each TOG domain to MT lattice-association activity. We compared cells with similar Crescerin1-GFP expression levels and classified MT lattice-binding as strong, weak, or no lattice-binding when Crescerin1-GFP co-localized with MTs completely, partially, or was diffuse in the cytoplasm, respectively (Figure 3.3, A-C).

Full-length Crescerin1 was found to strongly co-localize with MTs in 72.3 ± 2.4 % of transfected cells (Figure 3.3D). Mutating the intra-HEAT HR-A loop tubulin-binding region in TOG1 and TOG2 (P109E and Y364E respectively) did not appreciably alter MT association activity. In contrast, mutating the intra-HEAT HR-A loop tubulin-binding region in TOG3 and TOG4 to glutamate (W1274E and F1559E respectively) completely abrogated MT association. An N-terminal Crescerin1 truncation construct containing the central linker and TOG domains 3-4 (L-TOG-34, residues 577-1776) also had robust MT-association activity (Figure 3.4D). Crescerin1 L-TOG-34 MT association was fully ablated when the TOG4 HR-A loop was mutated. A smaller Crescerin1 N-terminal truncation construct containing only a small portion of the central linker and TOG domains 3-4 (L_c-TOG-34, residues 1119-1776) showed minimal MT association that was dependent on TOG3 and TOG4 HR-A loop tubulin-binding determinants. This data suggests that Crescerin1 TOG3 and TOG4 use canonical TOG domain intra-HEAT loop determinants to engage the straight tubulin conformation found in MTs and function synergistically with determinants in the central linker region to bind MTs. This also suggests that while the Crescerin1 N-terminal region encompassing TOG domains 1 and 2 has MT polymerization activity, it does not contribute dramatically to MT lattice-association in our cellular overexpression assay, a characteristic that is shared with the polarized pentameric TOG domain array of the ch-TOG protein family (Currie et al., 2011; Fox et al., 2014). Lastly, we note that constructs that lack TOGs 3 and 4 (1-1242 and 577-1242) were often severely mislocalized into large spherical cytoplasmic aggregates, many of which co-stained with the centrosomal marker pericentrin (Appendix 3.2).

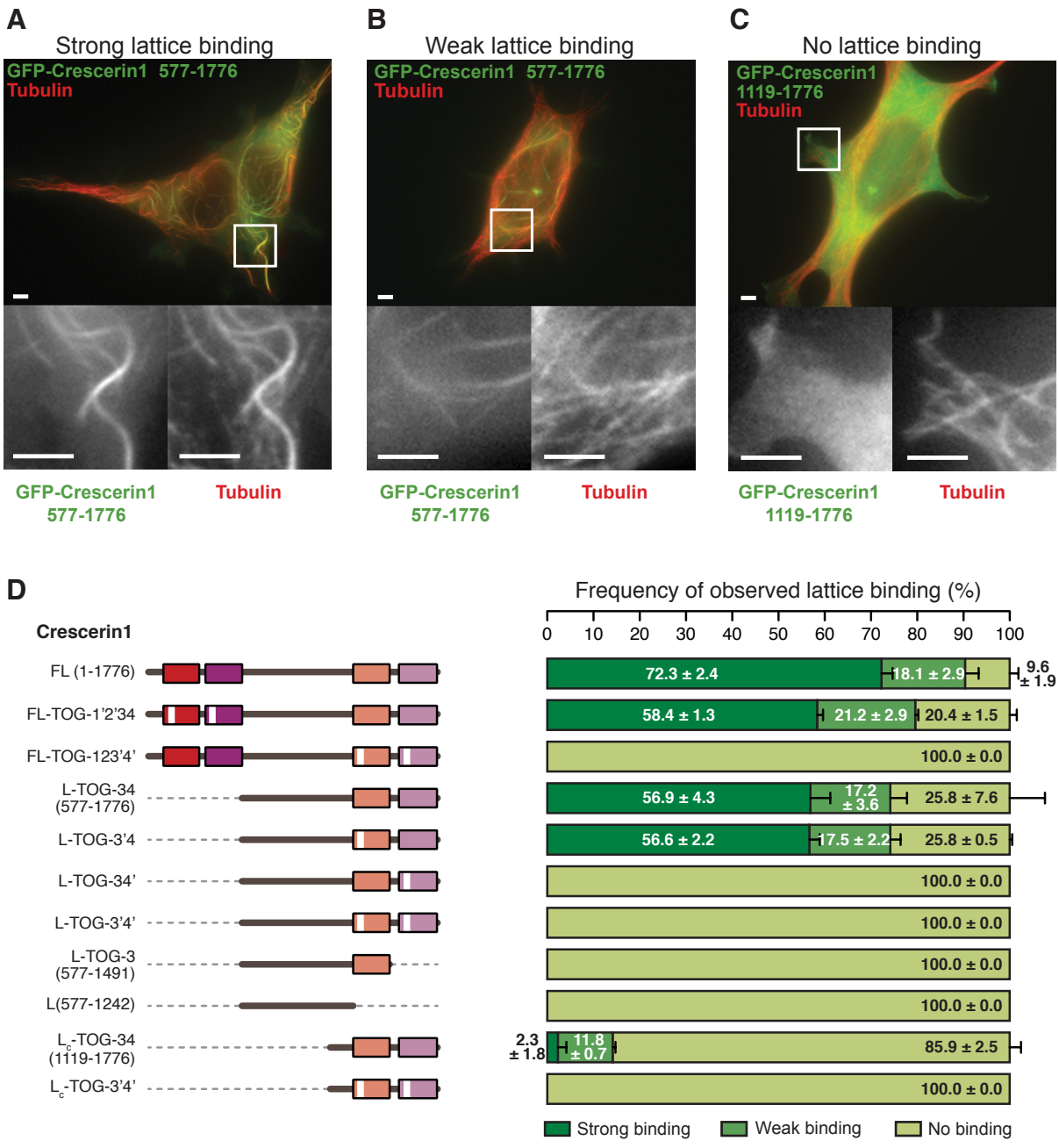

Figure 3.3. Crescerin1 C-terminal TOG domains have MT lattice-binding activity.
(A-C) Examples of strong (A), weak (B) and no MT lattice-association (C) by different Crescerin1 fragments. All scale bars = 5 µm. (D) Summary of MT lattice-binding observations in HEK-293 cells indicates the importance of the Crescerin1 central linker and C-terminal TOG domain pair for MT lattice-association. White vertical lines on select TOG domains indicate an HR A loop mutation that ablates tubulin-binding activity (TOG1:P109E; TOG2:Y364E; TOG3:W1274E; TOG4:F1559E).

3.5. Discussion

Although TOG domain-containing MT regulators have been studied since 1987, we have shown for the first time the localization of a TOG array containing protein in the primary cilium. Shortly after publication of our results, Mick *et al*. identified Crescerin1 in the primary cilia by proximity labeling using ascorbate peroxidase fused to a ciliary targeting sequence (residues 1-103 of NPHP3) as the probe (Mick et al., 2015). In their study, the total spectral counts observed for Crescerin1 was higher than that of known ciliary proteins like IFT52 (component of IFT-B), Sufu (a Hedgehog pathway protein) as well as Polycystin-2 (implicated in polycystic kidney disease, a common ciliopathy).

We have shown that sequences in the extreme N-terminal unstructured region of Crescerin1 influences its cilia localization. We also found that regions in the central linker of Crescerin1 were important for nuclear import and export of Crescerin1. Interestingly, the N-terminal cilia localization sequence also influenced nuclear localization further emphasizing the similarity between nuclear and ciliary import pathways. Utilizing multiple NLSs and NESs to fine tune nuclear, cytoplasmic and ciliary localization appear to be a common theme in another ciliary protein, RSP3 (Yan et al., 2015). The Verhey lab has previously shown that Importin-β2 (also known as Karyopherin- β2) was involved in transporting ciliary proteins like Kif-17 to the cilia (Kee et al., 2012). Importin-β2 recognizes sequence motifs known as PY-NLSs, which are found in nuclear proteins like hnRNP A1, hnRNP D, TAP, HuR, hnRNP F, hnRNP M and PQBP-1 (Lee et al., 2006). These motifs end with a conserved proline and tyrosine at the C-terminus and is preceded by either a hydrophobic patch or a basic patch as shown in Appendix 3.3A. Upon examining the Crescerin1 amino acid

sequence we found a PY-NLS like motif in residues 6-29, and additional sequences further downstream which have some but not all features of the consensus PY-NLS (Appendix 3.3B).

In a major deviation from ch-TOG and CLASP families, we did not find Crescerin1 at the plus ends of cytoplasmic microtubules. We also did not find any sequence motifs such as the SXIP or CAP-Gly domains that could confer binding to EB1 to recruit Crescerin1 to the plus tip. This raises the question, how does Crescerin1 localize to the dynamic plus ends of microtubules at the distal tip of the axoneme? One hypothesis is that Crescerin1 is coupled to the IFT machinery. A previous study in *C. elegans* has shown that the IFT-B components, CHE-13 and OSM-5 are necessary for the proper localization of the worm Crescerin homolog, CHE-12 to the cilia of sensory neurons (Bacaj et al., 2008). However, further experiments are necessary to establish the interactions of Crescerin1 with the IFT complex proteins in mammalian cells.

We found that the central linker with the C-terminal TOG(3+4) pair, when overexpressed in cells, can bind the lattice of cytoplasmic MTs. This parallels similar effects observed when a linker-TOG3-4 and a linker-TOG5 construct from the *Drosophila* ch-TOG family member Msps were overexpressed, yielding MT lattice association that was dependent on determinants in both the preceding linker and the TOG domain(s) (Currie et al., 2011). In contrast, Msps TOG1 and TOG2 do not appear to promote MT lattice association but have been shown to interact with free tubulin heterodimers over gel filtration, an activity that Msps TOG3 and TOG4 lack (Slep and Vale, 2007; Fox et al., 2014). This suggests that different TOG domains in the Msps array recognize different tubulin states: free tubulin

versus polymerized tubulin. Collectively, this leads us to hypothesize that the Crescerin TOG array may also be polarized with differential tubulin-binding activity, where the N-terminal TOG domains bind and promote tubulin incorporation into growing MTs while the C-terminal TOG pair affords MT association.

Searching the NCBI ClinVar database for human disease case studies that have variations in the Crescerin1 (FAM179B) gene, we found seven entries where large sections of chromosome 14 including the *FAM179B* gene were duplicated. Interestingly, in one of these cases, a shorter fragment spanning only six genes was duplicated, including the first exon of *FAM179B* gene (GRCh38/hg38 14q21.2(chr14:44283179-44978212)x3). This could possibly result in the expression of a truncated protein product containing the N-terminal 682 amino acids of Crescerin1, which includes TOG1, TOG2 and a short region of the central linker. The human subject in this case was reported to exhibit developmental defects. In our cellular assays we have observed that a truncated form of Crescerin1-GFP containing TOG1, TOG2 and central linker forms spherical aggregates in the cytoplasm which further co-stain with centrosomal markers like pericentrin (Appendix 3.2). Mislocalization of centrosomal proteins to aggregates could have detrimental effects on cell division and ciliogenesis, which may explain the developmental defects observed in the patient. However, further experiments are necessary to rule out the effects of overexpressing of the five other genes in the duplicated region of chromosome 14.

REFERENCES

Al-Bassam, J., and F. Chang. 2011. Regulation of microtubule dynamics by TOG-domain proteins XMAP215/Dis1 and CLASP. *Trends Cell Biol.* 21:604–614. doi:10.1016/j.tcb.2011.06.007.

Al-Bassam, J., H. Kim, G. Brouhard, A. van Oijen, S.C. Harrison, and F. Chang. 2010. CLASP promotes microtubule rescue by recruiting tubulin dimers to the microtubule. *Dev. Cell*. 19:245–258. doi:10.1016/j.devcel.2010.07.016.

Awata, J., S. Takada, C. Standley, K.F. Lechtreck, K.D. Bellve, G.J. Pazour, K.E. Fogarty, and G.B. Witman. 2014. NPHP4 controls ciliary trafficking of membrane proteins and large soluble proteins at the transition zone. *J. Cell Sci.* 127:4714–4727. doi:10.1242/jcs.155275.

Bacaj, T., Y. Lu, and S. Shaham. 2008. The conserved proteins CHE-12 and DYF-11 are required for sensory cilium function in *Caenorhabditis elegans*. *Genetics*. 178:989–1002. doi:10.1534/genetics.107.082453.

Barr, A.R., and F. Gergely. 2008. MCAK-independent functions of ch-Tog/XMAP215 in microtubule plus-end dynamics. *Mol. Cell. Biol.* 28:7199–7211. doi:10.1128/MCB.01040-08.

Brittle, A.L., and H. Ohkura. 2005. Mini spindles, the XMAP215 homologue, suppresses pausing of interphase microtubules in *Drosophila*. *EMBO J.* 24:1387–1396. doi:10.1038/sj.emboj.7600629.

Caparros-Martin, J.A., M. Valencia, E. Reytor, M. Pacheco, M. Fernandez, A. Perez-Aytes, E. Gean, P. Lapunzina, H. Peters, J.A. Goodship, and V.L. Ruiz-Perez. 2013. The ciliary EVC/EVC2 complex interacts with Smo and controls Hedgehog pathway activity in chondrocytes by regulating Sufu/Gli3 dissociation and Gli3 trafficking in primary cilia. *Hum. Mol. Genet.* 22:124–139. doi:10.1093/hmg/dds409.

Cevik, S., A.A.W.M. Sanders, E. Van Wijk, K. Boldt, L. Clarke, J. van Reeuwijk, Y. Hori, N. Horn, L. Hetterschijt, A. Wdowicz, A. Mullins, K. Kida, O.I. Kaplan, S.E.C. van Beersum, K. Man Wu, S.J.F. Letteboer, D.A. Mans, T. Katada, K. Kontani, M. Ueffing, R. Roepman, H. Kremer, and O.E. Blacque. 2013. Active transport and diffusion barriers restrict Joubert Syndrome-associated ARL13B/ARL-13 to an Inv-like ciliary membrane subdomain. *PLoS Genet.* 9:e1003977. doi:10.1371/journal.pgen.1003977.

Chih, B., P. Liu, Y. Chinn, C. Chalouni, L.G. Komuves, P.E. Hass, W. Sandoval, and A.S. Peterson. 2011. A ciliopathy complex at the transition zone protects the cilia as a privileged membrane domain. *Nat. Cell Biol.* 14:61–72. doi:10.1038/ncb2410.

Craige, B., C.C. Tsao, D.R. Diener, Y. Hou, K.F. Lechtreck, J.L. Rosenbaum, and G.B. Witman. 2010. CEP290 tethers flagellar transition zone microtubules to the membrane and regulates flagellar protein content. *J. Cell Biol.* 190:927–940.

doi:10.1083/jcb.201006105.

Cullen, C.F., P. Deak, D.M. Glover, and H. Ohkura. 1999. *mini spindles*: A gene encoding a conserved microtubule-associated protein required for the integrity of the mitotic spindle in Drosophila. *J. Cell Biol.* 146:1005–1018. doi:10.1083/jcb.146.5.1005.

Currie, J.D., S. Stewman, G. Schimizzi, K.C. Slep, A. Ma, and S.L. Rogers. 2011. The microtubule lattice and plus-end association of *Drosophila* Mini spindles is spatially regulated to fine-tune microtubule dynamics. *Mol. Biol. Cell*. 22:4343–4361. doi:10.1091/mbc.E11-06-0520.

Deshpande, G., L. Swanhart, P. Chiang, and P. Schedl. 2001. Hedgehog signaling in germ cell migration. *Cell*. 106:759–769.

Dishinger, J.F., H.L. Kee, P.M. Jenkins, S. Fan, T.W. Hurd, J.W. Hammond, Y.N.-T. Truong, B. Margolis, J.R. Martens, and K.J. Verhey. 2010. Ciliary entry of the kinesin-2 motor KIF17 is regulated by importin-β2 and RanGTP. *Nat. Cell Biol.* 12:703–710. doi:10.1038/ncb2073.

Dowdle, W.E., J.F. Robinson, Andreas Kneist, M.S. Sirerol-Piquer, S.G.M. Frints, K.C. Corbit, N.A. Zaghloul, G. Van Lijnschoten, L. Mulders, D.E. Verver, K. Zerres, R.R. Reed, T. Attie-Bitach, C.A. Johnson, J.M. Garcia-Verdugo, N. Katsanis, C. Bergmann, and J.F. Reiter. 2011. Disruption of a ciliary B9 protein complex causes Meckel syndrome. *Am. J. Hum. Genet.* 89:94–110. doi:10.1016/j.ajhg.2011.06.003.

Drabek, K., M. van Ham, T. Stepanova, K. Draegestein, R. van Horssen, C.L. Sayas, A. Akhmanova, T. ten Hagen, R. Smits, R. Fodde, F. Grosveld, and N. Galjart. 2006. Role of CLASP2 in microtubule stabilization and the regulation of persistent motility. *Curr. Biol.* 16:2259–2264. doi:10.1016/j.cub.2006.09.065.

Fox, J.C., A.E. Howard, J.D. Currie, S.L. Rogers, and K.C. Slep. 2014. The XMAP215 family drives microtubule polymerization using a structurally diverse TOG array. *Mol. Biol. Cell*. 25:2375–2392. doi:10.1091/mbc.E13-08-0501.

Galjart, N. 2010. Plus-end-tracking proteins and their interactions at microtubule ends. *Curr. Biol.* 20:R528–537. doi:10.1016/j.cub.2010.05.022.

Garcia-Gonzalo, F.R., K.C. Corbit, M.S. Sirerol-Piquer, G. Ramaswami, E. a Otto, T.R. Noriega, A.D. Seol, J.F. Robinson, C.L. Bennett, D.J. Josifova, J.M. García-Verdugo, N. Katsanis, F. Hildebrandt, and J.F. Reiter. 2011. A transition zone complex regulates mammalian ciliogenesis and ciliary membrane composition. *Nat. Genet.* 43:776–784. doi:10.1038/ng.891.

Goetz, S.C., and K. V Anderson. 2010. The primary cilium: a signalling centre during vertebrate development. *Nat. Rev. Genet.* 11:331–344. doi:10.1038/nrg2774.

Haycraft, C.J., B. Banizs, Y. Aydin-Son, Q. Zhang, E.J. Michaud, and B.K. Yoder. 2005. Gli2 and Gli3 localize to cilia and require the intraflagellar transport protein polaris for

processing and function. *PLoS Genet.* 1:e53. doi:10.1371/journal.pgen.0010053.

Hochman, E., A. Castiel, J. Jacob-Hirsch, N. Amariglio, and S. Izraeli. 2006. Molecular pathways regulating pro-migratory effects of Hedgehog signaling. *J. Biol. Chem.* 281:33860–33870. doi:10.1074/jbc.M605905200.

Hu, Q., L. Milenkovic, H. Jin, M.P. Scott, M. V Nachury, E.T. Spiliotis, and W.J. Nelson. 2012. A Septin diffusion barrier at the base of the primary cilium maintains ciliary membrane protein distribution. *Science.* 329:436–439. doi:10.1126/science.1191054.

Hurd, T.W., S. Fan, and B.L. Margolis. 2011. Localization of retinitis pigmentosa 2 to cilia is regulated by Importin β2. *J. Cell Sci.* 124:718–26. doi:10.1242/jcs.070839.

Kee, H.L., J.F. Dishinger, T.L. Blasius, C.-J. Liu, B. Margolis, and K.J. Verhey. 2012. A size-exclusion permeability barrier and nucleoporins characterize a ciliary pore complex that regulates transport into cilia. *Nat. Cell Biol.* 14:431–437. doi:10.1038/ncb2450.

Lacroix, B., K.G. Bourdages, J.F. Dorn, S. Ihara, D.R. Sherwood, P.S. Maddox, and A.S. Maddox. 2014. In situ imaging in *C. elegans* reveals developmental regulation of microtubule dynamics. *Dev. Cell*. 29:203–216. doi:10.1016/j.devcel.2014.03.007.

Leano, J.B., S.L. Rogers, and K.C. Slep. 2013. A cryptic TOG domain with a distinct architecture underlies CLASP-dependent bipolar spindle formation. *Structure*. 21:939–950. doi:10.1016/j.str.2013.04.018.

Lee, B.J., A.E. Cansizoglu, K.E. Suel, T.H. Louis, Z. Zhang, and Y.M. Chook. 2006. Rules for nuclear localization sequence recognition by Karyopherinβ2. *Cell*. 126:543–558. doi:10.1016/j.cell.2006.05.049.

Lemos, C.L., P. Sampaio, H. Maiato, M. Costa, L. V. Omel'yanchuk, V. Liberal, and C.E. Sunkel. 2000. Mast, a conserved microtubule-associated protein required for bipolar mitotic spindle organization. *EMBO J.* 19:3668–3682. doi:10.1093/emboj/19.14.3668.

Li, W., T. Miki, T. Watanabe, M. Kakeno, I. Sugiyama, K. Kaibuchi, and G. Goshima. 2011. EB1 promotes microtubule dynamics by recruiting Sentin in *Drosophila* cells. *J. Cell Biol.* 193:973–983. doi:10.1083/jcb.201101108.

Maki, T., A.D. Grimaldi, S. Fuchigami, I. Kaverina, and I. Hayashi. 2015. CLASP2 has two distinct TOG domains that contribute differently to microtubule dynamics. *J. Mol. Biol.* 427:2379–2395. doi:10.1016/j.jmb.2015.05.012.

McGlashan, S.R., M.M. Knight, T.T. Chowdhury, P. Joshi, C.G. Jensen, S. Kennedy, and C.A. Poole. 2010. Mechanical loading modulates chondrocyte primary cilia incidence and length. *Cell Biol. Int.* 34:441–446. doi:10.1042/CBI20090094.

Mick, D.U., R.B. Rodrigues, R.D. Leib, C.M. Adams, A.S. Chien, S.P. Gygi, and M. V. Nachury. 2015. Proteomics of primary cilia by proximity labeling. *Dev. Cell*. 1–16. doi:10.1016/j.devcel.2015.10.015.

Patel, K., E. Nogales, and R. Heald. 2012. Multiple domains of human CLASP contribute to microtubule dynamics and organization in vitro and in *Xenopus* egg extracts. *Cytoskeleton*. 69:155–165. doi:10.1002/cm.21005.

Polizio, A.H., P. Chinchilla, X. Chen, S. Kim, D.R. Manning, and N.A. Riobo. 2011. Heterotrimeric G_i proteins link hedgehog signaling to activation of Rho small GTPases to promote fibroblast migration. *J. Biol. Chem.* 286:19589–19596. doi:10.1074/jbc.M110.197111.

Popov, A. V., A. Pozniakovsky, I. Arnal, C. Antony, A.J. Ashford, K. Kinoshita, R. Tournebize, A.A. Hyman, and E. Karsenti. 2001. XMAP215 regulates microtubule dynamics through two distinct domains. *EMBO J.* 20:397–410. doi:10.1093/emboj/20.3.397.

Rich, D.R., and A.L. Clark. 2012. Chondrocyte primary cilia shorten in response to osmotic challenge and are sites for endocytosis. *Osteoarthr. Cartil.* 20:923–930. doi:10.1016/j.joca.2012.04.017.

Roberson, E.C., W.E. Dowdle, A. Ozanturk, F.R. Garcia-Gonzalo, C. Li, J. Halbritter, N. Elkhartoufi, J.D. Porath, H. Cope, A. Ashley-Koch, S. Gregory, S. Thomas, J.A. Sayer, S. Saunier, E.A. Otto, N. Katsanis, E.E. Davis, T. Attie-Bitach, F. Hildebrandt, M.R. Leroux, and J.F. Reiter. 2015. TMEM231, mutated in orofaciodigital and Meckel syndromes, organizes the ciliary transition zone. *J. Cell Biol.* 209:129–142. doi:10.1083/jcb.201411087.

Schneider, L., M. Cammer, J. Lehman, S.K. Nielsen, F. Guerra, Charles, I.R. Veland, C.M. Stock, E.K. Hoffmann, B.K. Yoder, A. Schwab, P. Satir, and S.T. Christensen. 2010. Directional cell migration and chemotaxis in wound healing response to PDGF-AA are coordinated by the primary cilium in fibroblasts. *Cell. Physiol. Biochem.* 25:279–292.

Schneider, L., C.A. Clement, S.C. Teilmann, G.J. Pazour, E.K. Hoffmann, P. Satir, and S.T. Christensen. 2005. PDGFRαα signaling is regulated through the primary cilium in fibroblasts. *Curr. Biol.* 15:1861–1866. doi:10.1016/j.cub.2005.09.012.

Singla, V. 2006. The primary cilium as the cell's antenna: Signaling at a sensory organelle. *Science.* 313:629–633. doi:10.1126/science.1124534.

Slep, K.C. 2009. The role of TOG domains in microtubule plus end dynamics. *Biochem. Soc. Trans.* 37:1002–1006. doi:10.1042/BST0371002.

Slep, K.C., and R.D. Vale. 2007. Structural basis of microtubule plus end tracking by XMAP215, CLIP-170, and EB1. *Mol. Cell*. 27:976–991. doi:10.1016/j.molcel.2007.07.023.

Sousa, A., R. Reis, P. Sampaio, and C.E. Sunkel. 2007. The *Drosophila* CLASP homologue, Mast/Orbit regulates the dynamic behaviour of interphase microtubules by promoting the pause state. *Cell Motil. Cytoskeleton*. 64:605–620. doi:10.1002/cm.20208.

Uchida, H., K. Arita, S. Yunoue, H. Yonezawa, Y. Shinsato, H. Kawano, H. Hirano, R. Hanaya, and H. Tokimura. 2011. Role of sonic hedgehog signaling in migration of cell lines established from CD133-positive malignant glioma cells. *J. Neurooncol.* 104:697–704. doi:10.1007/s11060-011-0552-2.

van der Vaart, B., C. Manatschal, I. Grigoriev, V. Olieric, S.M. Gouveia, S. Bjelic, J. Demmers, I. Vorobjev, C.C. Hoogenraad, M.O. Steinmetz, and A. Akhmanova. 2011. SLAIN2 links microtubule plus end-tracking proteins and controls microtubule growth in interphase. *J. Cell Biol.* 193:1083–1099. doi:10.1083/jcb.201012179.

Wang, Y., Z. Zhou, C.T. Walsh, and A.P. McMahon. 2009. Selective translocation of intracellular Smoothened to the primary cilium in response to Hedgehog pathway modulation. *Proc. Natl. Acad. Sci. U. S. A.* 106:2623–2628. doi:10.1073/pnas.0812110106.

Wheatley, D.N. 2005. Landmarks in the first hundred years of primary (9 + 0) cilium research. *Cell Biol. Int.* 29:333–339. doi:10.1016/j.cellbi.2005.03.001.

Widlund, P.O., J.H. Stear, A. Pozniakovsky, M. Zanic, S. Reber, G.J. Brouhard, A.A. Hyman, and J. Howard. 2011. XMAP215 polymerase activity is built by combining multiple tubulin-binding TOG domains and a basic lattice-binding region. *Proc. Natl. Acad. Sci. U. S. A.* 108:2741–2746. doi:10.1073/pnas.1016498108.

Williams, C.L., C. Li, K. Kida, P.N. Inglis, S. Mohan, L. Semenec, N.J. Bialas, R.M. Stupay, N. Chen, O.E. Blacque, B.K. Yoder, and M.R. Leroux. 2011. MKS and NPHP modules cooperate to establish basal body/transition zone membrane associations and ciliary gate function during ciliogenesis. *J. Cell Biol.* 192:1023–1041. doi:10.1083/jcb.201012116.

Wilson, C.W., and D.Y.R. Stainier. 2010. Vertebrate Hedgehog signaling: cilia rule. *BMC Biol.* 8:102. doi:10.1186/1741-7007-8-102.

Yan, R., X. Hu, W. Zhang, L. Song, J. Wang, Y. Yin, S. Chen, and S. Zhao. 2015. The mouse radial spoke protein 3 is a nucleocytoplasmic shuttling protein that promotes neurogenesis. *Histochem. Cell Biol.* 144:309–319. doi:10.1007/s00418-015-1338-y.

Yoder, B.K. 2007. Role of primary cilia in the pathogenesis of polycystic kidney disease. *J. Am. Soc. Nephrol.* 18:1381–1388. doi:10.1681/ASN.2006111215.

Zeng, H., J. Jia, and A. Liu. 2010. Coordinated translocation of mammalian Gli proteins and Suppressor of Fused to the primary cilium. *PLoS One*. 5:e15900. doi:10.1371/journal.pone.0015900.

CHAPTER 4: THE MICROTUBULE REGULATORY FUNCTION OF CHE-12 IS NECESSARY FOR PROPER CILIA DEVELOPMENT IN *C. ELEGANS*[1]

4.1. Summary

In *C. elegans*, the Crescerin family member, CHE-12 has previously been shown to be important for proper development of amphid cilia. However, the mechanism by which CHE-12 regulates cilia structure remains unclear. We hypothesized that the MT-binding activity of CHE-12's arrayed TOG domains is important for its function in the cilia. In this chapter, we have used Cas9-targeted homologous recombination to introduce mutations and create fluorescent protein fusions at the endogenous *che-12* genomic locus. By measuring cilia length and comparing chemosensory behavior of the wild-type and mutant *che-12* strains, we have shown that mutating key tubulin-binding residues in CHE-12's four TOG domains has a similar effect as deleting the entire *che-12* coding sequence from the *C. elegans* genome, thereby emphasizing the importance of CHE-12's TOG domains in regulating cilia structure and function.

4.2. Introduction

The free-living nematode *Caenorhabditis elegans* is an excellent model system for studying the biology of cilia and proteins involved in ciliopathies. Several genes associated

[1]Parts of this chapter previously appeared as an article in the journal Molecular Biology of the Cell. The original citation is as follows: Das, A., D.J. Dickinson, C.C. Wood, B. Goldstein, and K.C. Slep. 2015. Crescerin uses a TOG domain array to regulate microtubules in the primary cilium. *Mol. Biol. Cell*. 26:4248–4264. doi:10.1091/mbc.E15-08-0603.

with ciliopathies such as polycystic kidney disease (PKD), Bardet-Biedl syndrome (BBS), Meckel-Gruber syndrome (MKS) and nephronophthisis (NPHP) are conserved in *C. elegans* (Inglis et al., 2006). However, unlike vertebrates where a primary cilium appears in a wide variety of cell types, in *C. elegans* only a subset of sensory neurons are ciliated. The anatomy and function of each of the 60 ciliated neurons in *C. elegans* have been characterized, and specific behavioral patterns of the organism have been attributed to these neurons (Inglis et al., 2006). Thus, screening for nervous system defects has identified many cilia-related genes. In addition, the transparent body of the worm allows imaging of fluorescently tagged proteins in the live animal. The *C. elegans* genome has been fully mapped and well-established protocols are available for knocking down endogenous proteins and expressing recombinant transgenes. In recent years, CRISPR-based techniques for targeted genome editing in *C. elegans* have also been developed, which is a huge stride forward in terms of the precision of the genetic perturbations that can be made to the system (Dickinson et al., 2013).

Defects in *C. elegans* sensory cilia cause a wide variety of behavioral phenotypes, including defects in chemosensation, mechanosensation, thermosensation, male mating and entry into dauer state (Inglis et al., 2006; Bae and Barr, 2008). The major chemosensory organs in the *C. elegans* head are structures known as the amphid sensillae, located on the left and right sides, close to the anterior end of the worm (Figure 4.1). Each amphid sensilla is composed of twelve neurons (ASE, ADF, ASG, ASH, ASI, ASJ, ASK, ADL, AWA, AWB, AWC and AFD) and two accessory cells (Amphid sheath cell, AmSh; Amphid socket cell, AmSo). Eight of these twelve neurons have either a single or a pair of simple rod-like cilia (ASE/ ASG/ ASH/ ASI/ ASJ/ ASK, single cilia; ADF/ ADL, double cilia) that are exposed to the environment through a channel formed by the amphid sheath and socket cells,

and are known as amphid channel cilia. In wild-type worms, the amphid neurons can accumulate lipophilic dyes like FITC, DiO and DiI from the environment via the exposed amphid channel cilia. This dye-filling assay is commonly used to screen mutants for defects in cilia structure.

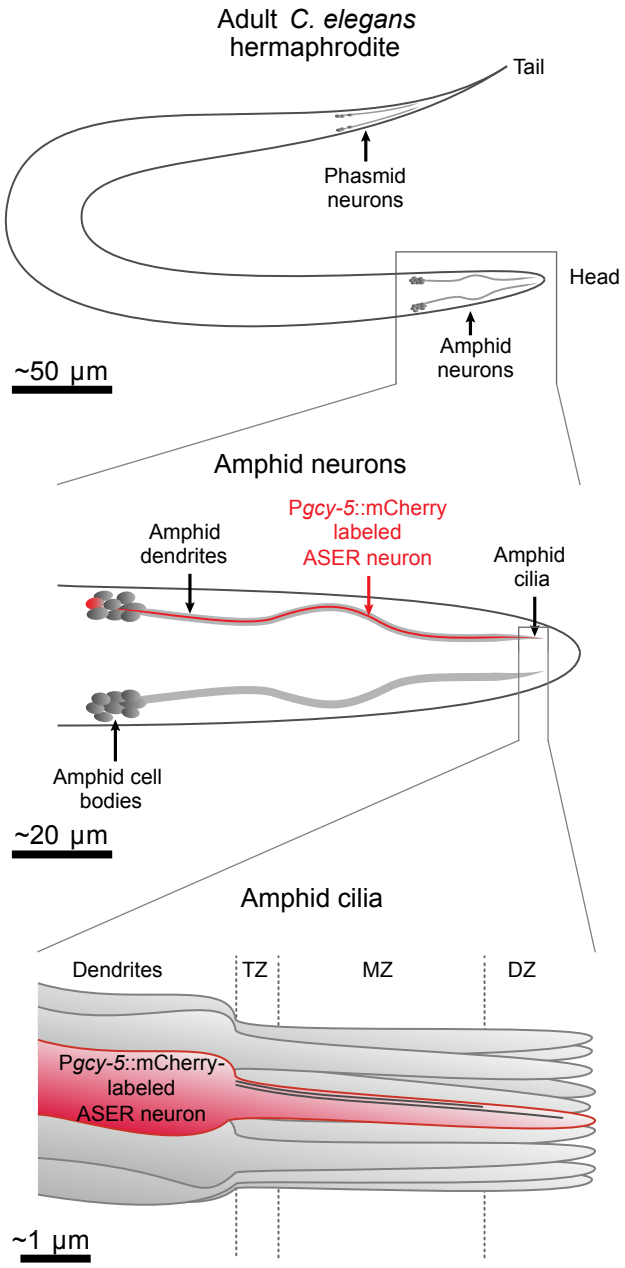

Figure 4.1. Diagram of amphid and phasmid sensillae.
Schematic showing the position of amphid and phasmid neurons in *C. elegans* (top). The amphid neurons each project a dendrite that extends toward the anterior end. These dendrites collectively bundle, and terminate in cilia (bottom). In our studies, we labeled the ASER amphid neuron using a P*gcy-5*::mCherry reporter (red).

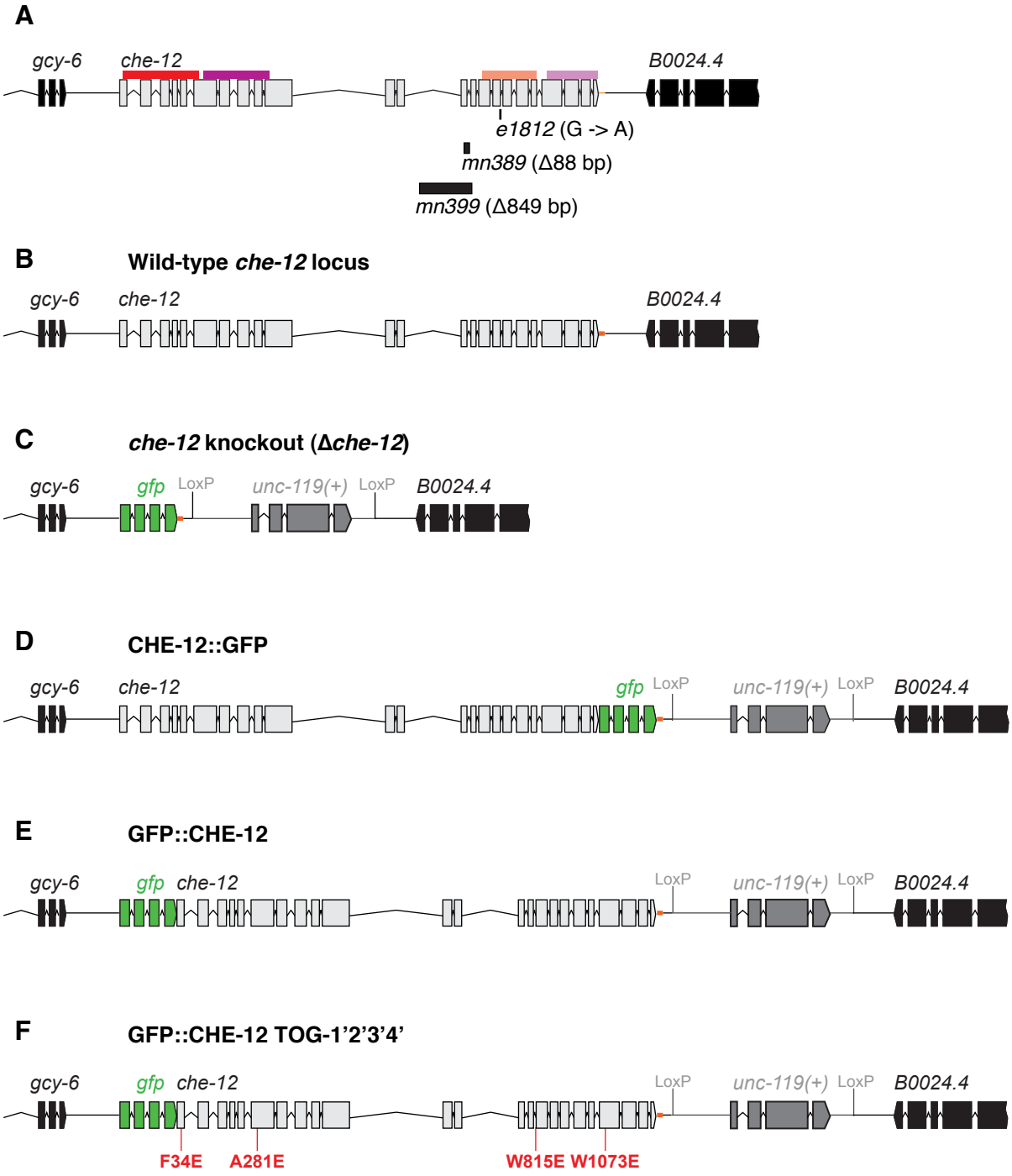

Figure 4.2. Map of *che-12* locus in *che-12* EMS mutant strains and CRISPR strains.
(A) Diagram of the *che-12* locus in the EMS mutant strains *e1812*, *mn389* and *mn399*, previously analyzed by Bacaj *et al*. and Perkins *et al*. The colored boxes on top of *che-12* coding region indicates the genomic location of CHE-12's TOG domain coding sequence and is color coded according to Figure 2.2. (B-F) Diagram showing the wild-type and modified *che-12* loci in the strains used in this study. Boxes indicate exons, bent lines indicate introns and straight lines indicate intergenic regions.

The ortholog of Crescerin1 in *C. elegans* is the protein CHE-12. Previously, three alleles of the *che-12* gene, *e1812*, *mn389* and *mn399* were isolated based on defects in dye-filling behavior. In 1986, Perkins *et al*., analyzed cross sections of the amphid sensilla in the *che-12 (e1812)* strain by electron microscopy and found that the channel cilia were shorter than wild-type and observed a lack of matrix in the lumen of the sheath channel (Perkins et al., 1986). In 2008, Bacaj *et al.*, further characterized the three *che-12* mutant alleles and found that in addition to defects in dye filling, the *che-12* animals showed defects in chemotaxis towards the soluble attractant NaCl and avoidance of a high osmolarity barrier. They also showed that *che-12* is expressed in the amphid neurons with simple rod-like cilia and two phasmid neurons in the tail region in a DAF-19 dependent manner (Bacaj et al., 2008). DAF-19 is a transcription factor that controls the expression of many cilia related genes in *C. elegans*. Bacaj *et al.,* then went on to show that CHE-12 localized to the cilia in the ASER amphid neuron, by specifically driving CHE-12::GFP overexpression in the ASER neuron under the control of the *gcy-5* promoter (Bacaj et al., 2008).

We have shown in our sequence analyses in Chapter 2 that CHE-12 has four TOG domains similar to the mammalian ortholog Crescerin1. The specific mutations in the *che-12 e1812*, *mn389* and *mn399* alleles effectively truncate the protein before or within TOG3 and are summarized in Figure 4.2A. Strain *mn399* has the largest deletion (Figure 4.2A) and exhibits the strongest deviation from wild-type chemotaxis and dye-filling behavior (Bacaj et al., 2008). However, since a large part of CHE-12 including TOG1 and TOG2 would possibly still be expressed in these mutant strains, we wondered whether the phenotypes observed in these three alleles were representative of a complete null mutation. In addition we wanted to study whether CHE-12's TOG domains play a role in regulating cilia structure

and cilia related behavior. To answer these questions we used recently described Cas9 targeted homologous recombination methods (Dickinson et al., 2013) to create several *C. elegans* strains bearing GFP fusions, deletions and point mutations at the endogenous *che-12* locus (Figure 4.2B-F). Editing the endogenous *che-12* locus preserves all native promoter elements, thereby minimizing the risk of non-specific phenotypes arising due to ectopic protein expression. In this chapter, we analyze the chemosensory behavior of these *C. elegans* strains and correlate behavior with the structure of amphid sensory cilia in the respective strains.

4.3. Experimental Procedures

4.3.1. C. elegans culture and strain construction

C. elegans strains were kept at 20 ºC and fed *E. coli* OP50 bacteria except where noted. Strain N2 was used as WT. To label the ASER neuron for imaging, we generated extrachromosomal arrays by injecting a plasmid encoding *Pgcy-5::mCherry* (a gift from Shai Shaham) together with the plasmid pRF4, which carries the dominant *rol-6(su1006)* marker (Mello et al., 1991). Appendix 4.1 shows a list of all strains generated and used in this study. All new *che-12* alleles reported in this study were generated using Cas9-triggered homologous recombination (Dickinson et al., 2013). For each modification to be made, we built a homologous repair template comprising the desired edited nucleotide sequence flanked on each side by 1.5 kb of unmodified genomic sequence. Each repair template also contained an *unc-119(+)* selectable marker flanked by *LoxP* sites. In addition, we generated a Cas9–sgRNA construct by inserting the desired target sequence into the vector pDD162 (Dickinson et al., 2013) using site-directed mutagenesis. Cas9 target sites were selected using

the CRISPR design tool available at http://crispr.mit.edu/ and are listed in Appendix 4.1. Young adults carrying an *unc-119(ed3)* mutant allele were injected with a plasmid mixture containing 50 ng/µL Cas9–sgRNA plasmid, 10 ng/µL homologous repair template, 10 ng/µL pMA122 (*Phsp-16.41::PEEL-1*), 10 ng/µL pGH8 (*Prab-3::mCherry*), 5 ng/µL pCFJ104 (*Pmyo-3::mCherry*) and 2.5 ng/µL pCFJ90 (*Pmyo-2::mCherry*). Injected animals were placed at 25 °C for 8-12 days, then heat shocked for 4 h at 34 °C to induce expression of the PEEL-1 toxin, which kills animals carrying extrachromosomal arrays. Plates carrying non-Uncoordinated animals that survived heat shock and lacked the mCherry co-injection were considered candidate knock-out/knock-in founders, and single worms from these plates were picked to establish lines. Genomic DNA was isolated from each line, and the presence of the desired genome modification was confirmed by PCR and sequencing. Only a single line from each independent plate was kept.

Appendix 4.2 shows the strategy for modifying the *che-12* locus using homologous recombination. To generate *che-12* knockout alleles, we designed a homologous repair template to delete the entire *che-12* coding sequence and replace it with *gfp*. This construct was injected into young adults of strain HT1593 (Maduro and Pilgrim, 1995) for Cas9-triggered homologous recombination as described above. To generate GFP-tagged WT and mutant *che-12* alleles at the endogenous locus, we first removed the *unc-119(+)* selectable marker from the *che-12* knockout strain LP177 by injecting Cre recombinase (Dickinson et al., 2013). The resulting Uncoordinated animals were used for a second round of Cas9-triggered homologous recombination to re-introduce the WT or mutant *che-12* gene.

4.3.2. Conditional endogenous tagging of C. elegans genes

The conditional tagging cassette (CTC) includes a Stop codon and a strong terminator sequence (*let-858* 3'UTR) bounded at either end by two LoxP sites within short synthetic introns, followed by the coding sequence of any fluorescent protein (Appendix 4.3A). We inserted a hygromycin resistance gene in the inter-genic region between the *che-12* and *B0024.4* genes for the selection of positive knock-in candidates. The CTC is introduced between the end of the coding sequence of the gene of interest and its stop codon using Cas9 targeted homologous recombination methods described above. Animals bearing a correct insertion of the CTC at the selected genetic locus express the untagged version of the protein. A cell/tissue specific promoter is then used to drive the expression of Cre-recombinase, in the specific cell/tissue where expression of the fluorescently tagged endogenous protein is desired. The Cre-recombinase will excise out the region enclosed within the LoxP sites in these specific cells, creating a fusion of the gene of interest and the fluorescent protein coding sequences, leading to cell/tissue-specific tagging of endogenous proteins. See Appendix 4.3A for an illustration of this strategy. For future experiments using this strategy we developed a more compact CTC where we included the hygromycin resistance gene between the end of the *let-858* 3'UTR and before the second LoxP site (Appendix 4.3E)

4.3.3. Chemotaxis assays

Chemotaxis plates with a linear NaCl gradient were prepared according to an established protocol (Luo et al., 2010). Briefly, 2% agar solutions in Chemotaxis buffer (50 mM Phosphate, 1 mM $CaCl_2$, 1 mM $MgCl_2$), with or without 60 mM NaCl, were prepared and sterilized by autoclaving. Before pouring, each petridish (circular, 8.5 cm diameter) was

labeled to mark the high-salt and low-salt ends and six parallel sections of equal width perpendicular to the gradient axis. The plates were uniformly elevated at the low-salt end. 20 ml of high-salt agar (containing 60 mM NaCl) was then poured into the plate and allowed to harden. This created a sloped agar block with maximum height at the high-salt end and barely covering the surface at the low-salt end. The plates were then laid flat and 20 ml of the low-salt agar (0 mM NaCl) was poured over the high-salt agar block to create a horizontal surface. Plates were incubated for 16 hours to allow NaCl to diffuse, creating a 0-60 mM NaCl gradient across the agar surface. Control isocratic chemotaxis plates were prepared using sterile chemotaxis agar supplemented with 30 mM NaCl.

The *C. elegans* strains were grown for 3 days on NGM plates seeded with bacteria to obtain a synchronous adult population. The worms were washed off the plates in chemotaxis buffer and collected in microcentrifuge tubes. The worms were allowed to settle to the bottom of the tube and washed three times with chemotaxis buffer to wash off the bacteria, embryos and juveniles. 150-300 adult worms, resuspended in 20 µl of chemotaxis buffer, were then pipetted into the plate center. Timing for the chemotaxis assay was initiated when the buffer evaporated completely and the worms started crawling on the agar surface. After 30 minutes the plates were cooled to 4 °C to paralyze the worms and the number of worms in each of six sectors along the plate's linear NaCl gradient were counted. We determined the normalized worm density for each sector, which we define as follows:

$$\text{Normalized density of sector X} = \frac{\dfrac{\text{No. of worms on sector X}}{\text{Total no. of worms on the plate}}}{\dfrac{\text{Area of sector X}}{\text{Total area of the plate}}}$$

By this measure, when the animals are uniformly distributed throughout the plate, the normalized density for each sector will be equal to one.

4.3.4. Dye-filling assay

Adult *C. elegans* hermaphrodites were washed off agar plates with M9 buffer and collected into 1.5 ml microcentrifuge tubes. The worms were allowed to settle to the bottom of the tube and washed three times in M9 buffer to wash off the bacteria. The worms were then resuspended in M9 buffer containing DiI (Anaspec, Fremont, CA) at a final concentration of 10 μg/ml and incubated at 20 °C for 3 hours. Post incubation, the worms were washed again in M9 buffer and transferred on a new agar plate to remove excess dye. After 5 minutes, the worms were mounted on thin agar pads made of 2.5% agar dissolved in M9 media supplemented with 10 mM NaN_3 to immobilize the animals. The worms were imaged using a Nikon Eclipse Ti microscope equipped with a 100X, 1.4 NA objective and a Yokogawa CSU-10 spinning disk head. A total of ~100 worms were imaged for each strain over the course of three experiments.

4.3.5. Fluorescence microscopy of C. elegans

For fluorescence microscopy of *C. elegans* strains, adult worms were mounted on thin agar pads made of 2.5% agar dissolved in M9 media. We used polystyrene nanoparticle beads (Polysciences, 2.5% by volume, 0.1 μm diameter) to immobilize the worms on the agar pad as described by Kim et al., 2013. The worms were imaged using a Nikon Eclipse Ti microscope equipped with a 100X, 1.4 NA objective and a Yokogawa CSU-10 spinning disk head.

For time-lapse imaging and FRAP of *C. elegans* amphid cilia, worms were mounted on thin agar pads made of 2.5% agar dissolved in M9 media supplemented with 10 mM

NaN_3 to immobilize the animals and imaged using VisiTech VT-HAWK microscope. Images were taken at 500 msec intervals for 5 seconds pre-bleach and 1 minute post-bleach.

4.3.6. Transmission electron microscopy of C. elegans

Adult *C. elegans* hermaphrodites were washed off agar plates with M9 buffer and collected into 1.5 ml microcentrifuge tubes. The worms were allowed to settle to the bottom of the tube and washed in M9 buffer to wash off the bacteria and then were fixed in 2% paraformaldehyde/2.5% glutaraldehyde in 0.1 M sodium cacodylate buffer, pH 7.4 with 0.05% $CaCl_2$. Samples were microwave irradiated using a PELCO BioWave® Pro microwave system (Ted Pella, Inc., Redding, CA) at 450 W to a temperature of 40 °C, allowed to cool to room temperature and stored at 4 °C for several days before processing. Following several washes in 0.1 M sodium cacodylate buffer, the samples were post-fixed in 1% osmium tetroxide/1.25% potassium ferrocyanide in 0.1 M sodium cacodylate buffer for 1 hour, followed by rinses in deionized water. (LP177 worms were encapsulated in agarose before the next step). Samples were dehydrated in a graded series of ethanol solutions (30%, 50%, 75%, 90%, 100%, 100%), followed by two changes in propylene oxide, and infiltration and embedment in Spurr's low viscosity epoxy resin (Polysciences, Inc., Warrington, PA). Ultrathin sections (70-80 nm) were cut using a diamond knife, mounted onto 200 mesh copper grids or Formvar-carbon coated copper slot grids and stained with 4% aqueous uranyl acetate and Reynold's lead citrate. Samples were observed using a LEO EM910 transmission electron microscope operating at 80 kV (Carl Zeiss Microscopy, LLC, Peabody, MA) and digital images were acquired using a Gatan Orius SC1000 CCD Digital Camera with Digital Micrograph 3.11.0 (Gatan, Inc., Pleasanton, CA).

4.4. Results

4.4.1. CHE-12 localizes to a subset of amphid and phasmid cilia in C. elegans

The *C. elegans* Crescerin homolog CHE-12 was previously reported to be required for the structure and function of cilia in the amphid neurons, a subset of sensory neurons in the head (Perkins et al., 1986; Bacaj et al., 2008). Previous studies using extrachromosomal arrays showed that the *che-12* promoter is active in amphid neurons and phasmid neurons, and that overexpressed CHE-12 localizes to cilia and that this localization was dependent on IFT particle B (Bacaj et al., 2008). To characterize endogenous CHE-12 expression and localization, we used Cas9-triggered homologous recombination (Dickinson et al., 2013) to insert *gfp* into the *che-12* locus, generating GFP::CHE-12 and CHE-12::GFP fusion proteins expressed under the control of all native regulatory elements (Figure 4.2, Appendix 4.1 and Appendix 4.2). We additionally expressed mCherry under control of the *gcy-5* promoter to label the ASER neuron, an amphid neuron with a single rod-like cilium (Figure 4.1). GFP::CHE-12 and CHE-12::GFP both localized to multiple sensory cilia in the head including the bundle of parallel amphid channel cilia (Figure 4.3A-B). CHE-12 also expressed in the phasmid neurons in the tail region, where it localized along the phasmid cilia with slight enrichment near the cilia base (Figure 4.3C). CHE-12 GFP constructs showed punctate localization along the amphid and phasmid cilia, which may reflect association with IFT particles.

We have also acquired time-lapse images of the amphid cilia in the CHE-12::GFP strain to observe the dynamics of CHE-12 within the cilia. We bleached the distal tip of the amphid cilia bundle and monitored fluorescence recovery over time. In addition to rapid

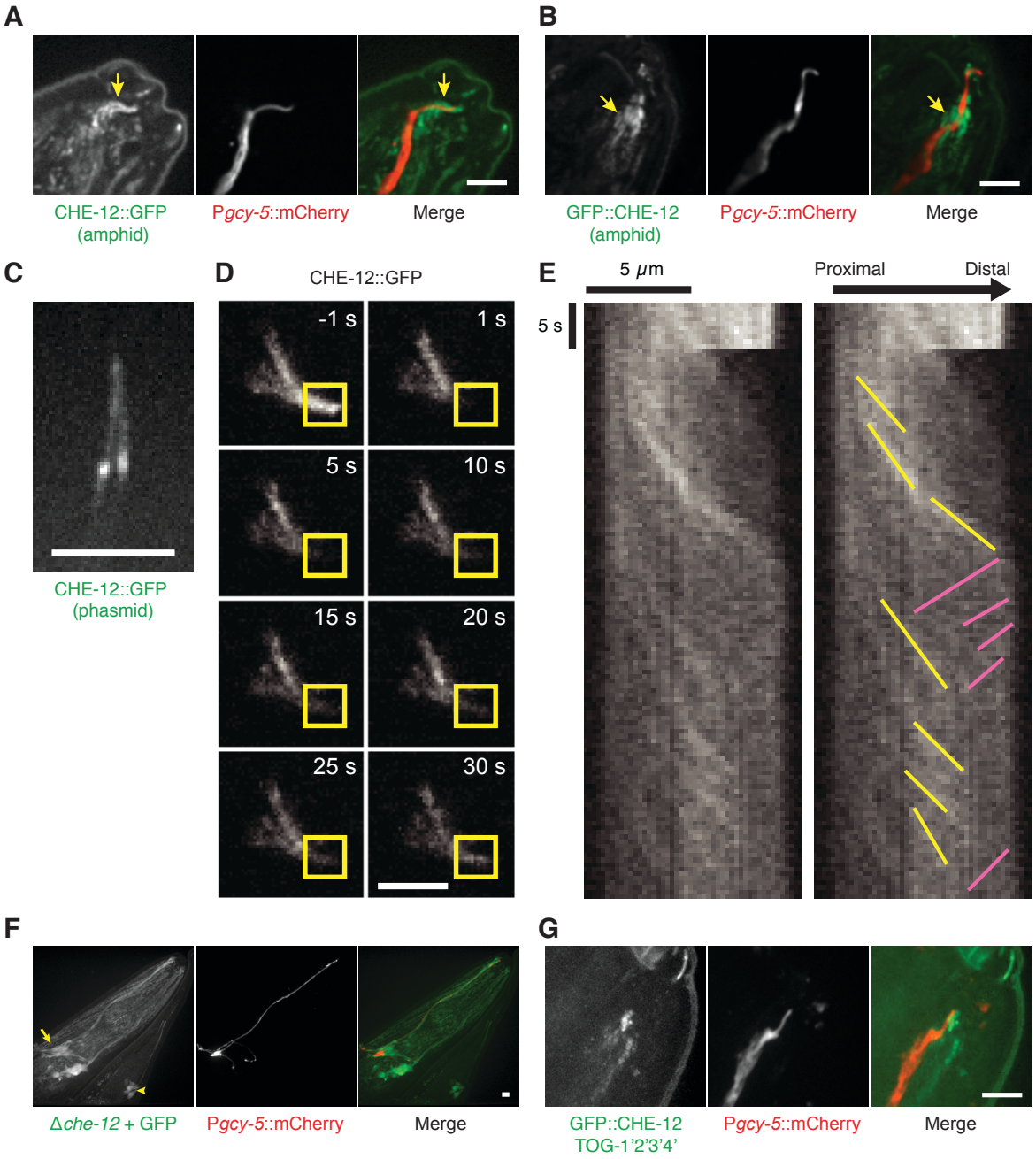

Figure 4.3. In *C. elegans*, the endogenously tagged Crescerin family member, CHE-12, localizes to cilia in amphid and phasmid neurons.
(A,B) CHE-12::GFP (A) and GFP::CHE-12 (B) localize to amphid cilia (yellow arrow). (C) CHE-12::GFP also localizes to the cilia in phasmid neurons (PHA, PHB). (D) Time-lapse images of the CHE-12::GFP strain showing recovery of CHE-12::GFP signal at the distal cilia tip after photo-bleaching the yellow boxed region. (E) Kymograph of data in D, showing anterograde CHE-12::GFP punctae moving along the cilium to quickly recover a photo-bleached region at the distal tip. Yellow lines = anterograde tracks; pink lines = retrograde tracks. (F) Low magnification view of the *C. elegans* head and tail region showing GFP expression in amphid (yellow arrow) and phasmid (yellow arrowhead) neurons in the Δ*che-12* strain. (G) In the GFP::CHE-12 TOG-1'2'3'4' strain, the mutated CHE-12 localizes to amphid cilia. The ASER neuron is labeled by the P*gcy-5*::mCherry reporter. All scale bars = 5 μm.

recovery at the tip we observed the movement of discrete punctae along the cilia in the anterograde direction with an average speed of 0.30 ± 0.09 μm/s (Figures 4.3D-E), suggesting that CHE-12 localization in the cilia is dynamic. Kymograph analysis also revealed retrograde movement with a speed of 0.36 ± 0.08 μm/s (Figure 4.3E).

The arrangement of amphid cilium in a bundle inside the amphid channel presented a challenge to follow a single fluorescent particle all the way from the cilia base to the distal tip. In order to better visualize CHE-12 dynamics in a single amphid cilium, we devised a strategy to fluorescently label endogenously expressing *che-12* in a single amphid neuron, the ASER neuron. Briefly, we introduced a conditional tagging cassette as outlined in Appendix 4.3A at the 3'-end of the *che-12* coding sequence using Cas9 targeted homologous recombination. We then used a ubiquitous or cell/tissue-specific promoter driven Cre-recombinase, expressed from an extra-chromosomal array to allow selective recombination in those specific cells and fuse the *che-12* coding sequence with mNeonGreen coding sequence. This strategy was successful in selectively labeling CHE-12 in the ASER neuron when we used *gcy-5* promoter driven Cre-recombinase (Appendix 4.3B-C). The conditionally tagged CHE-12::mNeonGreen fusion protein localized correctly to the ASER cilium (Appendix 4.3B-C). In contrast when we used a ubiquitous promoter such as *Peft-3* to drive the expression of Cre-recombinase, we observed CHE-12::mNeonGreen signal in all amphid neurons (Appendix 4.3D).

Two *che-12* mutant alleles, *mn389* and *mn399,* were previously shown to cause shortened amphid cilia (Bacaj et al., 2008). However, these two mutations truncate the CHE-12 protein after the second TOG domain, and may not be molecular null mutations. To

determine the effect of a complete loss of CHE-12 function, we used Cas9-triggered homologous recombination to delete the entire *che-12* coding sequence and replace it with *gfp* (Appendices 4.1 and 4.2). As expected, the resulting Δ*che-12* animals expressed GFP primarily in the amphid and phasmid sensory neurons, with GFP signal observed in the cell body and dendrite, overlapping with P*gcy-5*::mCherry expression in the ASER neuron (Figure 4.3F). We next tested a strain where we mutated a conserved hydrophobic residue on the predicted tubulin-binding surface of each TOG domain HR A intra-HEAT loop (F34, A281, W815, W1073) to glutamate (denoted TOG-1'2'3'4') as we did for Crescerin1 *in vitro* and cellular studies (Chapter 2, section 2.4.6 and Chapter 3, section 3.4.3) to ablate tubulin binding. We found that this mutant CHE-12 (CHE-12 TOG-1'2'3'4') was also able to localize correctly to the amphid cilia (Figure 4.3G).

4.4.2. CHE-12 is required for proper chemotaxis and dye-filling in amphid neurons.

C. elegans can sense and respond to a variety of environmental stimuli through their sensory neurons. Specifically, the ASE amphid neurons are specialized to detect soluble chemicals including cations (Na^+, K^+), anions (Cl^-), basic pH, cyclic nucleotides, certain amino acids, and other small molecules including biotin and serotonin (Ward, 1973; Bargmann and Horvitz, 1991; Bargmann, 2006). Functional ASE cilia enable worms to migrate along NaCl gradients and accumulate in regions of their preferred salt concentration (Luo et al., 2014). Previous work found that mutant *che-12(mn389)* animals were unable to chemotax along a NaCl gradient and showed concomitant defects in dye-uptake, an assay commonly employed to examine the fidelity of cilia in *C. elegans* (Bacaj et al., 2008). We asked whether completely deleting *che-12* or mutating the CHE-12 TOG domains would also

compromise chemotaxis along a NaCl gradient as well as the ability to take up dye.

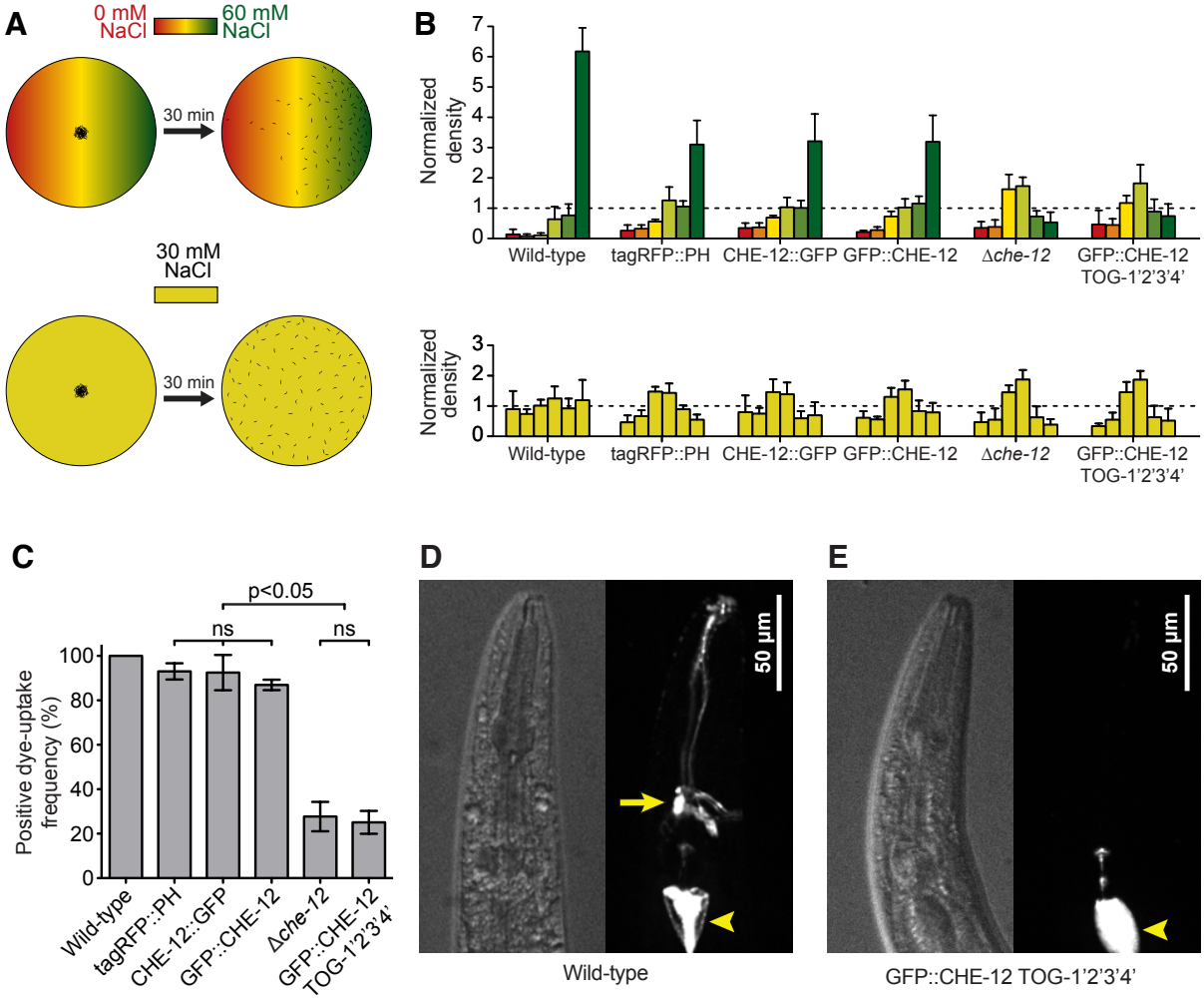

Figure 4.4. Deleting *che-12* or mutating tubulin-binding residues in CHE-12 TOG domains affects amphid cilia function.
(A) Schematic diagram of *C. elegans* chemotaxis assay on a 0-60 mM NaCl gradient (red-green) or 30 mM NaCl isocratic (yellow) agar plates. Worms are placed at the plate center and migration scored after 30 minutes. WT animals preferentially migrate toward 60 mM NaCl on the gradient plate but distribute uniformly on an isocratic plate. (B) Bar graph showing the normalized density (see Experimental Procedures) of worms in different sections of the plate. Error bars indicate standard deviations over the course of 4-5 experiments. (C) Quantitated results of DiI uptake assay. Error bars indicate standard deviations from three independent experiments. (D-E) Images showing strong dye-filling in WT (D) C. elegans amphid neurons (yellow arrow) and no dye-filling in GFP::CHE-12 TOG-1'2'3'4' amphid neurons (E). Gut staining due to feeding: yellow arrowhead. Scale bars = 50 µm.

We used an established chemotaxis assay in which worms were placed in the center of an agar plate containing either an isocratic 30 mM NaCl concentration (control plate), or a

linear 0-60 mM NaCl concentration gradient (Luo et al., 2010) (Figure 4.4A). As expected, WT worms (Strain N2) (Brenner, 2003) were uniformly distributed on control plates but accumulated in the high-salt area of plates containing the linear NaCl gradient (Figure 4.4B). CHE-12::GFP and GFP::CHE-12 strains also accumulated in the high-salt area, but were somewhat reduced in this bias compared to WT. A control strain, expressing a labeled non-neuronal protein (tagRFP::PH) in the same genetic background and containing the same *unc-119* rescue marker used in all Cas9-mediated recombination experiments in this study showed a similar reduction in chemotactic behavior, suggesting that the slightly reduced chemotactic behavior observed in the *gfp*-tagged *che-12* strains is due to *unc-119* replacement. In stark contrast to the WT and control strains, the distribution of Δ*che-12* worms on gradient plates was not different from their distribution on isocratic control plates, demonstrating that these animals are unable to sense and respond to a NaCl gradient (Figure 4.4B). The GFP::CHE-12 TOG-1'2'3'4' mutant strain phenocopied the Δ*che-12* strain, indicating that GFP::CHE-12 TOG-1'2'3'4', while properly localized, is non-functional as measured in this assay.

We performed a dye-uptake assay, which provides a quick readout for defects in cilia structure or organization. Wild-type worms with normal cilia are able to accumulate the lipophilic dye, DiI in their amphids when placed in the dye solution. However the Δ*che-12* and the GFP::CHE-12 TOG-1'2'3'4' mutant strains showed dramatically reduced dye-uptake frequencies compared to the wild-type or CHE-12::GFP and GFP::CHE-12 strains (Figure 4.4C-E). These observations suggest that deleting *che-12* or mutating the tubulin-binding residues of CHE-12's TOG domains compromises cilia structure. To test this, we next measure the lengths of the ASER cilium in these *C. elegans* strains.

4.4.3. CHE-12 is necessary for proper amphid cilia development and organization in C. elegans

To probe the role of CHE-12 in cilia structure, we first scored cilium length in ASER neurons using the P*gcy-5*::mCherry reporter to visualize the ASER dendrite and cilium (Figure 4.5A-B). ASER cilia in the wild-type (WT) N2 strain were 7.0 ± 1.7 μm in length. Strikingly, cilia in the Δ*che-12* strain were dramatically shorter, with a length of 3.2 ± 0.6 μm. The phenotype of the *che-12* alleles *mn389* and *mn399* that truncate CHE-12 after TOG2 are milder, with a ~30% decrease in cilia length for the *che-12(mn399)* mutant compared to WT (Bacaj et al., 2008). The more severe 54% decrease in cilia length that we observed in the Δ*che-12* animals suggests that the *mn399* strain may retain partial CHE-12 function and highlights the efficacy of Cas9-triggered homologous recombination to generate complete gene deletions with full loss of function phenotypes.

We also measured cilia length in the GFP-tagged CHE-12 strains. Both CHE-12::GFP and GFP::CHE-12 knock-in animals had cilia that were slightly shorter than WT (6.0 ± 1.5 μm and 5.9 ± 1.5 μm, respectively), suggesting that the terminal tag might have interfered slightly with CHE-12 function, though not as dramatically as the *che-12* deletion. Examination of the tagRFP::PH control strain used to analyze the effect of *unc-119* replacement on phenotypes showed amphid cilia lengths that did not deviate statistically from WT (Figure 4.5A-B).

We next asked whether CHE-12 uses canonical tubulin-binding determinants across its tetra-TOG domain array to promote proper cilia length. Strikingly, the GFP::CHE-12 TOG-1'2'3'4' mutant had amphid sensory cilia of dramatically reduced length (3.4 ± 0.6 μm compared to WT: 7.0 ± 1.7 μm) phenocopying the *che-12* knockout (3.2 ± 0.6 μm) (Figure

4.5A-B). These results strongly suggest that CHE-12 promotes proper cilia structure and length through mechanistic use of its TOG domain array's tubulin-binding activity.

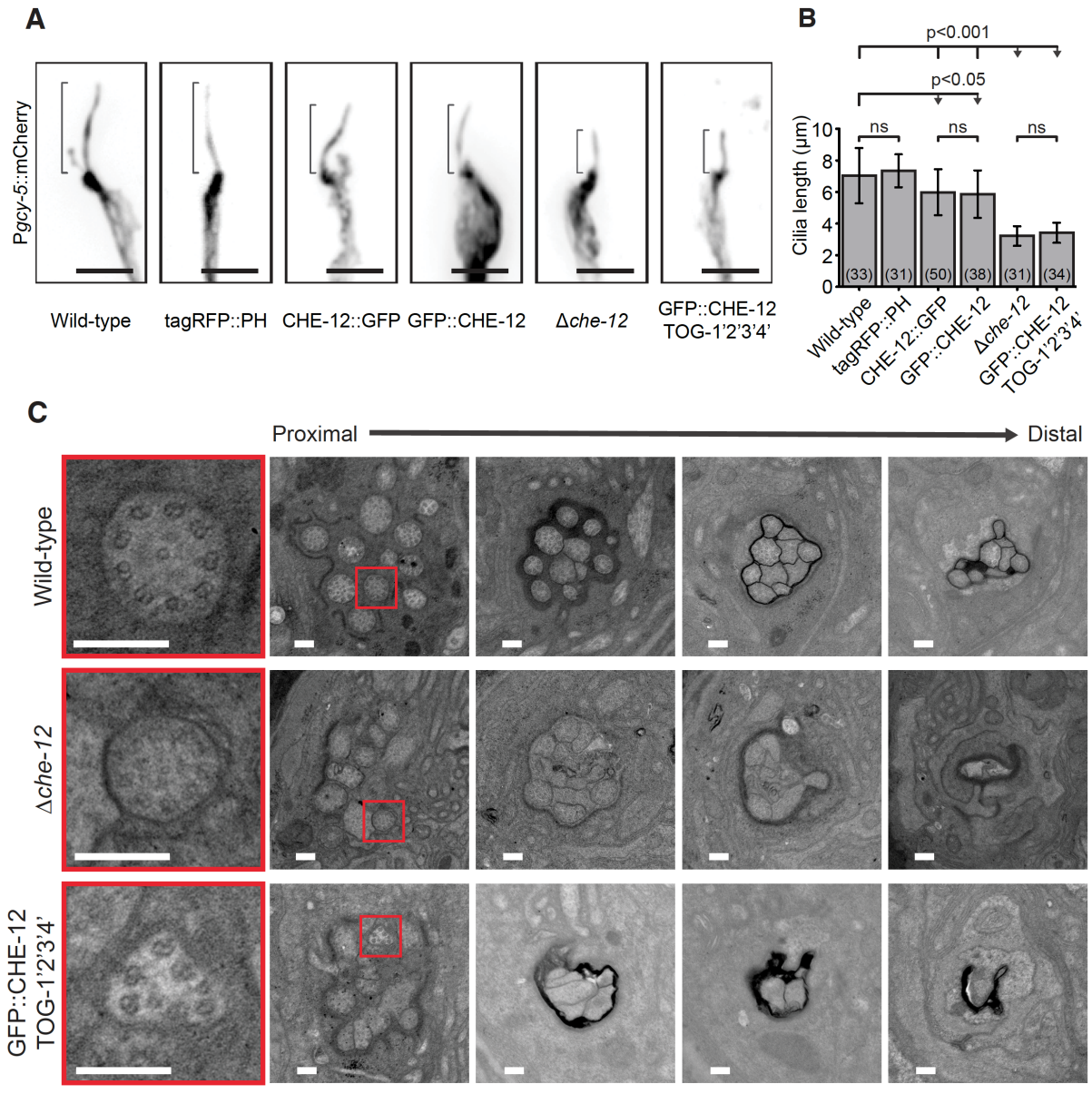

Figure 4.5. Deleting *che-12* or mutating tubulin-binding residues in CHE-12 TOG domains results in shorter and disorganized cilia in *C. elegans* amphid neurons.
(A) Images of the P*gcy-5*::mCherry labeled ASER dendrite with sensory cilium (bracket) from WT and mutant strains. Scale bars = 5 µm. (B) ASER cilium length for strains shown in A. Value in parentheses indicate number of cilia measured/strain; error bars indicate standard deviation. (C) Cross sectional transmission electron micrographs of amphid sensilla in WT, Δ*che-12*, and GFP::CHE-12 TOG-1'2'3'4' strains. Images on left are expanded views of smaller red-boxed regions on the right. Scale bars = 200 nm.

Previous electron microscopy work examining the mutant strain *che-12(mn389)* found ultrastructural defects in amphid cilia structure and the organization of MTs in these cilia (Bacaj et al., 2008). To determine what effect complete loss of CHE-12 function has on cilia ultrastructure, we examined cilia in WT, Δ*che-12*, and GFP::CHE-12 TOG-1'2'3'4' mutant worms using electron microscopy. In WT worms, the proximal sections of each of the 10 amphid channel cilia run parallel to each other forming a well-organized bundle, with most cilia exhibiting the canonical ring of nine doublet MTs surrounding a variable number of central singlet MTs (Figure 4.5C). These bundled cilia become smaller, and more tightly packed towards their distal end but the ring of nine doublet MTs is still evident. In contrast, Δ*che-12 and* GFP::CHE-12 TOG1'2'3'4' mutant worm cilia had poorly defined MT architecture at their proximal ends and no apparent MTs toward their distal ends. Cilia within the bundles appeared disorganized and did not run strictly parallel to each other as in WT, which could account for decreased MT visibility on EM cross-sections.

4.5. Discussion

We have shown that GFP tagged CHE-12 expressed at endogenous levels localizes to the amphid channel cilia and phasmid cilia. In addition, we observed GFP::CHE-12 and CHE-12::GFP localize to a few other cilia in the head region whose cellular identity we were not able to establish. One possible hypothesis is that these unidentified cilia belong to the IL2 neurons, which possess simple rod-like cilia exposed to the environment and are chemosensory in nature. Further experiments expressing IL2 specific markers in the CHE-12::GFP and GFP::CHE-12 strains are necessary to test this hypothesis. We also showed that the localization of CHE-12 to the cilia is dynamic and observed the movement of distinct

punctae in the anterograde and retrograde direction, reminiscent of IFT-coupled movement. Although the previous study by Bacaj *et al*. concluded that CHE-12 may be coupled to IFT, specifically IFT-B, they did not observe IFT-like movements of CHE-12::GFP in the cilia (Bacaj et al., 2008). One possible explanation for this is that extrachromosomal transgenic arrays containing low copy numbers of *che-12* pro::*che-12*::GFP transgene causes CHE-12 expression at levels higher than endogenous, which is sufficient to mask IFT-dependent dynamics in the cilia. However, the speeds of our observed punctae were slower than that previously reported for IFT. This is likely the result of using sodium azide to immobilize the worms for imaging, since sodium azide depletes cellular ATP levels, which in turn affects the movements of the dynein and kinesin IFT motors. In the future, these experiments should be repeated using different means to immobilize the animals that do not affect IFT transport rates.

We observed higher penetrance of the dye-filling defects and shorter cilia in the Δ*che-12* and CHE-12 TOG-1'2'3'4' strains compared to the previously described *che-12* mutant strains *e1812*, *mn389* and *mn399*. This suggests that in each of these strains, the respective truncated CHE-12 protein retained partial activity. Further experiments are necessary to parse out the specific roles of each of the four TOG domains in CHE-12 by selectively mutating individual or a subset of TOG domains.

In our electron microscopy analysis of the amphid cilia in the Δ*che-12* and CHE-12 TOG-1'2'3'4' strains, we found that in addition to being shorter in length compared to the wild-type, the amphid cilia in these two strains were disorganized. In the wild-type animals, the amphid cilia were roughly parallel to the anterior-posterior body axis. However, in the

Δ*che-12* and CHE-12 TOG-1'2'3'4' strains, the amphid cilia lay at various angles to the anterior-posterior body axis, such that the axonemal MTs were not visible in the cross sections for many of the cilia. Perkins *et al*. previously noted that the *che-12 (e1812)* mutant lacked matrix in the lumen of the amphid sheath channel, which is normally secreted by the amphid sheath cell. (Perkins et al., 1986). Whether the disorganization of the amphid cilia is caused due to the lack of matrix in the sheath cell is yet to be determined. Further investigations are necessary to understand the role of CHE-12 in matrix production and secretion in the sheath cell.

REFERENCES

Bacaj, T., Y. Lu, and S. Shaham. 2008. The conserved proteins CHE-12 and DYF-11 are required for sensory cilium function in *Caenorhabditis elegans*. *Genetics*. 178:989–1002. doi:10.1534/genetics.107.082453.

Bae, Y.-K., and M.M. Barr. 2008. Sensory roles of neuronal cilia: cilia development, morphogenesis, and function in *C. elegans*. *Front. Biosci.* 13:5959–5974. doi:10.2741/3129.

Bargmann, C. 2006. Chemosensation in *C. elegans*. *In* WormBook. 1–29.

Bargmann, C.I., and H.R. Horvitz. 1991. Chemosensory neurons with overlapping functions direct chemotaxis to multiple chemicals in *C. elegans*. *Neuron*. 7:729–742. doi:10.1016/0896-6273(91)90276-6.

Brenner, S. 2003. Nature's gift to science (Nobel lecture). *ChemBioChem*. 4:683–687. doi:10.1002/cbic.200300625.

Dickinson, D.J., J.D. Ward, D.J. Reiner, and B. Goldstein. 2013. Engineering the *Caenorhabditis elegans* genome using Cas9-triggered homologous recombination. *Nat. Methods*. 10:1028–1034. doi:10.1038/nmeth.2641.

Inglis, P.N., G. Ou, M.R. Leroux, and J.M. Scholey. 2006. The sensory cilia of *Caenorhabditis elegans*. *In* WormBook. 1–22.

Kim, E., L. Sun, C. V. Gabel, and C. Fang-Yen. 2013. Long-term imaging of *Caenorhabditis elegans* using nanoparticle-mediated immobilization. *PLoS One*. 8:1–6. doi:10.1371/journal.pone.0053419.

Luo, L., J. Greenwood, E. Soucy, D. Kim, and A. Samuel. 2010. Making linear chemical gradients in agar. *Worm Breeder's Gaz.* 18:24–25.

Luo, L., Q. Wen, J. Ren, M. Hendricks, M. Gershow, Y. Qin, J. Greenwood, E.R. Soucy, M. Klein, H.K. Smith-Parker, A.C. Calvo, D.A. Colon-Ramos, A.D.T. Samuel, and Y. Zhang. 2014. Dynamic encoding of perception, memory, and movement in a *C. elegans* chemotaxis circuit. *Neuron*. 82:1115–1128. doi:10.1016/j.neuron.2014.05.010.

Maduro, M., and D. Pilgrim. 1995. Identification and cloning of unc-119, a gene expressed in the *Caenorhabditis elegans* nervous system. *Genetics*. 141:977–988.

Mello, C.C., J.M. Kramer, D. Stinchcomb, and V. Ambros. 1991. Efficient gene transfer in *C. elegans*: extrachromosomal maintenance and integration of transforming sequences. *EMBO J.* 10:3959–3970.

Perkins, L.A., E.M. Hedgecock, J.N. Thomson, and J.G. Culotti. 1986. Mutant sensory cilia in the nematode *Caenorhabditis elegans*. *Dev. Biol.* 117:456–487. doi:10.1016/0012-

1606(86)90314-3.

Ward, S. 1973. Chemotaxis by the nematode *Caenorhabditis elegans*: identification of attractants and analysis of the response by use of mutants. *Proc. Natl. Acad. Sci. U. S. A.* 70:817–821. doi:10.1073/pnas.70.3.817.

CHAPTER 5: DISCUSSION AND FUTURE DIRECTIONS

5.1. Why is Crescerin specific to cilia and how does this compare and contrast with the regulation of MT dynamics in the cytoplasm?

Extensive work has characterized MAPs that regulate cytoplasmic MTs including investigations that probe the roles and mechanisms of the TOG array proteins ch-TOG and CLASP. While MAPs affect MT dynamics, a key underlying factor is the concentration of tubulin and its ability to diffuse throughout the cytoplasm. This contrasts with components at the cilium tip where the singlet microtubule plus ends reside. In this diffusion-limited space, a small fraction of the tubulin that is present diffuses in from the cytoplasm while the major fraction is transported to the cilia distal tip via IFT to reach the concentration required for MT polymerization, particularly during the non-equilibrium phase of ciliogenesis when the flux of IFT-coupled tubulin is greatest (Craft et al., 2015). Previous studies have identified cilia-specific tubulin isoforms in *C. elegans* (Hao et al., 2011) as well as in mammals (Jensen-Smith et al., 2003; Péchart et al., 1999). These tubulin isotypes are coupled to IFT and are actively transported to the distal tip (Hao et al., 2011; Bhogaraju et al., 2013). Little is known about the critical concentration of these tubulin isotypes or their dynamics, but models that predict how cilia of fixed length are generated and maintained rely on specific parameters that include the flux of tubulin to and from the cilia tip as well as the parameters of ciliary microtubule dynamics (Ludington et al., 2015). Recent work has observed that the tubulin diffusion rate is slower at the cilia tip than at other ciliary regions, which suggests

that non-polymerized tubulin engages in macromolecular interactions with ciliary tip components (Craft et al., 2015). The differential nature of tubulin isotype availability, as well as the difference in MT dynamics in the cytoplasm versus the distal cilia tip suggests that additional, cilia-specific MT regulators are required to regulate ciliary MTs. We suggest that these differential requirements underlie the need for Crescerin in the cilium. Just as ch-TOG and CLASP are part of larger regulatory complexes, we anticipate that Crescerin interacts with other regulators of ciliary MT dynamics, coordinating phases of polymerization and depolymerization, driving polymerization during ciliogenesis, or oscillating between short phases of polymerization and depolymerization during the maintenance phase to retain a cilium of proper length. With these observations we re-classify Crescerin as a third conserved TOG-domain containing protein family found in ciliated and flagellated eukaryotes, specialized for MT regulation in cilia. However, many questions remain to be addressed in the future to fully understand the mechanism underlying Crescerin's role in regulating cilia structure and function. Some of these outstanding questions are described below.

5.2. Future directions

We have shown that in *C. elegans*, CHE-12 is necessary for generation of proper amphid cilia and binding of tubulin to CHE-12's TOG domains is necessary for this function. It remains to be seen how CHE-12's TOG domains modulate MT dynamics at the distal cilia tip. A comparison of the fluorescence recovery rates of photobleached tubulin in amphid cilia of the wild type vs. the CHE-12 TOG mutant strains can indicate differences in tubulin turnover rates in the cilia. However, the amphid cilia is able to develop partially in the Δ*che-12* strain, reaching about ~45% of the WT length on average. Thus, the question arises

whether CHE-12 is required for ciliogenesis or maintenance of the cilium length after formation. In order to test this, we can specifically deplete CHE-12 in adult worms after normal cilia have already formed, and monitor ciliary tubulin dynamics post depletion. CHE-12-depletion in adult worms can be achieved by multiple approaches, namely, using an auxin-degron system (Nishimura et al., 2009) or by conditionally deleting CHE-12 in adults using a modified version of the conditional tagging scheme discussed in Chapter 4. Another hypothesis is that CHE-12 may preferentially recognize tubulin isotypes that specifically localize to the distal ends of the axoneme (e.g. TBA-5) (Hao et al., 2011) and stabilize these regions, such that only these regions of the axoneme are lost in absence of functional CHE-12.

We have also observed IFT-like dynamics of CHE-12 within the amphid cilia. Previous studies have shown that CHE-12 requires IFT-B components, specifically CHE-13 and OSM-5, to localize to the cilia (Bacaj et al., 2008). Tubulin transport within the cilia is also largely dependent on IFT, especially during cilia growth (Hao et al., 2011; Bhogaraju et al., 2013; Craft et al., 2015), although diffusive transport may also be relevant (Ludington et al., 2015). The N-terminal Calponin Homology (CH) domain of IFT-81 and the N-terminal positively charged region of IFT-74 together form a tubulin-binding site (Bhogaraju et al., 2013). It is not known whether CHE-12 functions as an additional link between IFT and tubulin. Dual color time-lapse imaging of fluorescently labeled CHE-12 and tubulin is necessary to analyze whether CHE-12 and tubulin punctae co-localize or move independently of each other along the cilia. It is also not known which IFT proteins may directly interact with CHE-12 and whether these interactions are conserved across species. Expressing BirA or APEX tagged CHE-12 and Crescerin1 in *C. elegans* and mammalian

cells respectively, can lead to identification of potential interaction partners (Roux et al., 2012; Lam et al., 2014; Mick et al., 2015).

In addition to interactions with tubulin and IFT components, the Crescerin family proteins may also interact with the transporter protein, Importin-β2, which facilitates entry of proteins like KIF17 and RP2 into the ciliary compartment (Dishinger et al., 2010; Hurd et al., 2011; Kee et al., 2012). We have shown that mouse Crescerin1 contains multiple signal motifs, different combinations of which target the protein to the nucleus, cytoplasm or cilia. We found that Crescerin1 contains multiple PY-NLS like sequences at its N-terminus. PY-NLSs are typically recognized by Importin-β2 (Lee et al., 2006; Xu et al., 2010) for nuclear import in presence of a Ran-GTP gradient across the nuclear membrane. Further experiments are necessary to conclusively prove that Crescerin1's PY-NLS can bind to Importin-β2 and that this interaction is necessary for its import into the ciliary compartment.

In *C. elegans*, *che-12* expression is restricted to a small set of sensory neurons that have a simple rod-shaped cilium. Interestingly, CHE-12 is absent in amphid neurons that have winged or branched cilia (AWA, AWB, AWC, AFD) as well as many others of the total 60 ciliated neurons in the adult hermaphrodite. It is yet unknown whether ciliogenesis in these neurons follow a different mechanism or these neurons express a different protein with similar function as CHE-12. In mammalian systems, different tissues have diversified cilia that perform highly specialized functions, as well as two closely related Crescerin genes. Further work will be necessary to fully understand Crescerin1 and Crescerin2 expression and function in different cell types. Whether knockdown of Crescerin in mammalian cells leads to shorter cilia remains to be investigated.

We have seen that Crescerin's C-terminal TOG domains bind to the MT-lattice in cells while the N-terminal pair promotes MT nucleation *in vitro*. Whether TOG domains from Crescerin2 also show similar tubulin binding activity as Crescerin1 TOGs 3 and 4 is yet unknown. This suggests that the Crescerin1 C-terminal TOG domains preferentially bind to straight tubulin while the N-terminal TOG domains prefer binding to bent tubulin heterodimers. It is also unknown whether each TOG domain in Crescerin acts independently or in a cooperative manner to regulate MT dynamics. Further structural analysis of TOGs 1, 3 and 4 is necessary to determine the underlying cause of differential tubulin binding between these domains. In addition, preferential binding of the different TOG domains to straight or bent tubulin should further be probed through experiments such as co-sedimentation microtubules, analytical ultracentrifugation and analytical size-exclusion chromatography. These experiments can be carried out under conditions that favor the stabilization of the either the polymerized state (paclitaxel, GMPCPP) or unpolymerized state (low temperature) of microtubules. Lastly, rates of polymerization, pause, catastrophe and rescue of labeled microtubules in presence of different Crescerin1 TOG domains should be carefully analyzed by TIRF microscopy in a simplified cell free system to better understand the role of each TOG domain.

REFERENCES

Bacaj, T., Y. Lu, and S. Shaham. 2008. The conserved proteins CHE-12 and DYF-11 are required for sensory cilium function in *Caenorhabditis elegans*. *Genetics*. 178:989–1002. doi:10.1534/genetics.107.082453.

Bhogaraju, S., L. Cajanek, C. Fort, T. Blisnick, K. Weber, M. Taschner, N. Mizuno, S. Lamla, P. Bastin, E. a Nigg, and E. Lorentzen. 2013. Molecular basis of tubulin transport within the cilium by IFT74 and IFT81. *Science*. 341:1009–1012. doi:10.1126/science.1240985.

Craft, J.M., J.A. Harris, S. Hyman, P. Kner, and K.F. Lechtreck. 2015. Tubulin transport by IFT is upregulated during ciliary growth by a cilium-autonomous mechanism. *J. Cell Biol.* 208:223–237. doi:10.1083/jcb.201409036.

Dishinger, J.F., H.L. Kee, P.M. Jenkins, S. Fan, T.W. Hurd, J.W. Hammond, Y.N.-T. Truong, B. Margolis, J.R. Martens, and K.J. Verhey. 2010. Ciliary entry of the kinesin-2 motor KIF17 is regulated by importin-β2 and RanGTP. *Nat. Cell Biol.* 12:703–710. doi:10.1038/ncb2073.

Hao, L., M. Thein, I. Brust-Mascher, G. Civelekoglu-Scholey, Y. Lu, S. Acar, B. Prevo, S. Shaham, and J.M. Scholey. 2011. Intraflagellar transport delivers tubulin isotypes to sensory cilium middle and distal segments. *Nat. Cell Biol.* 13:790–798. doi:10.1038/ncb2268.

Hurd, T.W., S. Fan, and B.L. Margolis. 2011. Localization of retinitis pigmentosa 2 to cilia is regulated by Importin β2. *J. Cell Sci.* 124:718–726. doi:10.1242/jcs.070839.

Jensen-Smith, H.C., R.F. Luduena, and R. Hallworth. 2003. Requirement for the βI and βIV tubulin isotypes in mammalian cilia. *Cell Motil. Cytoskeleton*. 55:213–220. doi:10.1002/cm.10122.

Kee, H.L., J.F. Dishinger, T.L. Blasius, C.-J. Liu, B. Margolis, and K.J. Verhey. 2012. A size-exclusion permeability barrier and nucleoporins characterize a ciliary pore complex that regulates transport into cilia. *Nat. Cell Biol.* 14:431–437. doi:10.1038/ncb2450.

Lam, S.S., J.D. Martell, K.J. Kamer, T.J. Deerinck, M.H. Ellisman, V.K. Mootha, and A.Y. Ting. 2014. Directed evolution of APEX2 for electron microscopy and proximity labeling. *Nat. Methods*. 12:51–54. doi:10.1038/nmeth.3179.

Lee, B.J., A.E. Cansizoglu, K.E. Suel, T.H. Louis, Z. Zhang, and Y.M. Chook. 2006. Rules for nuclear localization sequence recognition by Karyopherinβ2. *Cell*. 126:543–558. doi:10.1016/j.cell.2006.05.049.

Ludington, W.B., H. Ishikawa, Y. V. Serebrenik, A. Ritter, R.A. Hernandez-Lopez, J. Gunzenhauser, E. Kannegaard, and W.F. Marshall. 2015. A systematic comparison of mathematical models for inherent measurement of ciliary length: How a cell can

measure length and volume. *Biophys. J.* 108:1361–1379. doi:10.1016/j.bpj.2014.12.051.

Mick, D.U., R.B. Rodrigues, R.D. Leib, C.M. Adams, A.S. Chien, S.P. Gygi, and M. V. Nachury. 2015. Proteomics of primary cilia by proximity labeling. *Dev. Cell*. 1–16. doi:10.1016/j.devcel.2015.10.015.

Nishimura, K., T. Fukagawa, H. Takisawa, T. Kakimoto, and M. Kanemaki. 2009. An auxin-based degron system for the rapid depletion of proteins in nonplant cells. *Nat. Methods*. 6:917–922. doi:10.1038/nmeth.1401.

Péchart, I., M.L. Kann, N. Levilliers, M.H. Bré, and J.P. Fouquet. 1999. Composition and organization of tubulin isoforms reveals a variety of axonemal models. *Biol. Cell*. 91:685–697. doi:10.1016/S0248-4900(00)88532-9.

Roux, K.J., D.I. Kim, M. Raida, and B. Burke. 2012. A promiscuous biotin ligase fusion protein identifies proximal and interacting proteins in mammalian cells. *J. Cell Biol.* 196:801–810. doi:10.1083/jcb.201112098.

Xu, D., A. Farmer, and Y.M. Chook. 2010. Recognition of nuclear targeting signals by Karyopherin-β proteins. *Curr. Opin. Struct. Biol.* 20:782–790. doi:10.1016/j.sbi.2010.09.008.

APPENDIX 2.1: CH-TOG FAMILY OF TOG DOMAIN CONTAINING PROTEINS

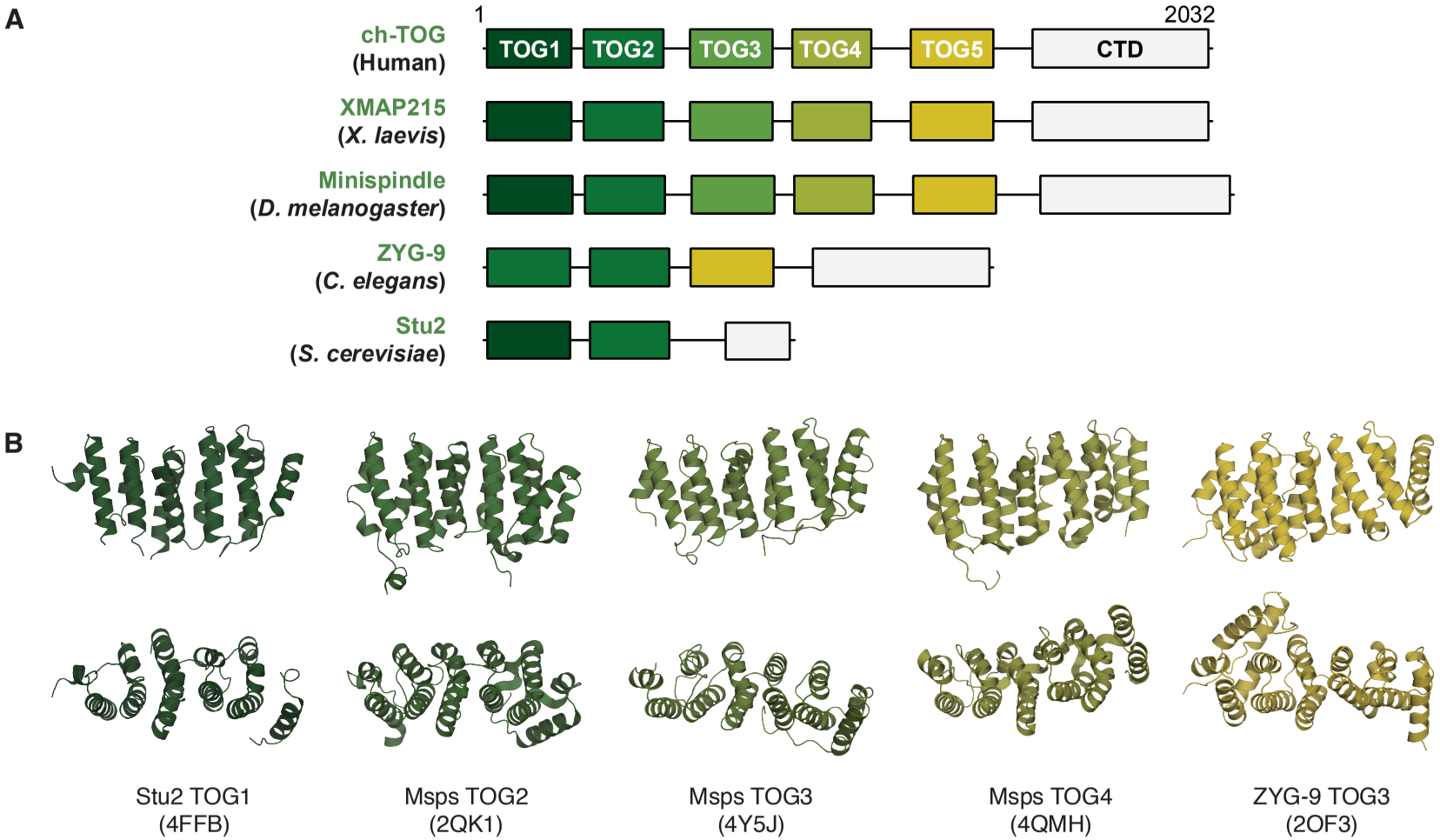

Appendix 2.1. ch-TOG family of TOG domain containing proteins.
(A) Diagram showing the TOG domain arrays in the ch-TOG family proteins. The domains are color coded according to sequence similarity across species. For example, ZYG-9 TOG3 is similar to ch-TOG TOG5. (B) Structures of ch-TOG family TOG domains from different species solved to date and colored according to A. The PDB IDs are shown in parentheses below the respective structure.

APPENDIX 2.2: CLASP FAMILY OF TOG DOMAIN CONTAINING PROTEINS

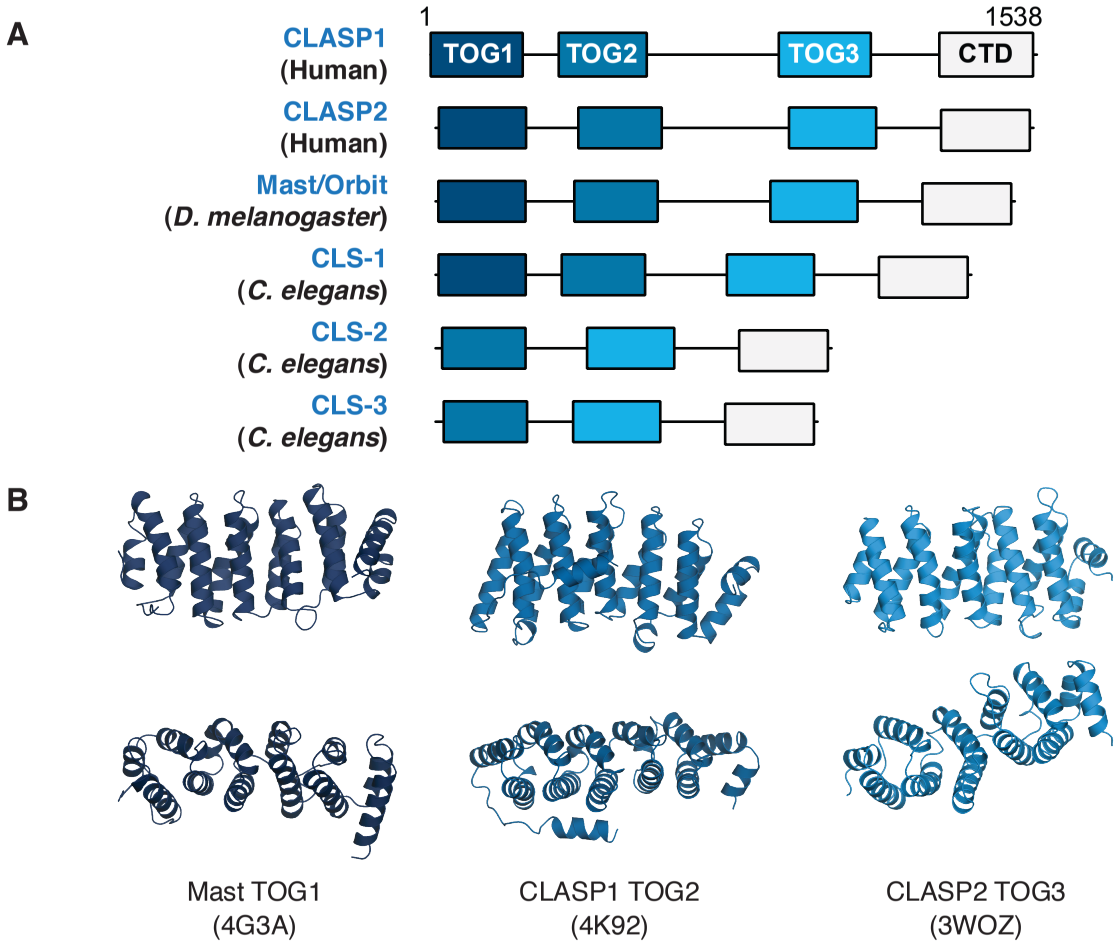

Appendix 2.2. CLASP family of TOG domain containing proteins.
(A) Diagram showing the TOG domain arrays in the CLASP family proteins. The domains are color coded according to sequence similarity across species. For example, CLS-2 TOG2 is similar to CLASP1 TOG3. (B) Structures of CLASP family TOG domains from different species solved to date and colored according to A. The PDB IDs are shown in parentheses below the respective structure.

APPENDIX 2.3: NCBI SEQUENCE IDENTIFIERS FOR CRESCERIN HOMOLOGS IN DIFFERENT SPECIES.

	Name	Organism	NCBI accession no.	No. of amino acids
Crescerin1 (FAM179B) sub-family	Mouse	*Mus musculus*	AAI72117.1	1776
	Human	*Homo sapiens*	XP_005267508.1	1773
	Xenopus	*Xenopus tropicalis*	XP_004917198.1	1164
	Sea urchin	*Strongylocentrotus purpuratus*	XP_783976.2	780
	Drosophila	*Drosophila melanogaster*	NP_608498.3	1655
	C. elegans	*Caenorhabditis elegans*	NP_001256204.1	1282
	Hydra	*Hydra vulgaris*	XP_004205896.1	1192
	Sea anemone	*Nematostella vectensis*	XP_001640509.1	602
	T. adhaerens	*Trichoplax adhaerens*	XP_002113545.1	728
	Sponge	*Amphimedon queenslandica*	XP_003385576.1	1433
	Chlamydomonas	*Chlamydomonas reinhardtii*	XP_001697989.1	761
	Tetrahymena	*Tetrahymena thermophila*	EAR96856.2	2132
	Paramecium	*Paramecium tetraurelia*	XP_001435910.1	1007
Crescerin2 (FAM179A) sub-family	Mouse	*Mus musculus*	XP_006524459.1	1148
	Human	*Homo sapiens*	XP_006712017.1	1028
	Xenopus	*Xenopus tropicalis*	XP_004914873.1	996
	Sea urchin	*Strongylocentrotus purpuratus*	XP_785383.3	655
	Hydra	*Hydra vulgaris*	XP_002157731.2	480
	T. adhaerens	*Trichoplax adhaerens*	XP_002113544.1	1063

APPENDIX 2.4: CRYSTALLOGRAPHIC DATA, PHASING AND REFINEMENT STATISTICS FOR THE CRESCERIN1 TOG2 STRUCTURE

	Native	SeMet derivative
Space group	$P2_12_12$	$P2_12_12$
Unit cell: (Å)		
a	72.4	72.3
b	48.5	48.4
c	68.0	68.2
Wavelength (Å)	0.97926	0.97933
Resolution range (Å)	50 – 2.20 (2.28 – 2.20)	50 - 2.37 (2.45 – 2.37)
Measured reflections	89456	92009
Unique reflections	12609	18721
Redundancy	7.1 (6.8)	4.9 (4.2)
Completeness (%)	99.9 (99.8)	99.9 (99.1)
I/σ	16.6 (4.0)	20.4 (8.4)
R_{sym} (%)	11.9 (57.9)	8.0 (22.6)
Figure of Merit	0.83	
Refinement (Å)	34.65 – 2.20 (2.29 – 2.20)	
R_{work}	0.18 (0.20)	
R_{free}	0.24 (0.25)	
Ramachandran favored (%)	97.9	
Ramachandran allowed (%)	2.1	
RMSD bond lengths (Å)	0.011	
RMSD bond angles (°)	1.185	
Mean B (min/max) ($Å^2$)	35.0 (11.9/99.4)	

Values in parentheses indicate the highest resolution shell.

APPENDIX 2.5: CRESCERIN FAMILY TOG1 SEQUENCE ALIGNMENT

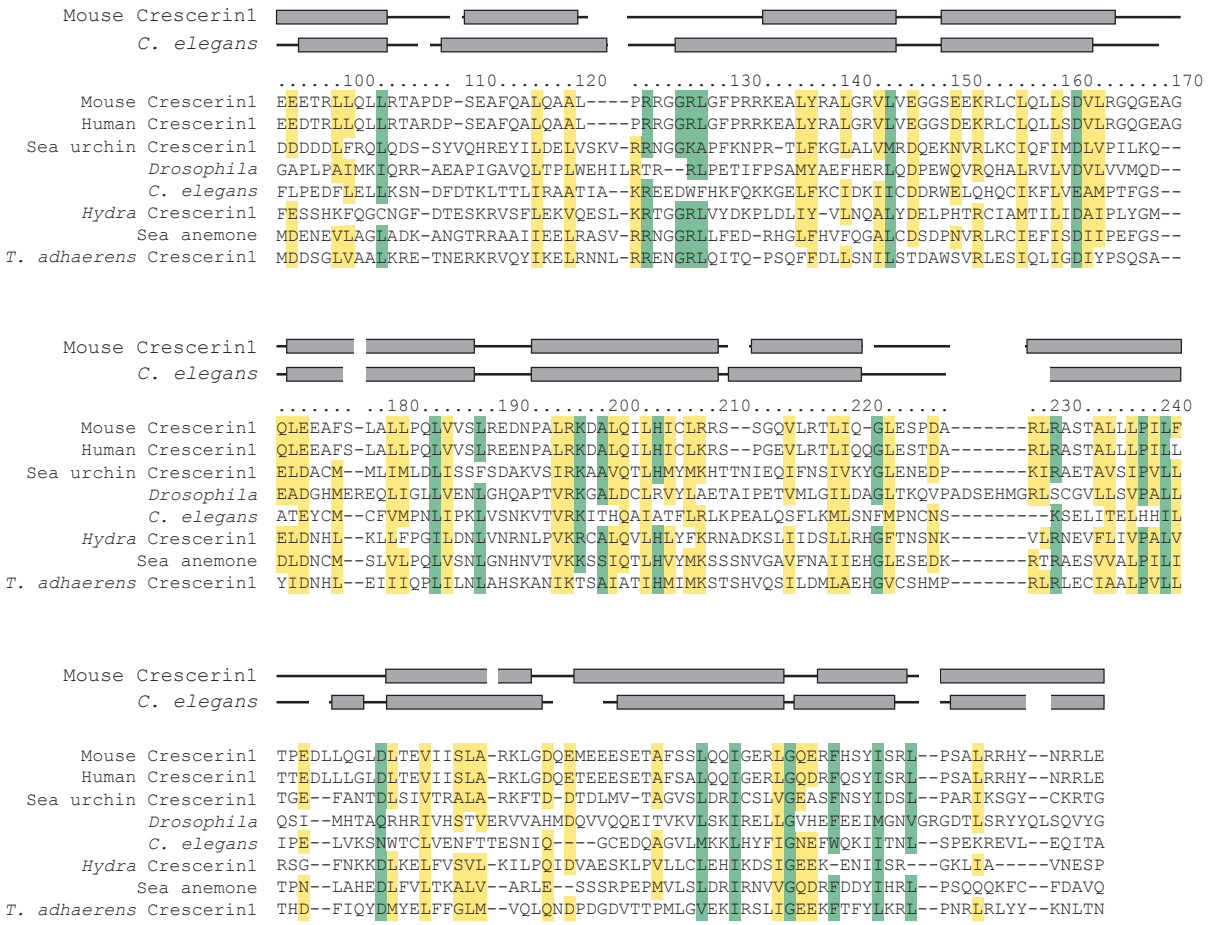

Appendix 2.5. Crescerin family TOG1 sequence alignment.
Sequence alignment of all TOG1-like domains in different species (all dark red domains in Figure 2.2. Residues that are identical or similar in 75% or more of the aligned sequences are highlighted in green and yellow respectively. The residue numbers of the mouse Crescerin1 sequence used in this alignment is shown above the alignment. The predicted alpha helices and connecting loops for this domain in mouse Crescerin1 and *C. elegans* CHE-12 are shown as grey boxes and black lines respectively.

APPENDIX 2.6: CRESCERIN FAMILY TOG2 SEQUENCE ALIGNMENT

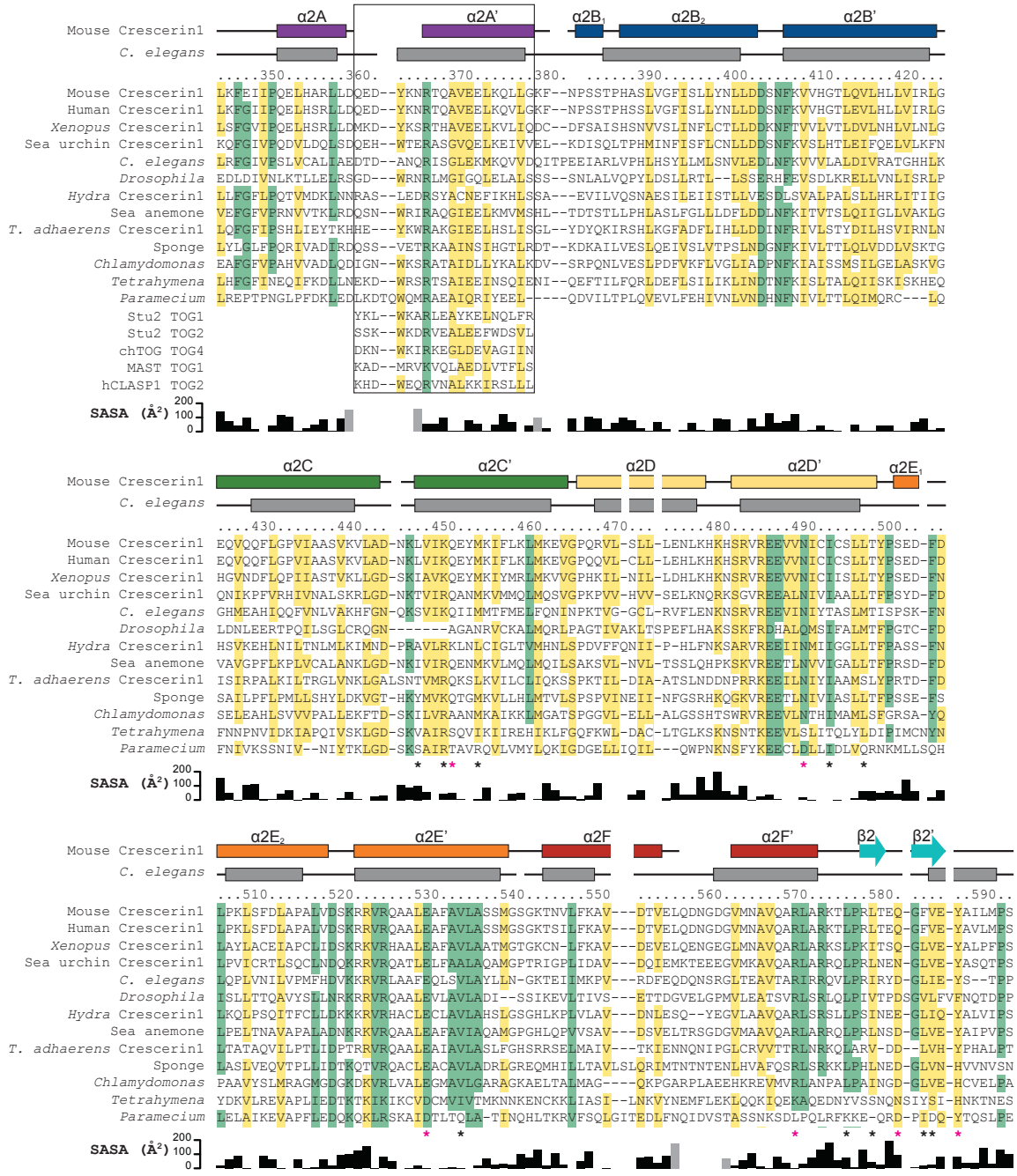

Appendix 2.6. Crescerin family TOG2 sequence alignment.
Sequence alignment of all TOG2-like domains in different species (all dark purple domains in Figure 2.2). Residues that are identical (green) or similar (yellow) in 75% or more of the aligned sequences are highlighted. The residue numbers of the mouse Crescerin1 sequence are shown above the alignment. The secondary structures for mouse Crescerin1 TOG2 as observed in the crystal structure are shown as boxes and colored according to Figure 2.5A. The predicted α-helices and connecting loops for *C. elegans* CHE-12 TOG2 are shown as grey boxes and black lines respectively. The solvent accessible surface area (SASA) for each residue as computed from the crystal structure of Crescerin1 TOG2 is shown as black bars except for residues with incompletely modeled side-chains or those flanking unmodeled regions (grey). Asterisks denote the residues involved in polar (pink) or hydrophobic (black) interactions between the β-hairpin and HRs C-F.

APPENDIX 2.7: CRESCERIN FAMILY TOG3 SEQUENCE ALIGNMENT

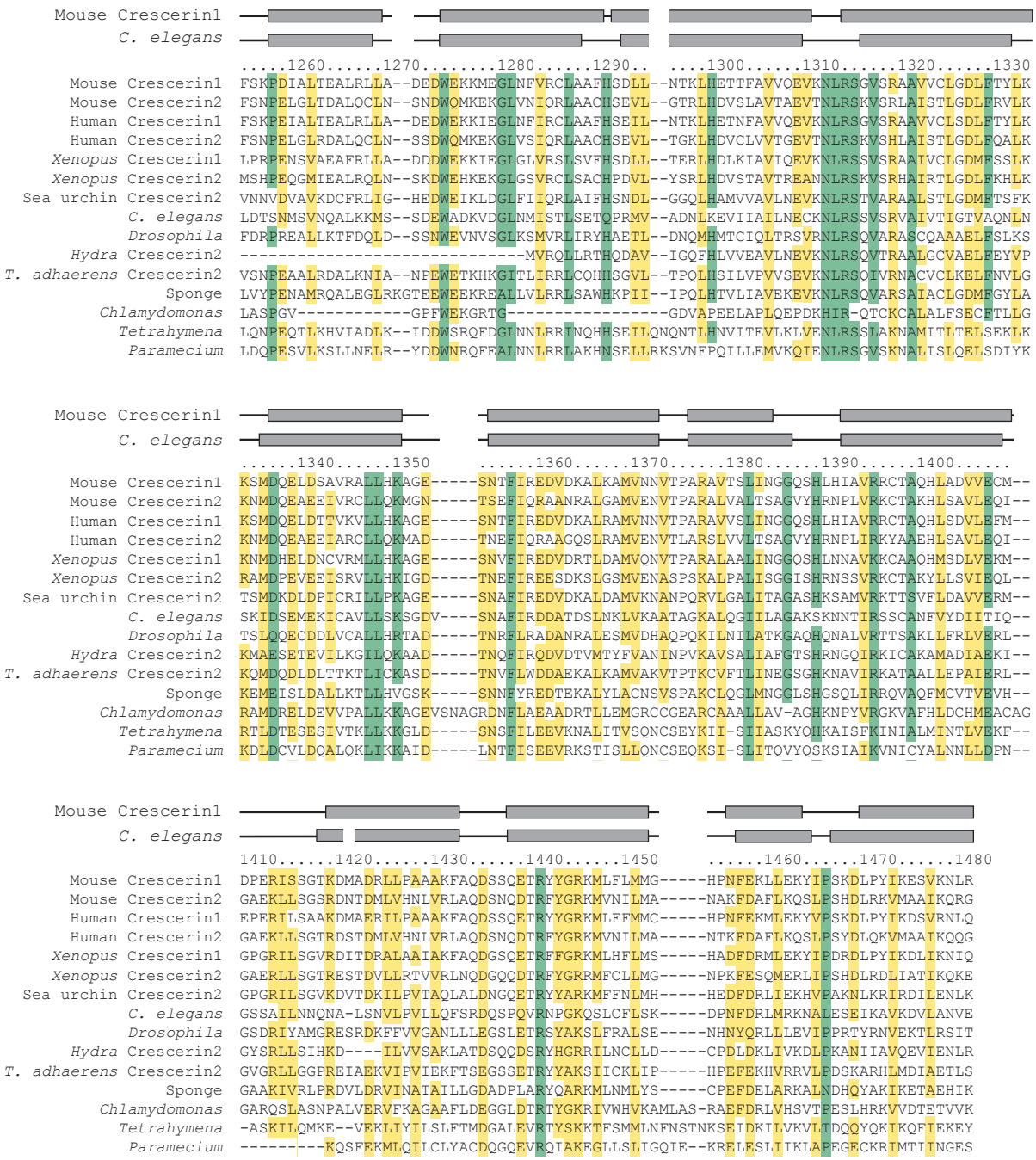

Appendix 2.7. Crescerin family TOG3 sequence alignment.
Sequence alignment of all TOG3-like domains in different species (all light orange domains in Figure 2.2). Residues that are identical or similar in 75% or more of the aligned sequences are highlighted in green and yellow respectively. The residue numbers of the mouse Crescerin1 sequence used in this alignment is shown above the alignment. The predicted alpha helices and connecting loops for this domain in mouse Crescerin1 and *C. elegans* CHE-12 are shown as grey boxes and black lines respectively.

APPENDIX 2.8: CRESCERIN FAMILY TOG4 SEQUENCE ALIGNMENT

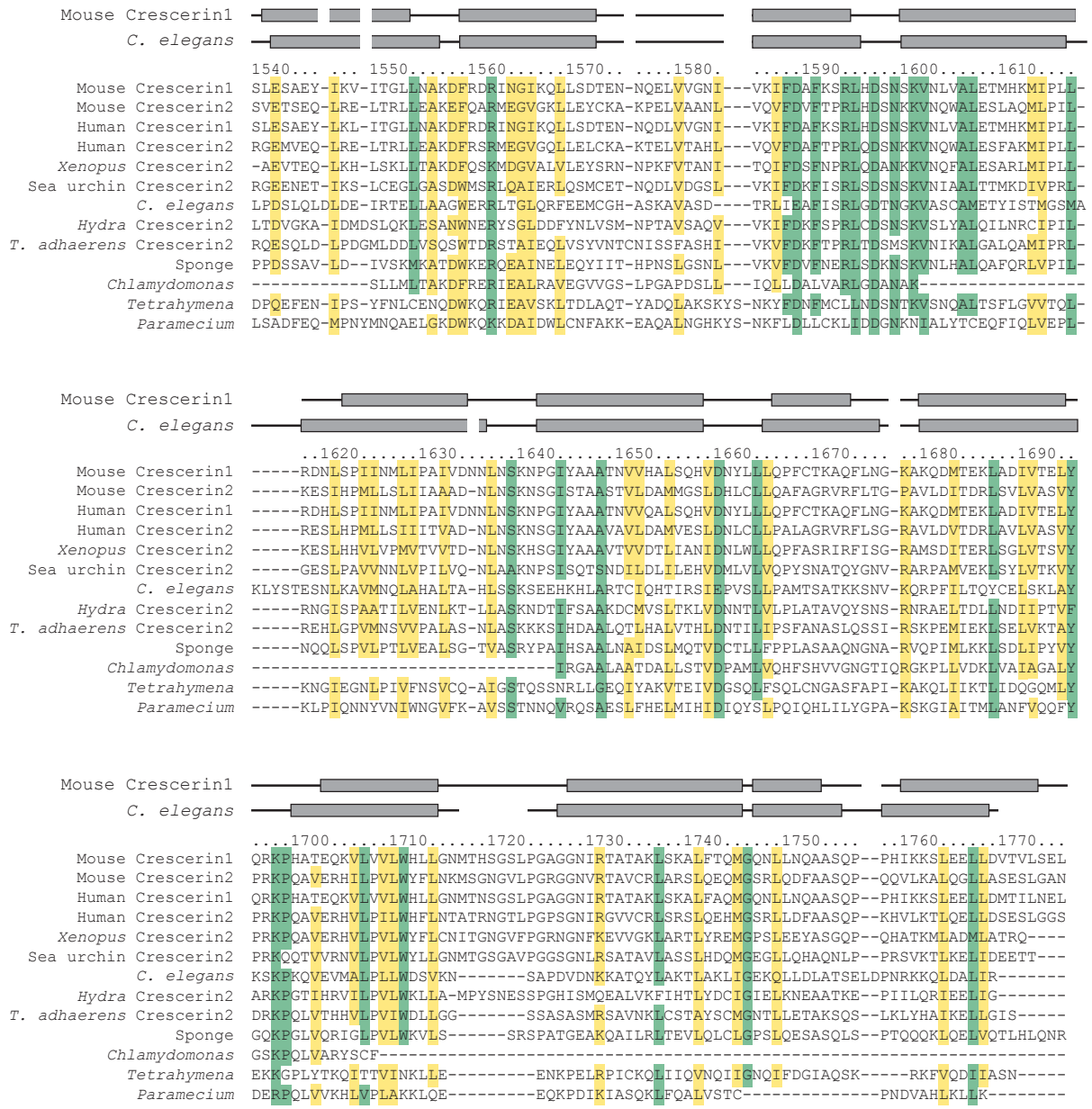

Appendix 2.8. Crescerin family TOG4 sequence alignment.
Sequence alignment of all TOG4-like domains in different species (all light purple domains in Figure 2.2). Residues that are identical or similar in 75% or more of the aligned sequences are highlighted in green and yellow respectively. The residue numbers of the mouse Crescerin1 sequence used in this alignment is shown above the alignment. The predicted alpha helices and connecting loops for this domain in mouse Crescerin1 and *C. elegans* CHE-12 are shown as grey boxes and black lines respectively.

APPENDIX 2.9: CIRCULAR DICHROISM OF CRESCERIN1 TOG DOMAINS

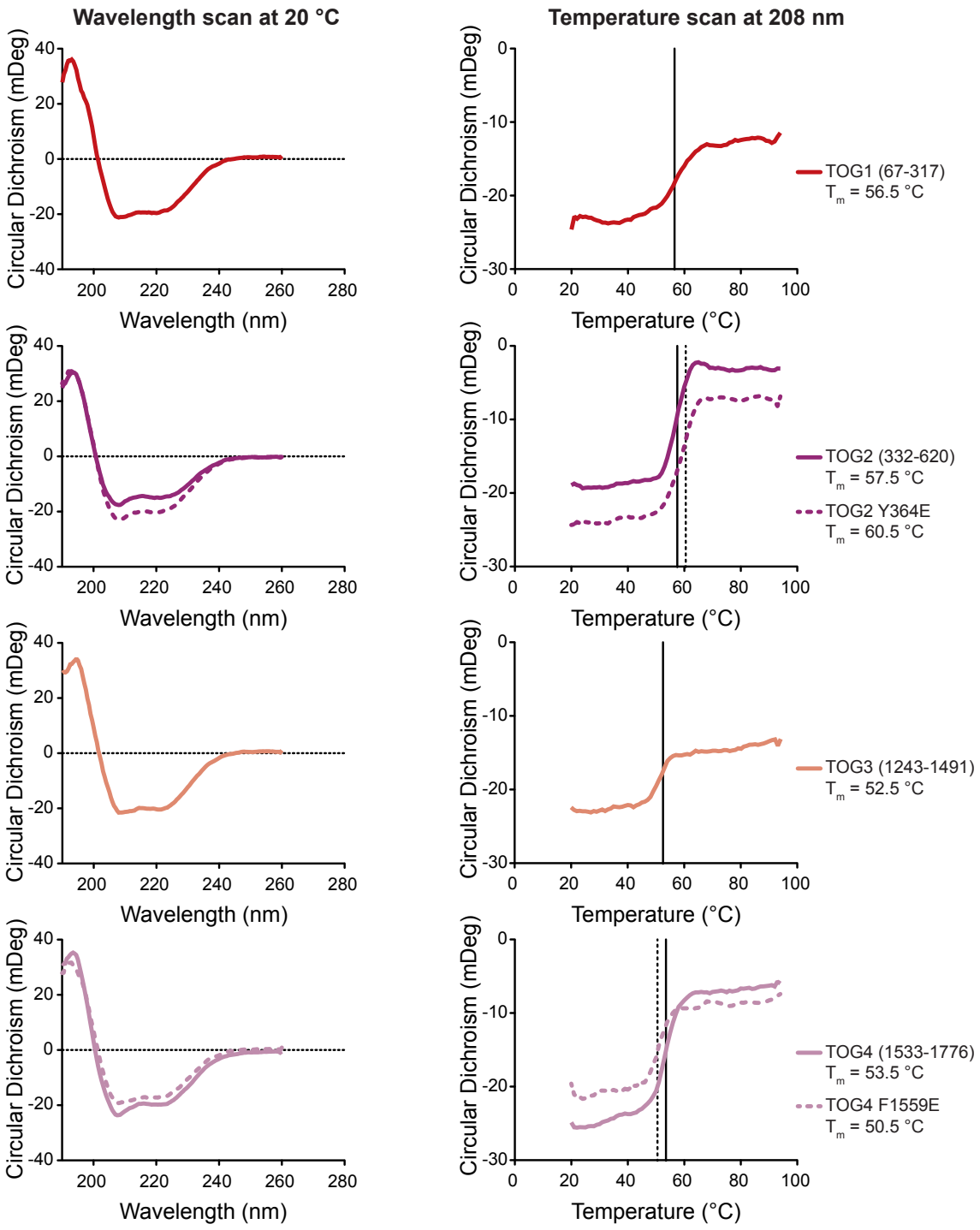

Appendix 2.9. Circular dichroism of Crescerin1 TOG domains.
Circular dichroism analysis of all single TOG domain constructs used for *in vitro* MT polymerization assays (Figure 2.8B). For each construct, wavelength scans reveal spectra characteristic of alpha helical proteins. Temperature scans show a sigmoidal shape indicative of co-operative unfolding that is not dramatically altered when conserved tubulin-binding determinants are mutated in TOG2 or TOG4.

APPENDIX 3.1: OVER-EXPRESSED CRESCERIN1 ASSOCIATES WITH CYTOPLASMIC MICROTUBULES

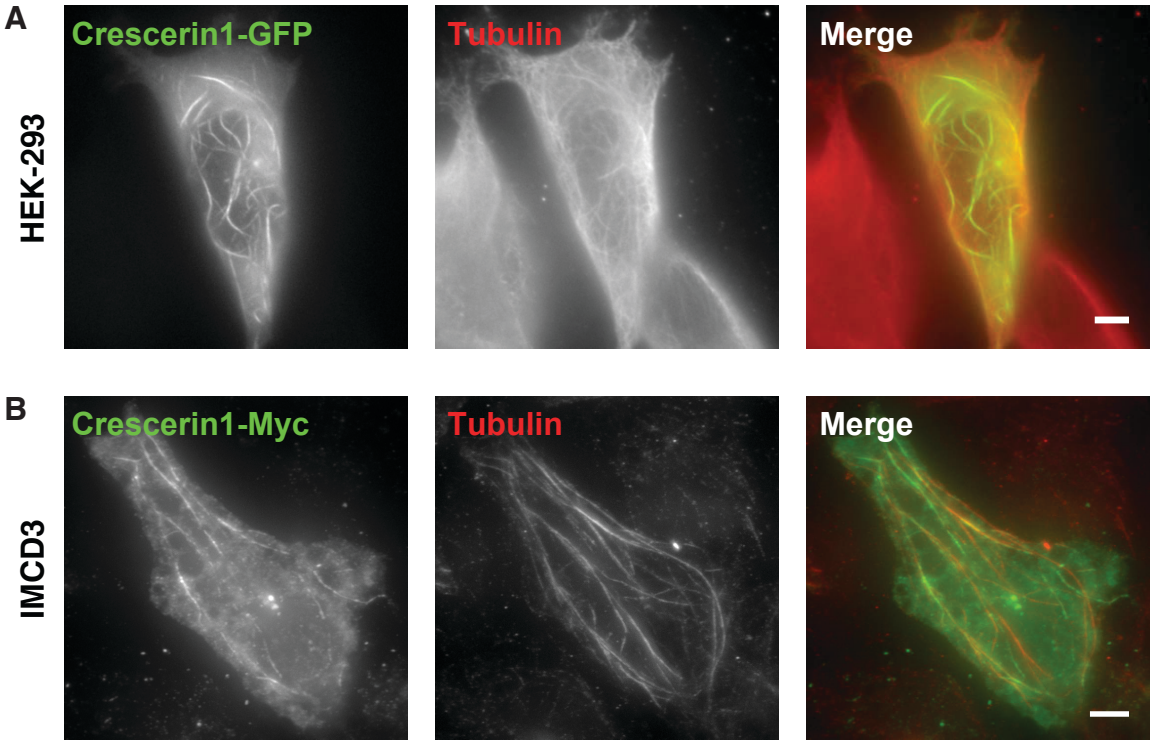

Appendix 3.1. Over-expressed Crescerin1 associates with cytoplasmic microtubules.
(A-B) Over-expressed Crescerin1 associates with cytoplasmic MTs in HEK-293 cells (A) and IMCD3 cells (B). All scale bars = 5 μm.

APPENDIX 3.2: CRESCERIN1 CONSTRUCTS SPANNING RESIDUES 1-1242 AND 577-1242 MISLOCALIZE TO LARGE CYTOPLASMIC PUNCTAE

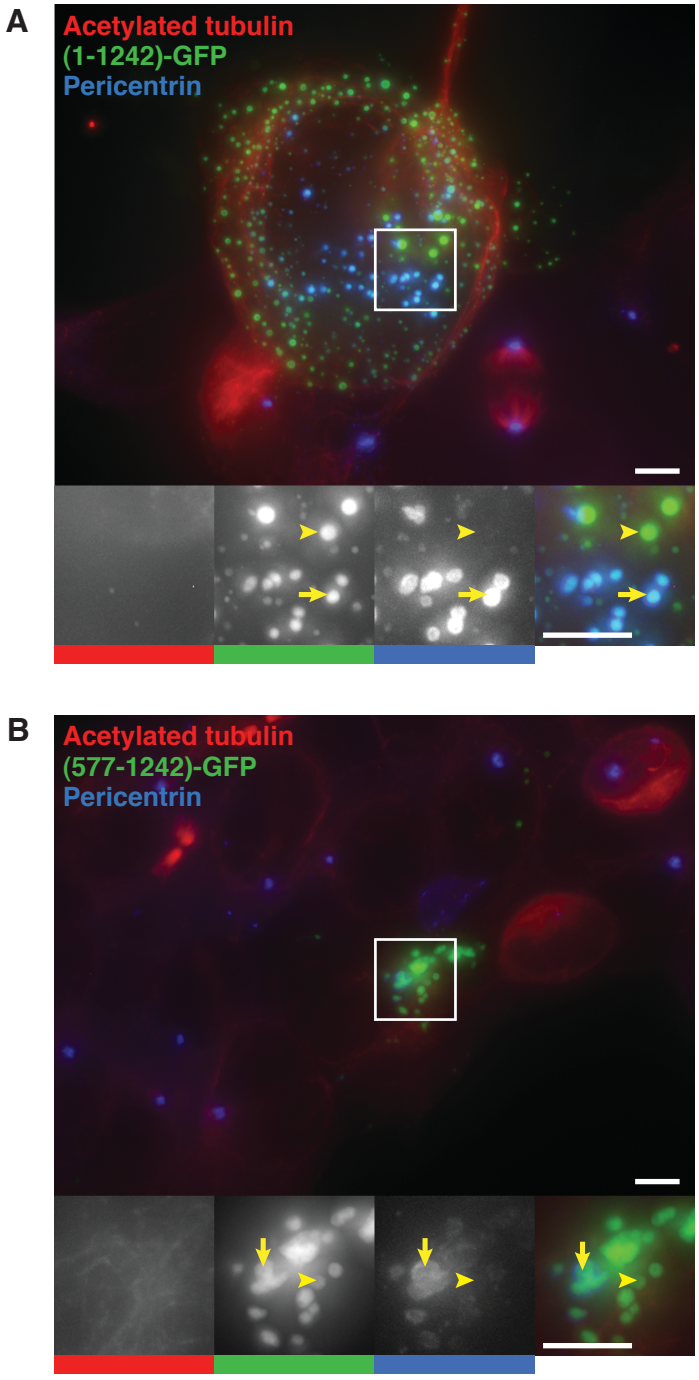

Appendix 3.2. Crescerin1 constructs spanning residues 1-1242 and 577-1242 mislocalize to large cytoplasmic punctae.
GFP tagged Crescerin1 constructs spanning residues 1-1242 (A) and 577-1242 (B) mislocalize to large cytoplasmic punctae that often co-stained with the antibody against the basal body/centrosome marker, Pericentrin (Yellow arrow). Yellow arrowheads denote punctae with GFP signal that do not co-stain with the anti-Pericentrin antibody.

APPENDIX 3.3: PY-NLS SEQUENCES FROM KNOWN IMPORTIN-β2 BINDING PROTEINS AND CRESCERIN1

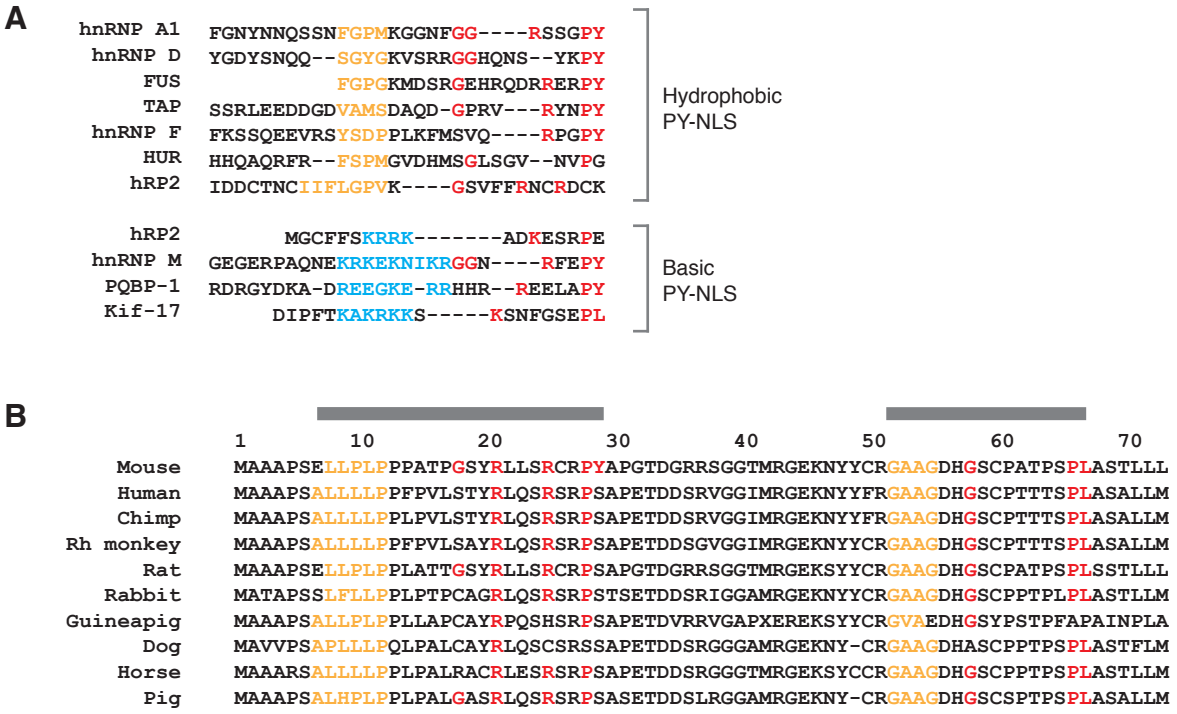

Appendix 3.3. PY-NLS sequences from known Importin-β2 binding proteins and Crescerin1.
(A) Alignment of sequences from hydrophobic PY-NLSs (top) and basic PY-NLSs (bottom) reveal a conserved residues (red) and hydrophobic (yellow) or basic (blue) patches. (B) Two hydrophobic PY-NLS like sequences at the N-terminus of mammalian Crescerin1. The residue numbers of mouse Crescerin1 are shown above the alignment.

APPENDIX 4.1: LIST OF *C. ELEGANS* STRAINS USED IN THIS STUDY AND THEIR GENOTYPES.

Strain name	Genotype	Reference	Cas9 site selected for strain generation (5'-3')
N2	Wild Type	(Brenner, 2003)	N/A
HT1593	*unc-119(ed3)* III	(Maduro and Pilgrim, 1995)	N/A
LP176	*unc-119(ed3)* III; *che-12(cp25[che-12::GFP + LoxP unc-119(+) LoxP])* V	This study	GGAAAAACAATTG CTTGACTTGG
LP177	*unc-119(ed3)* III*; che-12(cp26[Δ1-1282 + GFP + LoxP unc-119(+) LoxP])* V	This study	GAGCCGCAACGAT AGCAAAACGG
LP193	*cpSi20[Pmex-5::TagRFP-T::PLCδ-PH ::tbb-2 3'UTR + unc-119(+)]* II; *unc-119(ed3)* III	Gift from C. Higgins	N/A
LP198	*unc-119(ed3)* III*; che-12(cp34[gfp::che-12 + LoxP unc-119(+) LoxP])* V	This study	CCGCCGGAGAGCA AAAGCTCATC
LP200	*unc-119(ed3)* III*; che-12(cp36[gfp::che-12 F34E A281E W815E W1073E + LoxP unc-119(+) LoxP])* V	This study	CCGCCGGAGAGCA AAAGCTCATC
LP204	*cpEx17[Pgcy-5::mCherry + rol-6(su1006)]*	This study	N/A
LP205	*unc-119(ed3)* III*; che-12(cp26[Δ1-1282 + GFP + LoxP unc-119(+) LoxP])* V*; cpEx18[Pgcy-5::mCherry + rol-6(su1006)]*	This study	N/A
LP206	*unc-119(ed3)* III*; che-12(cp34[gfp::che-12 + LoxP unc-119(+) LoxP])* V*; cpEx19[Pgcy-5::mCherry + rol-6(su1006)]*	This study	N/A
LP207	*unc-119(ed3)* III*; che-12(cp36[gfp::che-12 F34E A281E W815E W1073E + LoxP unc-119(+) LoxP])* V*; cpEx20[Pgcy-5::mCherry + rol-6(su1006)]*	This study	N/A
LP285	*unc-119(ed3)* III*; che-12(cp25[che-12::GFP + LoxP unc-119(+) LoxP])* V*; cpEx28[Pgcy-5::mCherry + rol-6(su1006)]*	This study	N/A
LP286	*cpSi20[Pmex-5::TagRFP-T::PLCδ-PH ::tbb-2 3'UTR + unc-119(+)]* II; *unc-119(ed3)* III; *cpEx29[Pgcy-5::mCherry + rol-6(su1006)]*	This study	N/A
LP313	*che-12(cp77[che-12::loxP::che-12 3'UTR::let-858 3'UTR::loxP::mNG + HygR]) V*	This study	GGAAAAACAATTG CTTGACTTGG

APPENDIX 4.2: GENOME EDITING IN *C. ELEGANS*

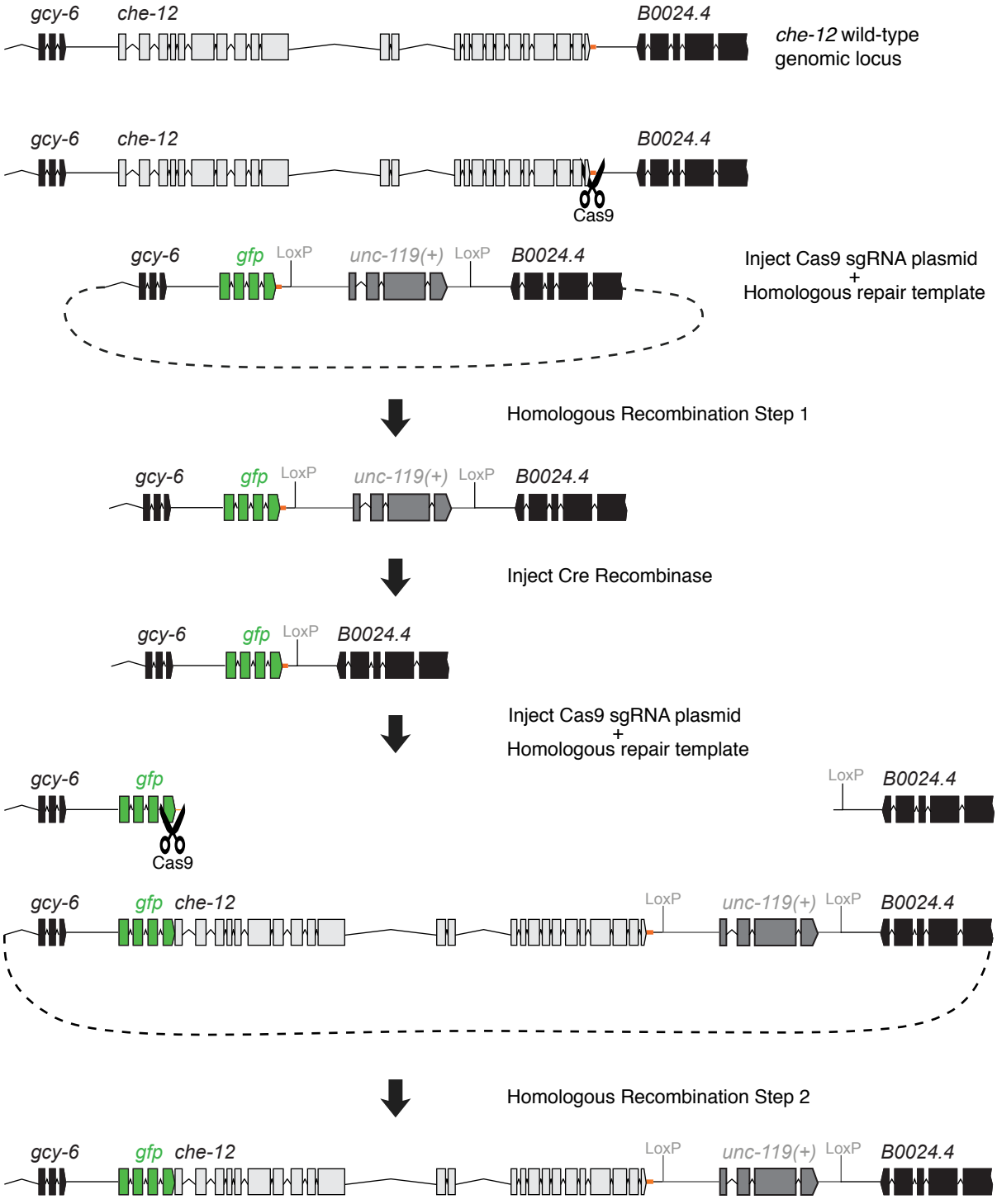

Appendix 4.2. Genome editing in *C. elegans*.
Diagram outlining the steps to generate *C. elegans* strains with targeted modifications at the *che-12* locus. Exons, introns and intergenic regions are shown as boxes, bent lines and straight lines, repectively. The *che-12* 3'UTR is shown in orange.

APPENDIX 4.3: CONDITIONAL ENDOGENOUS TAGGING OF *C. ELEGANS* GENES

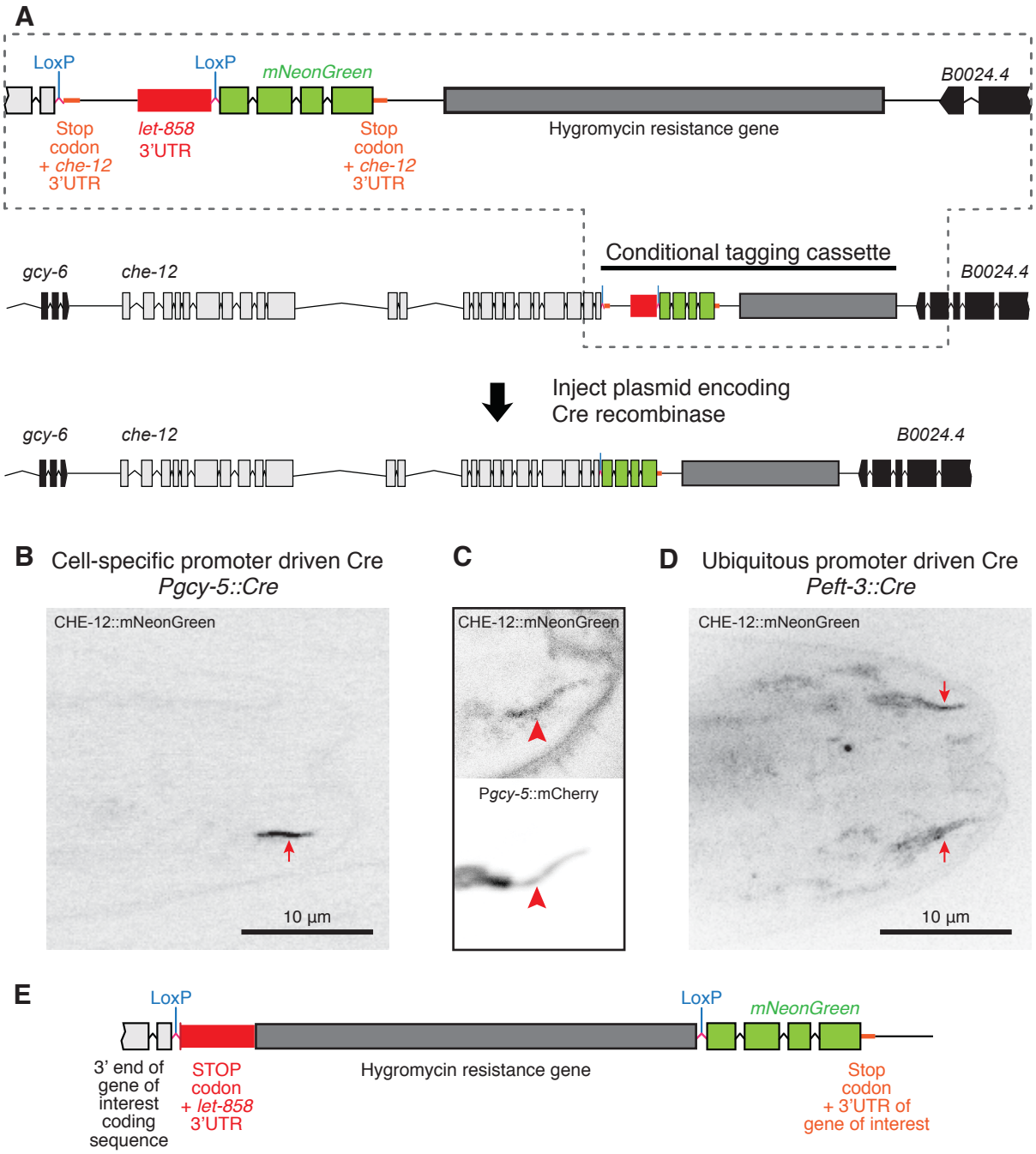

Appendix 4.3. Conditional endogenous tagging of *C. elegans* genes.
(A) Diagram outlining the strategy for the conditional tagging of *che-12*. (B) Expressing P*gcy-5* driven Cre-recombinase in the conditionally tagged *che-12* strain results in mNeonGreen labeled CHE-12 expression specifically in a single neuron (red arrow). (C) CHE-12::mNeonGreen localizes to the P*gcy-5*::mCherry labeled ASER cilium (red arrowhead). (D) Expressing P*eft-3* driven Cre-recombinase in the conditionally tagged *che-12* strain results in mNeonGreen labeled CHE-12 expression multiple amphid neurons and localizes to both left and right amphid cilia bundles (red arrows). (E) Map of the modified CTC for future experiments featuring a rearrangement of modules for a more compact design.